

DESIGN AND SYNTHESIS  
OF  
ACOUSTIC SURFACE WAVE  
FILTERS

by

William R. Donnison, B. Sc. (Hon)

PART A: MCMASTER (ON CAMPUS) PROJECT\*

A Report Submitted to the School of Graduate Studies  
in Partial Fulfilment of the Requirements  
for the Degree  
Master of Engineering

Department of Engineering Physics

McMaster University

Hamilton, Ontario, Canada

April, 1976

\* One of the two Project Reports: The other part is designated  
PART B: INDUSTRIAL PROJECT

MASTER OF ENGINEERING

MCMASTER UNIVERSITY

ENGINEERING PHYSICS

HAMILTON, ONTARIO

TITLE: Design and Synthesis of Acoustic Surface Wave Filters

AUTHOR: William R. Donnison, B. Sc. (Hon) (Trent University)

SUPERVISOR: Dr. Colin Kydd Campbell

NUMBER OF PAGES: viii, 134

TABLE OF CONTENTS

|  | <u>Page</u> |
|--|-------------|
| Acknowledgement  | i           |
| Abstract   | ii          |
| List of Tables   | iii         |
| List of Figures  | iii         |
| Computer Programmes  | viii        |
| INTRODUCTION .....   | 1           |
| SECTION I: SURFACE WAVE DEVICES .....                      | 4           |
| 1. The Basic Device Concept .....                          | 4           |
| 2. The Basic Form of the Surface Acoustic Wave...          | 5           |
| 3. The Basic Interdigital Transducer .....                 | 8           |
| SECTION II: MODELLING OF THE INTERDIGITAL TRANSDUCER ..... | 14          |
| 1. Mason Equivalent Circuit .....                          | 14          |
| 2. Impulse Model of Surface Transducers .....              | 20          |
| SECTION III: BANDPASS FILTER SYNTHESIS .....               | 30          |
| 1. Design Procedures .....                                 | 30          |
| 2. Experimental Procedures .....                           | 55          |
| RESULTS: 1. Parameter Listings .....                       | 69          |
| 2. Theoretical-Experimental Comparison .....               | 70          |
| 3. Discussion of Results .....                             | 72          |
| CONCLUSIONS: .....   | 74          |

TABLE OF CONTENTS

|   | Page |
|---|------|
| APPENDIX #1: Slow Transmission-Line Analogy ..... | 76   |
| APPENDIX #2: Computer Programmes                  | 82   |
| 1. Design Programme                               | 83   |
| 2. Mask Co-ordinate Programme                     | 87   |
| TABLES .....                                      | 88   |
| FIGURES .....                                     | 89   |
| REFERENCES .....                                  | 132  |

## ACKNOWLEDGEMENT

The author wishes to express his appreciation to Dr. Colin Campbell for his guidance and encouragement throughout the course of this project. The author also wishes to acknowledge the excellent work of Mrs. Hazel Coxall in typing the final form of this report.

## ABSTRACT

This report describes the basic physical properties of surface wave devices and design procedures necessary to realize filter functions from such devices. The mathematical form of the surface wave is presented. Filter models based on this wave are reviewed and the strong relationship between device geometry and resultant transfer functions is developed.

Design and experimental procedures adopted for the synthesis of a surface-wave filter used for colour T.V. I.F. strips are given. Two such filters are actually made in the laboratory and experimental-theoretical results are compared. Results obtained indicate good agreement between theory and experiment, and clearly demonstrate the superiority of surface wave filters over conventional L-C filters in high frequency applications.

LIST OF TABLES

|  | <u>Page</u> |
|--|-------------|
| Table I: - Transition Width and Ripple for a Bessel Weighting<br>Function of time duration $2\tau$ (from Reference #1) | 88          |

LIST OF FIGURES

|  | <u>Page</u> |
|--|-------------|
| Figure 1 - Block Diagram of a surface-wave device<br>(from Reference #2).  | 89          |
| Figure 2 - Displacement due to surface acoustic waves on an<br>isotropic solid (from Reference #2).  | 90          |
| Figure 3 - Basic structure of an interdigital transducer<br>(from Reference #3).   | 91          |
| Figure 4 - Side View of an Interdigital Transducer<br>(from Reference #3).<br>(a) Generation mode<br>(b) Detection mode  | 92          |
| Figure 5 - "Mason Equivalent Model" of a section of<br>transducer (from Reference #1).   | 93          |
| Figure 6 - Complete electrical equivalent of a section of<br>a transducer (from Reference #1).   | 94          |
| Figure 7 - Models of Complete transducers (from Reference #1)<br>(a) 3-Port model showing the two acoustic and one<br>electrical ports<br>(b) Equivalent circuit as reviewed from the<br>electrical port | 95          |

LIST OF FIGURES

|   | <u>Page</u> |
|---|-------------|
| Figure 8 - Acoustic elements associated with the transducer model (from Reference #1).                                | 96          |
| (a) Acoustic conductance  |             |
| (b) Acoustic susceptance  |             |
| Figure 9 - Comparison between surface-wave transducer and transversal filter (from Reference #1)                      | 97          |
| (a) Surface wave impinging upon the transducer from the left  |             |
| (b) Block representation of operation of a transversal filter (from Reference #1)                                     |             |
| Figure 10 - Typical arrangement for a surface wave device (from Reference #1).  | 98          |
| Figure 11 - Two-transducer arrangement with the one on the left being of the apodized class.                          | 99          |
| Figure 12 - Acoustic field response of an apodized transducer (from Reference #3).                                    | 100         |
| Figure 13 - Schematic showing method of time response determination from the transducer geometry (from Reference #4). | 101         |
| Figure 14 - Determination of effective transducer time responses (from Reference #4)                                  | 102         |
| (A) Apodized transducer with constant centre-to-centre finger spacings.   |             |
| (B) Demonstration of strip analysis technique   |             |

LIST OF FIGURES

|  | <u>Page</u> |
|--|-------------|
| (C) Time response associated with the strip shown in (B).  |             |
| (D) Effective time response of the apodized transducer in (A).   |             |
| Figure 15 - Magnitude of time response for a rectangular bandpass, linear phase filter.  | 103         |
| Figure 16 - Imaginary component of time response for rectangular bandpass, linear phase filter.  | 104         |
| Figure 17 - "Haystack" colour T.V. video I.F. response (reconstructed from information provided by Electrohome Electronics Corporation). | 105         |
| Figure 18 - Modeling the frequency response of two apodized transducers (from Reference #4).   | 106         |
| Figure 19 - Form of the initial input data to the Fast Fourier Programme.  | 107         |
| Figure 20 - The Kaiser Weighting Function (from Reference #1).   | 108         |
| Figure 21 - Effect on frequency response due to time response truncation after the fifth zero.   | 109         |
| Figure 22 - Effect on frequency response due to time response truncation after the second zero.  | 110         |
| Figure 23 - Determining the phase from the group delay.  | 111         |
| Figure 24 - Kaiser-optimized frequency response for truncation after the fifth zero.   | 112         |

LIST OF FIGURES

|   | <u>Page</u> |
|---|-------------|
| Figure 25 - Kaiser-optimized frequency response for truncation after the second zero.   | 113         |
| Figure 26 - Universal admittance curves for surface-wave transducers on Lithium Niobate and Quartz substrates (from Reference #4).                  | 114         |
| Figure 27 - Electrical Matching for Input Transducers (from Reference #4).  | 115         |
| Figure 28 - Transducer Efficiency versus Beamwidth (from Reference #1).   | 116         |
| Figure 29 - Finger-edge reflection from a surface wave transducer (from Reference #1).  | 117         |
| Figure 30 - Use of split-finger transducer geometry to reduce effects of finger-edge reflections (from Reference #1).                               | 118         |
| Figure 31 - Dummy fingers used to reduce wavefront distortion (from Reference #1).  | 119         |
| Figure 32 - Harmonic amplitude versus metalization ratio for fundamental, third and fifth harmonic operation of the transducer (from Reference #1). | 120         |
| Figure 33 - Geometrical outline for filter #1-100x.   | 121         |
| Figure 34 - Geometrical outline for filter #2-100x.   | 122         |
| Figure 35 - Mask for filter #1-5x.  | 123         |
| Figure 36 - Mask for filter #2-5x.  | 124         |

LIST OF FIGURES

|  | <u>Page</u> |
|--|-------------|
| Figure 37 - Observed response of filter #1.  | 125         |
| Figure 38 - Observed response of filter #2.  | 126         |
| Figure 39 - Photographs of response of filter #1.                                    | 127         |
| (a) Magnitude response as measured on<br>Alfred Network Analyzer.                    |             |
| (b) Response as observed on Hewlett-<br>Packard Phase-Magnitude Analyzer.            |             |
| Figure 40 - Photographs of Response of filter #2.                                    | 128         |
| (a) Magnitude response as measured on<br>Alfred Network Analyzer.                    |             |
| (b) Response as observed on Hewlett-Packard<br>Phase-Magnitude Analyzer.             |             |
| Figure 41 - Photographs of equipment used in processing<br>the surface-wave filters. | 129         |
| (a) The Rubylith cutting table.  |             |
| (b) The Photo-Reduction Camera.  |             |
| (c) The annealing furnace.   |             |
| (d) The Photo-resist spinner.  |             |
| Figure 42 - Photographs of equipment used in processing<br>the surface-wave filters. | 130         |
| (a) The Vacuum evaporation system.   |             |
| (b) The Sweep-Network Analyzer and Oscilloscope<br>used in magnitude measurements.   |             |
| (c) The completed filters shown in their test<br>packages.                           |             |

LIST OF FIGURES

|   | <u>Page</u> |
|---|-------------|
| (c) The completed filters shown in their test packages.   |             |
| Figure A1 - Surface-wave transducer characteristics based on the transmission line analogy (from Reference #5). | 131         |
| (a) Uniform transmission line of characteristic impedance $Z_0$ with periodically spaced excitation potentials. |             |
| (b) 3-port electrical equivalent circuit of the complete transducer.  |             |

COMPUTER PROGRAMMES

|  | <u>Page</u> |
|--|-------------|
| Programme #1 - Determination of required response for transducer given the frequency response characteristics of the filter. | 83          |
| Programme #2 - Determination of finger length, polarity and position for a linear phase type filter.                         | 87          |

## THE SURFACE ACOUSTIC WAVE BANDPASS

### FILTER INTRODUCTION

#### A Brief Historical Note:

In 1885 Lord Rayleigh showed that stable modes of mechanical displacement waves could exist on the surface of a solid. From then till 1957 when Viktorov wrote his work on similar waves little attention was paid to them. It was recognized that if the solid under consideration was of a piezoelectric nature, then electric fields were attendant to the mechanical fields, and vice-versa. Therefore, in the early 1960's much research work was carried out to try to determine an efficient manner of converting electrical impulses applied to these surfaces into mechanical surface waves.

Major breakthroughs occurred in the years 1966 and 1968. In 1966 G. A. Coquin and H. F. Tiersten published a paper "Analysis of the Excitation and Detection of Piezoelectric Surface Waves in Quartz by Means of Surface Electrodes".<sup>(7)</sup> This paper put on firm mathematical foundations the form of the generated waves and demonstrated clearly the potential of the interdigital transducer configuration as a means of accomplishing the necessary conversion. In 1968 Campbell and Jones' paper "A Method for estimating optimal crystal cuts and propagation directions for excitation of piezoelectric surface waves"<sup>(8)</sup> was used as a basis for orienting the transducer configuration on the substrate by the Stanford Group. They were able to report conversion losses as low as 4 db over a 20% bandwidth on Lithium Niobate.

With such firm confirmation of the basic interdigital transducer

configuration research on practical applications in this area was greatly enhanced. Since this time applications of the basic principles has resulted in a wide variety of devices such as delay lines, frequency filters, oscillators, fixed and programmable analogue matched filters, convolvers and correlators, and even devices related to display. Much of the basic design work for frequency filters, delay lines and matched filters has now been achieved, and highly reliable design synthesis and device manufacture processes established. In this work emphasis is on the development of frequency filters, specifically for application in television I.F. strips.

SECTION I

SURFACE WAVE DEVICES

## 1. The Basic Device Concept

The Basic operation concept common to all surface-wave devices is the conversion of electrical signals into the mechanical equivalent represented by the surface wave. This is accomplished by the interdigital transducer. The generated acoustic wave is propagated in a specified direction along the medium until it encounters a second interdigital transducer. This transducer performs the inverse of the first, and converts the impinging surface wave disturbance into its electrical equivalent. Figure #1<sup>(2)</sup> shows the basic blocks necessary to realize a surface-wave device.

Several features of this basic structure which has caused attention to be paid to them are:<sup>(2)</sup>

- (i) Due to the planar nature of these structures the fabrication methods developed for intergrated circuits may be extended to these devices. Specifically, the standard photolithography techniques may be used.
- (ii) Device performance is almost completely specified by the geometry of the transducers. This fact, coupled with point number (i) allows one to incorporate the complete transducer design into the masks, thus increasing the repeatability of performance in batch manufacturing schemes.
- (iii) Since the surface wave velocity is approximately  $10^{-5}$  times the speed of electromagnetic waves, this allows spatial compression of a converted electrical signal by the same factor.
- (iv) Since the information transmitted by these devices is on the surface, it is accessible at all points. This allows greatly increased

freedom in signal processing.

- (v) Since the wave is stable, it is to a large extent unaffected by electric and magnetic fields, and to a lesser extent to temperature.

## 2. The basic form of the Surface Acoustic Wave <sup>(6)</sup>

Acoustic surface waves are elastic displacement waves which propagate near the stress-free boundary of a solid and decay with depth. The basic physical equations necessary to derive the form of the waves are:

- (i) The equations of state for a piezoelectric medium

$$T_{ij} = c_{ijkl} S_{kl} - e_{ijk} E_k \quad (6) \quad (1)$$

$$D_i = e_{ijk} S_{jk} + \epsilon_{ij} E_j \quad (2)$$

Here  $E_j$  are the components of the electric field;  $D_i$  the components of the electric displacement;  $c_{ijkl}$  the elastic constants for the piezoelectric medium;  $e_{ijk}$ , the piezoelectric constants relating stresses to electric fields; and  $\epsilon_{ij}$ , the permittivities measured at constant strain;  $T_{ij}$  is the second rank stress tensor, and  $S_{kl}$  is the second rank strain tensor. The usual convention of summing over repeated indicies is used in the above equations.

- (ii) The equations of motion as given by Newtons Second Law

$$\rho(\partial^2 \mu_i / \partial t^2) = (\partial T_{ij} / \partial x_j) \quad (3)$$

where  $\rho$  is the density of the material and  $\mu_i$  are the components of the particle displacement.

(iii) Gauss's Law for an insulator

$$\text{div } D = 0 \quad (4)$$

The usual cases studied are for the class of piezoelectric materials known as the "weak coupling class". For this class of materials the piezoelectric constants  $e_{ijk}$  are much less in magnitude than the permittivities  $\epsilon_{ij}$  and the equation for  $D_i$  may be expressed to a good approximation as

$$D_i = \epsilon_{ij} E_j$$

Also, the strain components are related to the displacement components through the usual relationship

$$S_{ij} = \frac{1}{2} [(\partial u_i / \partial x_j) + (\partial u_j / \partial x_i)] \quad (5)$$

The Boundary conditions under which the above equations are solved are that the stress components normal to surface of the piezoelectric medium be equal to zero.

Results of such studies indicate the existence of stable surface waves. The general form for a displacement  $u_i$  propagating in the  $x_i$  direction of a surface normal to the  $x_3$  direction is<sup>(5)</sup>

$$u_i = \sum_{j=1}^3 c_j \exp \left[ -a_j \omega x_3 / v_s \right] \exp \left[ i\omega(t - x_1 / v_s) \right] \quad (6)$$

The amplitude  $c_j$ , the surface wave velocity  $v_s$ , and the roots  $a_j$  are found by making this equation satisfy both the equation of motion and the above mentioned boundary conditions. As indicated by the form of the displacement equations if the roots  $a_j$  are real then the resultant waves are travelling waves in the  $\chi_1$  direction and decaying exponentially in the  $\chi_3$  direction; i.e. the surface normal.

In the case of solids which are isotropic the basic tensor relationships are replaced by the much simplified scalar form of relationships. That is to say that the c's, s's and  $\epsilon$ 's become direction independent and their normal matrix representation becomes a simple scalar number. It was this type of solid which Lord Rayleigh considered in his paper of 1885. For this case the surface-wave velocity may be approximated by

$$v_s = v_t \frac{0.87 + 1.12\nu}{1 + \nu} \quad (5) \quad (7)$$

where  $\nu$  is Poisson's ratio. As  $\nu$  varies from 0 to 0.5, the surface phase velocity varies from  $0.87v_t$  to  $0.96v_t$ , where  $v_t$  is the bulk shear wave velocity. Note that  $v_s$  is less than  $v_t$  and that it is also independent of frequency. Thus the surface wave is nondispersive. At the surface the motion of the material particle is counter-clockwise and elliptical, having a component perpendicular to the surface and another component parallel to the wave vector. The plane described by the propagation vector and the normal surface vector is referred to as the sagittal plane.

For anisotropic single crystals the full tensor forms of the

equations must be used and the problem becomes much more complex. The velocity cannot be expressed in closed form and computer methods are required to find the velocity along each direction. It is also possible to find for the anisotropic case that the surface wave velocity may exceed the bulk wave velocity along certain directions. This condition gives rise to "leaky" waves being generated into the solid. Also, the  $a_j$ 's of the solution may occur in complex conjugate pairs, so that amplitude decay into the solid is an exponential times a trigonometric function. The particle motion may also have three components so that the three-dimensional elliptical motion is not in the sagittal plane and the power flow is parallel to the wave vector only along selected pure-mode axes.

A considerable amount of research has been carried out in an attempt to solve the basic equations for as many of the known piezoelectric crystals as possible. Good theoretical-experimental agreement has been found in most cases, resulting in the compilation of tables which give the most important physical parameters of piezoelectrics used in surface wave devices. For more detail on the basic form of the surface wave I refer you to the references at the end of this paper.

In figures 2(a) and (b) <sup>(2)</sup> I have shown the displacements due to surface acoustic waves on an isotropic solid.

### 3. The Basic Interdigital Transducer

As mentioned in the historical note at the beginning, the fundamental structure used in the generation and manipulation of surface waves is the so-called "interdigital transducer". This structure is universally accepted as the most efficient and reliable method of generating and

controlling the waves. This structure is shown in figure #3.<sup>(3)</sup> Most striking is the simplicity of the geometry. Even so, this structure allows for a remarkable degree of control over the generated wave.

Associate with the structure are the following parameters

$W$  = finger overlap length

$a$  = finger width

$d$  = distance between adjacent fingers

$L$  = transducer length

The following points about the structure are immediately clear.

- (i) If an electrical impulse is applied between the buss bars marked + and - then adjacent fingers will be subjected to equal magnitude, but oppositely directed electric field distributions.
- (ii) The beamwidth of any generated acoustic wave resulting from the response of adjacent fingers to the applied impulse will be equal to the amount of finger overlap  $W$  for the adjacent pair.
- (iii) The direction of the radiated wave will be along a line perpendicular to the line defining the beamwidth. In the diagram this direction is marked  $\underline{k}$ . Note that this point does not preclude the possibility that the energy flow may not be along the direction  $\underline{k}$ . This would be the case if the direction  $\underline{k}$  did not correspond to a "pure-mode" direction of the piezoelectric material to which the interdigital transducer is adhered.

What is not clear is the form of the generated acoustic wave between the adjacent fingers. It will be noticed that in analysing this case from first principles that the basic equations become subject to new

boundary conditions. Specifically, the section of piezoelectric surface covered by the metalized fingers becomes subjected to the following boundary condition. In Gauss's law one must use the fact that the tangential component of the electric field is zero on the metallized fingers and the normal component of the electric displacement is continuous across the solid-vacuum interface. Secondly, and more difficult to incorporate, is the fact that the metallized fingers supply loading to the surface. This changes the condition that the normal components of stress on the surface be equal to zero. Also to be recognized is that the metallized fingers represent a "short" to the electric field attendant to the acoustic wave. These conditions clearly demonstrate that deriving an exact solution to the form of the acoustic surface disturbance produced by the interdigital transducer is by no means a trivial problem.

This problem has resulted in the development of various equivalent circuits to describe the results of exciting the interdigital transducer. Which model is used depends on the dominant specifications of the device being designed and on the number of second order effects it is necessary to include. However, we may gain insight into the frequency response of the simple transducer by considering figure #4(b).<sup>(3)</sup> This figure represents a surface wave impinging upon a uniform N-finger pair transducer. The output from such a transducer will be the vector addition over all sections.<sup>(10)</sup> All contributions will have the same magnitude but each will be progressively shifted in phase by a quantity  $\delta$ , where  $\delta = \frac{\omega\lambda}{2V}$  where V is the surface wave velocity. The total output will then be given by

$$E_t = E_0 e^{j\omega t} \left[ 1 - e^{j\delta} + e^{2j\omega} + \dots + (-1)^{n-1} e^{j(n-1)\delta} \right] \quad (8)$$

where  $E_0$  = peak output voltage from the transducer. The alternate plus and minus signs of the series arise due to the fact that adjacent fingers are connected to buss bars of opposite polarity. At the synchronous frequency  $\omega_0$ ,  $\delta = \pi$  and all terms in the series equal +1.

At frequencies near  $\omega_0$  we get for the total voltage

$$E_t = 2NE_0 \frac{\sin(N\pi \frac{\Delta\omega}{\omega_0})}{N\pi \frac{\Delta\omega}{\omega_0}} e^{j(\omega t - (2N-1)\frac{\pi\Delta\omega}{2\omega_0})} \quad (9)$$

where  $\Delta\omega = \omega - \omega_0$  and we have assumed that

$$\sin(\pi\Delta\omega/2\omega_0) \sim \pi\Delta\omega/2\omega_0$$

From this we see that the frequency response is of the  $\sin x/x$  form and that the phase response is linear. In the following section of this report I will introduce two approaches to equivalent circuit models of the interdigital transducer. One is based on a physical picture of the transducer and is called the Mason equivalent circuit. The other approach makes use of the connection between the time and frequency domain descriptions of systems through the Fourier Transform. It is this latter approach that is usually favoured for the design of filters, and is the approach used by the author in designing bandpass filters. However, since the Mason equivalent circuit yields a good physical understanding of the device, an outline of the approach will be included in the report. For details of this equivalent circuit I refer you to the original paper "Analysis of Interdigital Surface Wave Transducers by Use of an Equivalent Circuit Model" by W. R. Smith et. al., IEEE Transactions on Microwave

Theory and Techniques, Vol. MTT-17, No. 11, November 1969.

SECTION II

MODELLING OF THE INTERDIGITAL TRANSDUCER

### 1. Mason Equivalent Circuit <sup>(1,11)†</sup>

Consider Figure#4 <sup>(3)</sup> which shows a side view of an interdigital transducer in both the generation and detection mode. From the generation mode it is most clear that in any model representing the interdigital transducer one must use a 3-port representation. Two of the ports will be acoustic, representing waves propagating to the left and to the right of the transducer. A third port will be electrical in nature representing the forcing or response term depending on whether the transducer is in the generation or detection mode. Also, since the fingers of the transducer are composed of metal, then there will exist interelectrode capacity between adjacent fingers.

Since the wave is travelling on a acoustic medium one would naturally introduce an acoustic impedance associated with the material. It is also necessary that the transducer be symmetrical with respect to both the acoustic ports and the electric port.

These considerations led to the development of the "Mason Equivalent Circuit" <sup>(1,11)</sup> model of a section of transducer as shown in Figure#5. This model, also known as the cross-field model has the applied electric field normal to the acoustic propagation vector. Associated with this model are the following quantities

(i) Characteristic impedance  $Z_0 = \rho v A$

(ii) transit angle  $\phi = \pi \omega / \omega_0 = 2\pi L / \lambda$

(iii) resonant frequency  $\omega_0 = \pi v / L$

† The development presented here follows references (1,11).

(iv) static capacity of section  $C_L$

(v) Acoustic to electric transformer ratio  $\phi = Wd/s$  where

$\rho$  = density of piezoelectric material

$A$  = cross-sectional area

$v$  = acoustic surface-wave velocity

$W$  = acoustic beamwidth

$d, s$  = appropriate piezoelectric and compliance constants.

A completely electrical equivalent is produced by noting the following facts. For the acoustic ports we have that

$$\frac{F_i}{\mu_i} = Z_0 \quad (10)$$

Now we want an equivalent electric impedance so we wish  $\frac{e_i}{i_i}$ . If we make the substitutions  $e_i = F_i/\phi$  and  $i_i = \phi\mu_i$  then

$$\frac{e_i}{i_i} = \frac{F_i/\phi}{\phi\mu_i} = \frac{1}{\phi^2} \left( \frac{F_i}{\mu_i} \right) = Z_0/\phi^2 \quad (10')$$

Therefore the complete electrical equivalence consists of changing the characteristic impedance from  $Z_0$  to  $Z_0/\phi^2$ . This electrical equivalence is shown in Figure#6.

The quantity  $Z_0/\phi^2 = R_0$  is related to fundamental constants of the section through  $R_0 = \pi/\omega_0 C_L K^2$  where  $K^2$  is a electromechanical coupling constant for the piezoelectric material used.

In modelling a complete transducer<sup>(1,11)</sup> from this equivalent circuit one interconnects a number of sections numerically equal to the number of fingers in the transducer. The acoustic ports for successive sections are cascaded, while the electrical terminals are connected in

parallel with the polarity of successive transformers chosen to correspond with the relative polarity of corresponding finger pairs. It is clear that complete freedom exists for each section as far as the values of  $W$ ,  $a$  and  $L$  are concerned. Hence each section will have its own characteristic impedance, transit angle, transformer turns ratio and interelectrode capacitance. This being the case, modelling of a complete transducer on this equivalent circuit can become quite complex, and will in general require a computer for the evaluation of the transducer performance.

However, one simple case may be analysed in closed form. This is the case of the  $N$ -finger pair uniform transducer of the kind mentioned in the introduction and shown in Figure#3. For this case the values of  $W$ ,  $a$  and  $L$  are constant from section to section.

The usual starting point of this analysis is the development of the admittance matrix for a single section. <sup>(1,11)</sup> Then using recursion relationships based on the aforementioned manner of section interconnections a complete transducer admittance matrix is developed. The admittance matrix is defined through the relationship

$$[I] = [Y] [V] \quad (11)$$

From the fact that the Mason equivalent circuit is a 3-port, and that there are symmetries in the model we have the expanded expression for the circuit of Figure#6

$$\begin{bmatrix} I_{i'-1} \\ I_{i'} \\ I_i \end{bmatrix} = \begin{bmatrix} Y_{11} & Y_{12} & Y_{13} \\ Y_{12} & Y_{11} & -Y_{13} \\ Y_{13} & -Y_{13} & Y_{33} \end{bmatrix} \begin{bmatrix} e_{i'-1} \\ e_{i'} \\ e_i \end{bmatrix} \quad (11')$$

From the first line expansion we have  $I_{i'-1} = Y_{11} e_{i'-1} + Y_{12} e_{i'} + Y_{13} e_i$ .

To determine  $Y_{11}$  then we have

$$Y_{11} = \left. \frac{I_{i'-1}}{e_{i'-1}} \right|_{e_{i'}, e_i = 0}$$

Considering the circuit model we see that with  $e_i = 0$ ,  $i_i = 0$  and the admittance is  $-jR_0^{-1}(\tan \theta)^{-1} = -jG_0 \cot \theta$ . In a similar manner the other components of  $[Y]$  are filled in, resulting in the expression for the admittance matrix of a single section as

$$\begin{bmatrix} I_{i'-1} \\ I_{i'} \\ I_i \end{bmatrix} = jG_0 \begin{bmatrix} -\cot \theta & \csc \theta & -\tan \theta/2 \\ \csc \theta & -\cot \theta & -\tan \theta/2 \\ -\tan \theta/2 & \tan \theta/2 & 2\tan \theta/2 + \frac{\omega C}{G_0} \end{bmatrix} \begin{bmatrix} e_{i'-1} \\ e_{i'} \\ e_i \end{bmatrix} \quad (1)$$

(11")

where  $G_0 = R_0^{-1}$ . Note that the symmetry of the equivalent circuit is clearly preserved in this matrix. Terms originating from the equivalent acoustic ports contain the total phase angle  $\theta$ . This reflects the fact that if one shorts out the electric port then acoustic waves propagating past the section are unaffected by the port. Similarly, all admittance terms involving electric-acoustic port interactions are symmetrical and the fact that waves are generated equally in both directions from the section.

For a complete transducer one uses the recurrision formulæ

$$\begin{bmatrix} I_{i'-1} \\ I_{i'} \\ I_i \end{bmatrix} = \boxed{Y} \begin{bmatrix} e_{i'-1} \\ e_{i'} \\ e_i \end{bmatrix} \quad (1) \quad (12)$$

which yields the admittance matrix for a complete transducer of  $2N$  sections as

$$\begin{bmatrix} I_{1'} \\ I_{2'} \\ I \end{bmatrix} = jG_0 \begin{bmatrix} -\cot 2N\theta & \csc 2N\theta & -\tan \theta/2 \\ \csc 2N\theta & -\cot 2N\theta & -\tan \theta/2 \\ -\tan \theta/2 & 4N\tan\theta/2 + \omega C_T/G_0 & E \end{bmatrix} \begin{bmatrix} E_{1'} \\ E_{2'} \\ E \end{bmatrix} \quad (13)$$

where

$$C_T = 2NC \text{ and } \theta = 2\pi L/\lambda = \pi\omega/\omega_0 ,$$

where the port terms are as in Figure 7(a). In Figure 7(b) is an equivalent circuit as viewed from the electrical input for the total transducer. The elements of this circuit are

- (i)  $G_T(\omega)$  = acoustic conductance of transducer, and represents the acoustic power generated by the transducer due to electrical excitation.
- (ii)  $B_T(\omega)$  = acoustic susceptance of transducer, and represents the stored energy/cycle in the transducer configuration.

(iii)  $C_T$  = an additive susceptance term due to the interelectrode capacitance of the transducer.

The total admittance for the transducer is then (1,11)

$$Y_T(\omega) = G_T(\omega) + j(B_T + \omega C_T) \quad (14)$$

Using the above admittance matrix, with the acoustic ports terminated in the characteristic impedance  $R_0$  the values of  $G_T(\omega)$  and  $B_T(\omega)$  are respectively

$$G_T(\omega) = 2G_0 \tan^2 \frac{\theta}{2} \sin^2 N\theta \quad (15)$$

$$B_T(\omega) = G_0 \tan \frac{\theta}{2} \left[ 4N + \tan \frac{\theta}{2} \sin 2N\theta \right] \quad (16)$$

For frequencies near the fundamental resonance at  $\omega_0$  then (1,11)

$$G_T(\omega) = 8N^2 G_0 \left( \frac{\sin x}{x} \right)^2 \quad (15')$$

$$B_T(\omega) = 9N^2 G_0 \left( \frac{\sin 2x - 2x}{2x} \right) \quad (16')$$

where  $X = N\pi \left( \frac{\omega - \omega_0}{\omega_0} \right)$ .

Note that since  $\lim_{X \rightarrow 0} \frac{\sin X}{X} = 1$

and that for  $X \ll 1$   $\sin X = X$  then we see that the radiation conductance term is a maximum for  $\omega = \omega_0$  and that the susceptance term is 0 at  $\omega = \omega_0$  and remains small for values of  $\omega$  near  $\omega_0$ . Plots of these functions are

shown in Figure#8. Note that the  $\frac{\sin x}{x}$  response agrees with the result obtained in the introduction based on a simple vector addition approach.

The next model to be considered is the so-called "impulse" approach. This model yields equivalent results for the uniform transducer as does the above circuit. But further, it allows one to determine the expected frequency response of the transducer, when the values of W, a and L vary from section to section, in a much more convenient manner.

## 2. The Impulse Model of Surface Transducers <sup>(1,4)†</sup>

Although the previously mentioned equivalent circuit model provides good understanding to the physical operation of the interdigital transducer, it fails in respect to its ability to yield a clear insight into the frequency response of a transducer. It is only for the simplest case of the uniform transducer that closed form expressions for the response can be obtained. To overcome this, a synthesis approach based on a mathematical relationship known as the Fourier transform was introduced.

In Figure 9(A) <sup>(1)</sup> is shown a surface wave impinging upon a surface-wave transducer. Shown in Figure 9(B) is a functional block diagram of a transversal filter. It is clearly evident that the interdigital transducer satisfies the requirement of 9(B). In the matching procedure we identify the various W's representing adjacent finger overlap as being proportional to the amplitude of the voltage supplied by a given finger pair to the load resistor. The  $\tau$ 's represent the propagation delay of the surface wave from finger pair to finger pair. It is thus evident that the output from the interdigital transducer may be mathematically expressed as

† The development of the model of this section is based on that presented in references (1,4).

$$H(\omega) = \sum_{n=1}^N W_n e^{j\omega x_n/v} \quad (1) \quad (17)$$

where  $x_n$  represents the location of the  $n^{\text{th}}$  finger pair and  $v$  is the surface wave velocity. The form of this equation is exactly the same as that of sampled Fourier transform. This realization immediately leads to a very useful synthesis approach to surface wave filters.

It is known from mathematics that the frequency response and time response of a system form a Fourier transform pair: (12)

$$H(\omega) = \frac{1}{\sqrt{2\pi}} \int_{-\infty}^{+\infty} h(t) e^{-j\omega t} dt \quad (18)$$

$$h(t) = \frac{1}{\sqrt{2\pi}} \int_{-\infty}^{+\infty} H(\omega) e^{j\omega t} dt \quad (19)$$

We also have the "time convolution theorem" which states: (12)

$$\text{If } F[h_1(t)] = H_1(\omega) \text{ and } F[h_2(t)] = H_2(\omega)$$

$$\text{then } F[h_1(t) * h_2(t)] = H_1(\omega) H_2(\omega) \quad (20)$$

where the star represents convolution defined as

$$h(t) = \int_{-\infty}^{+\infty} h_1(\tau) h_2(t-\tau) d\tau \quad (21)$$

These relationships are immediately adaptable to surface-wave filters. From the block diagram of Figure #1 we know that every surface wave device must have associated with it two transducers separated by some distance along the surface of a piezoelectric media. Each transducer has associated

with it a time response. A third response is associated with the dispersionless time delay between transducers. If one of the transducers is made of uniform overlap equal to a greater than the maximum overlap of the second transducer which may have varying finger lengths, then the convolution theorem may be used. Then, the time response of the two transducers will be the convolution of their individual responses

$$h(t) = \int_{-\infty}^{+\infty} h_1(\tau) h_2(t-\tau) d\tau \quad (21')$$

and the frequency response will be given by

$$H(\omega) = H_1(\omega) H_2(\omega) \quad (22)$$

If we consider Figure #10<sup>(1,4)</sup> showing a typical device arrangement then we can write the transfer function  $V_2/V_1$  as

$$\frac{V_2}{V_1} = H_{\text{Tot}}(\omega) = H_1(\omega) e^{-j\omega\tau} H_2(\omega) \quad (1) \quad (23)$$

where  $H_1(\omega)$  = frequency response of transducer #1.

$H_2(\omega)$  = frequency response of transducer #2.

$e^{-j\omega\tau}$  = dispersionless delay between centre of transducers.

Figure #11 shows a device arrangement for which the above transfer function is valid. The transducer on the left has varying finger overlap, a property which defines it as an "apodized transducer". The transducer on the right is of uniform overlap, the value of which is equal to the

maximum overlap of the one on the left. It is important to note that if both transducers are apodized then this simple transfer function is no longer valid. More will be said on this subject later.

In Figure#12 is shown the acoustic field response of such a transducer, based on the approximation shown in Figure#13. In this approximation one assumes that one half of a sine wave may be placed between centres of adjacent fingers. What is important to note is the direct relationship between the geometry of the structure and the generated acoustic response. The fundamental frequency of the wave is given by the centre-to-centre spacing of adjacent fingers. The magnitude is given by the amount of overlap of adjacent fingers. Thus one can accurately control the frequency and magnitude (in the sense of acoustic beamwidth) of the acoustic wave generated at any point of the transducer array by simply varying the geometric parameters. Since acoustic surface waves are dispersionless (velocity of propagation independent of frequency) we can use the simple relationship  $t_n = \lambda_n/v$  to convert from the spatial to temporal specification of the response.

We are now in a position to compare this approach with that given by the Mason equivalent circuit. Referring to Figure#13 which uses the above-mentioned assumption we set up the impulse response for this circuit. The interdigital transducer shown has uniform overlap and variable centre-to-centre spacing of adjacent fingers. The width-to gap ratio is kept constant. To set up the response<sup>(4)</sup> one places one-half cycle of a sine wave between centres of adjacent fingers for which there is a polarity reversal. Then one multiplies the amplitude of each half-cycle by a scaling factor  $f_{inst}^{3/2}$  where  $f_{inst}$  = the instantaneous frequency as

dictated by the centre-to-centre spacing of the finger pair under consideration. Another multiplication factor is also needed to account for the dependence of the radiated acoustic amplitude on the interelectrode capacitance. The appropriate factor is  $4k\sqrt{C}$  where  $k$  is the coupling constant and  $C$  is the capacitance/finger pair. Then, the impulse response is given by

$$h(t) = 4k\sqrt{C} f_{\text{inst}}^{3/2}(t) \sin \omega_i t \quad (4) \quad (24)$$

where

$$\omega_i(t) = 2\pi \int_0^t f_i(\tau) d\tau .$$

Now, if  $f_{\text{inst}}$  is a constant as for the case of constant centre-to spacing of adjacent fingers, and all adjacent fingers are connected to opposite buss bars then the appropriate  $h(t)$  will be

$$h(t) = f_0^{3/2} 4k\sqrt{C} \sin \omega_0 t \quad (25)$$

The Fourier transform  $F [h(t)]$  is now taken, resulting in

$$H(\omega) = 2k\sqrt{C}f_0 N \frac{\sin x}{x} \exp(-j\omega N/2f_0) \quad (4) \quad (26)$$

where  $x = N\pi(\omega - \omega_0)/\omega_0$  as in the case of the Mason equivalent circuit.

Notice again we have the  $\frac{\sin x}{x}$  response and the linear phase shift with frequency as before. We also need to determine the acoustic conductance term  $G_a(\omega)$  and the associated acoustic susceptance  $B_a(\omega)$  as was done for the former equivalent circuit.

In determining  $G_a(\omega)$  we recognize this term represents the electric to acoustic conversion in the interdigital transducer. The energy content  $E$  of a non-periodic function can be defined by the integral equation

$$E = \int_{-\infty}^{+\infty} |h(t)|^2 dt \quad (12) \quad (27)$$

Now, according to Parseval's theorem (12)

$$E = \int_{-\infty}^{+\infty} |h(t)|^2 dt = \int_{-\infty}^{+\infty} |H(\omega)|^2 d\omega \quad (28)$$

This simply states that the energy content in the time domain must equal that in the frequency domain. Now, for the interdigital transducer, if we want the energy delivered per unit frequency we have

$$\begin{aligned} E(\omega) &= \frac{\partial E}{\partial \omega} = \frac{\partial}{\partial \omega} \left[ \int_{-\infty}^{+\infty} |H(\omega)|^2 d\omega \right] \quad (12) \\ &= |H(\omega)|^2 \quad (29) \end{aligned}$$

Since energy is radiated from each direction of the interdigital transducer, then we must multiply by 2

$$\therefore E(\omega) = 2 |H(\omega)|^2 = G_a(\omega)$$

$$\therefore G_a(\omega) = 2 |H(\omega)|^2 \quad (30)$$

Now, we must determine the acoustic susceptance term  $B_a(\omega)$ . To determine this we make use of the causality of the physical system and the following

relationship. If  $H(\omega) = F[\tilde{h}(t)] = R(\omega) + j X(\omega)$  then  $R(\omega)$  and  $X(\omega)$  satisfy the relationships

$$R(\omega) = \frac{1}{\pi} \int_{-\infty}^{+\infty} \frac{X(\omega')}{\omega - \omega'} d\omega' \quad (31)$$

$$X(\omega) = -\frac{1}{\pi} \int_{-\infty}^{+\infty} \frac{R(\omega')}{\omega - \omega'} d\omega' \quad (32)$$

These relationships are known as the Hilbert Transforms. In the case of the interdigital transducer we have  $F[\tilde{h}(t)] = H(\omega) = G_a(\omega) + jB_a(\omega)$ . Therefore we can determine the value of  $B_a(\omega)$  as

$$B_a(\omega) = -\frac{1}{\pi} \int_{-\infty}^{+\infty} \frac{G_a(\omega')}{\omega - \omega'} d\omega' \quad (33)$$

We can use these results in determining the terms  $G_a(\omega)$  and  $B_a(\omega)$  for the N-pair unapodized transducer. We have

$$G_a(\omega) = 2 |H(\omega)|^2 = H(\omega)^* H(\omega) \quad (30')$$

For the case of the transducer in question

$$H(\omega) = 2k\sqrt{Cf_0} N \frac{\sin x}{x} \exp(-j\omega N/2f_0) \quad (34)$$

$$\therefore G_a(\omega) = 4k^2 C^2 f_0^2 N^2 \frac{\sin^2 x}{x^2} = G_0 \frac{\sin^2 x}{x^2} \quad (4) \quad (35)$$

Then

$$B_a(\omega) = -\frac{G_0}{N^2 \pi^3} \int_{-\infty}^{+\infty} \frac{\sin^2 N \left[ \frac{\pi(\omega - \omega_0)}{\omega_0} \right] \omega_0^2}{(\omega - \omega_0)^3} d\omega \quad (36)$$

where  $x = N\pi(\omega - \omega_0)/\omega_0$  was substituted. The evaluation of this integral is quite complex and results obtained are

$$B_a(\omega) = \frac{G_0(\sin 2x - 2x)}{2x^2} \quad (4) \quad (37)$$

These agree completely with the results obtained for the N-finger pair uniform transducer considered in the Mason equivalent circuit case.

If the filter desired has one transducer of the apodized type then the closed form results of the above are no longer valid. For this case we must perform the "strip analysis"<sup>(4)</sup> as indicated in Figure#14. The transducer is divided into narrow strips which have uniform overlap. The function  $h_0(t)$  has the same finger placement (i.e. number of cycles) as does the original transducer, and is of unit width. The function  $W(t)$  describes the envelope of the finger overlap. Then the appropriate expression for the input admittance of the apodized transducer is given by

$$G_a(\omega) = \sum_{i=1}^N \frac{1}{2} \left| \int_{t_1(W_i)}^{t_2(W_i)} h_0(t) \exp(-j\omega t) dt \right|^2 \Delta W_i \quad (4) \quad (38)$$

Examining this expression we note that within the absolute value signs the expression is that of the Fourier transform of the strip  $i$ , with time beginning and end points  $t_1(W_i)$  and  $t_2(W_i)$  as dictated by the overlap envelope. Then, because each strip will generate this amount of acoustic energy one must sum over all strips to arrive at the total expression. This expression is in general time consuming for overlap functions of any complexity. Since  $N$  Fourier transforms are required in the evaluation, this expression becomes costly to determine on computer facilities.

However, there exists approximate expressions <sup>(1,4)</sup> for  $G_a(\omega)$  which allow universal admittance graphs to be developed. In design procedures, these are usually used in determining  $G_a(\omega)$  and  $B_a(\omega)$  for the apodized transducer. More will be said on this subject in the design section of the report.

The last component of input admittance to be determined is the interelectrode capacitance. The appropriate method for this is

(13)

$$C_1 = \frac{C_{1,2}}{2}, \quad C_p|_{p=2 \text{ to } n-1} = \frac{C_{p-1,p} + C_{p,p+1}}{2}, \quad C_m = \frac{C_{n-1,n}}{2} \quad (39)$$

where the C's are given in terms of the acoustic beamwidth and finger width to gap ratio as

$$\frac{C}{W} = (\epsilon_s + 1) \left[ 6.5 \left(\frac{a}{L}\right)^2 + 1.08 \left(\frac{a}{L}\right) + 2.37 \right] \quad (1) \quad (40)$$

where  $\epsilon_s$  is the effective dielectric constant for the chosen sagittal plane.

This concludes the description of the basic models invented to describe the physical nature and frequency behaviour of interdigital transducers. In the next section the design and experimental procedures used by the author in realizing a bandpass filter will be discussed. Limitations of the basic approach and second order effects which must be considered are also included.

SECTION III

BANDPASS FILTER SYNTHESIS

### 1. Design Procedures

In bandpass filter design one is given the required frequency response in terms of magnitude and group delay. That is

$$H(\omega) = R(\omega) + jX(\omega) = |H(\omega)| e^{j\theta(\omega)} \quad (41)$$

where  $|H(\omega)|$  is the magnitude spectrum of  $H(\omega)$  and  $\phi(\omega)$  the phase spectrum. The group delay is related through the relationship

$$t_g = - \frac{\partial \phi(\omega)}{\partial \omega} \quad (42)$$

to the phase spectrum. Since as was discussed earlier, one can accurately control the form of the time response  $h(t)$  of the transducer, then one can use the Fourier transform theorem to determine the form of  $h(t)$  given a  $H(\omega)$

$$h(t) = \frac{1}{\sqrt{2\pi}} \int_{-\infty}^{+\infty} H(\omega) e^{j\omega t} d\omega \quad (42')$$

This then is the basic design approach. One takes the required frequency response, determines the corresponding time response and then designs the geometry of the interdigital transducer according to the following procedure. One evaluates the magnitude  $|H(t)|$  and the imaginary part  $\text{Im } H(t)$ . The fingers for the transducer are then located at those points in time where the relative phasing is  $0^\circ$  or  $180^\circ$  i.e. the imaginary part equals 0. The length of the fingers is determined by the magnitude of the time response for that point in time. The polarity of fingers is

then given by the slope of the imaginary part at those points where it is equal to 0. Figures#(15) and#(16) show the magnitude and imaginary part respectively of the time response obtained from a rectangular bandpass in the frequency domain.

However, usual specifications and practical considerations prevent one from carrying out this exact plan. The frequency specifications are of such a form as to prevent writing them in a closed form analytic expression. Secondly, the limits on the Fourier transform are from  $-\infty$  to  $+\infty$ . This means that the transducer must be of infinite extent. This certainly could never be carried out. Thirdly, it is implicit in the above mentioned design procedure that only certain points in time are used in describing the response. The time response determined through the Fourier transform is non-periodic and continues in time. The transducer can only offer a sampled version of this response. This fact brings into question the effects of sampling rates on the desired response.

The frequency specifications problem requires one to use a numerical method to determine Fourier transform. Up until this last decade the problem was great, even for digital computers. However, a new algorithm, called the Fast Fourier Transform, has now come into existence. It has largely done away with the problem, but not completely. The cost of enacting the algorithm on a computer is still sufficiently high as to be an economic consideration in designing the filter. The question of truncating the limits of the Fourier transform yields ripples in the pass-band response of the filter. These ripples are known as Gibb's phenomena. They are characterized by an amplitude independent of the truncation time. The number of ripples is equal to the number of

sidelobes present in the truncated time response.<sup>(1)</sup> Methods of controlling Gibb's phenomena are contained in methods used to taper the truncation.<sup>(1)</sup> This general method is known as optimizing the response.<sup>(1)</sup>

We are now in a position to consider the specific design procedure for an actual filter. The filter required is one for the intermediate frequency section of an electrohome color television. Figure#18 shows the magnitude and group delay required in the frequency domain. This particular type of response is for a solid state color television. It is known in the trade as the "haystack response". The centre frequency of the filter is 44.25 MHz, with major traps occurring at 41.25 and 47.25 MHz. Thus, the required bandwidth is 6 MHz, and the fractional bandwidth is

$$\frac{6}{44.25} \times 100 = 13.5\%$$

The transition width is defined for this case as the frequency interval from the - 3 db point of the main passband to the highest point on the first out-of-band sidelobe and is for this case slightly assymetrical. On the lower passband end it is 2.25 MHz, and on the upper end it is 2.75 MHz. The maximum magnitude of the first out-of-band sidelobe on the lower frequency end is - 35 db, and on the upper frequency end the maximum value is - 30 db. The group delay is a constant 660 nanoseconds for frequencies above 43.75 MHz and rises along a quadratic curve from the 43.75 MHz point to the 41.25 MHz point to a value of 1.0 microsecond. These summarize the major specifications of the filter.

The first design decision to be made is how to divide the required

response between the input and output transducer. The choices available are (1) two unapodized transducers; (2) two apodized transducers; (3) one apodized transducer and one unapodized. Choice number (1) is immediately eliminated since with this configuration only responses of the form:

$$\left(\frac{\sin x_1}{x_1}\right) \left(\frac{\sin x_2}{x_2}\right) \text{ are realizable.}$$

Choice number (3) on the other hand results in frequency response characteristics of the form

$$H_{\text{TOTAL}}(\omega) = \sum_{s=1}^Q H_{1s}^*(\omega) H_{2s}(\omega) \exp(-jkd) \quad (43)$$

as shown in Figure#18. From this expression it is clear that response is dependent upon two apodization functions each of which must be divided into strips. Then the Fourier transform of each must be evaluated and multiplied together. Finally, all such responses must be added over the total number of strips. This approach is clearly most complex. If we consider choice number (2), then looking in the equation above we see that since for the unapodized transducer all of the strip transforms will be the same, then we can take this response out of the summation sign. Then, if #1 is unapodized

$$H_{\text{TOT}} = H_1(\omega) \sum_{s=1}^Q H_{2s}(\omega) \exp(-jkd) \quad (44)$$

Now, if we examine Figure#14(D) we see that the effective time response for an apodized transducer used in an apodized-unapodized arrangement is

that of a time pulse with amplitude given directly by the finger overlap. This unambiguous time response is exactly what is required for producing reasonable design procedures. The resulting total response then for such a pair is then given by the expression

$$\begin{aligned} H_{\text{TOT}}(\omega) &= F \left[ h_1(t) * h_{2 \text{ eff}}(t) e^{-jkd} \right] \\ &= H_1(\omega) H_{2 \text{ eff}}(\omega) e^{-jkd} \end{aligned} \quad (45)$$

Now, if it can be arranged that  $H_1(\omega)$  is approximately a constant, then

$$H_{\text{TOT}} = \text{CONSTANT} \left[ H_{2 \text{ eff}}(\omega) e^{-jkd} \right] \quad (46)$$

Thus, all of the magnitude response will be placed in the one apodized transducer. This is a clearly desirable situation and is the one chosen. The condition of  $H_1(\omega)$  being a constant can be quite reasonably approximated by choosing the transducer as broadband as possible. From the form of  $G_a(\omega)$  for a uniform transducer we had that the bandwidth was inversely proportional to the length of the transducer. It is shown in literature<sup>(4)</sup> that a uniform transducer of 4 finger pairs built on the Lithium Niobate substrate has a maximum percentage bandwidth of 24%. That is to say that at 12% of  $\omega_0$  on each of  $\omega_0$ , the response will only be down -3 db. Since the % bandwidth required by the T.V. filter is only 13.5%, then the use of the above mentioned type of uniform transducer yields a very good approximation to the constant required for  $H_1(\omega)$ . It will also be shown later that this transducer arrangement allows acoustic and electrical matching

across its total bandwidth.

The next step to be made is in determining the shape of the time response of the apodized transducer necessary to fulfill the requirements in the frequency domain. Since the response is non-standard one must use a computer to simulate responses. Specifically, a Fast Fourier Transform Subroutine is required. This subroutine evaluates the Fourier Transform of a given input function. The input function must be specified in the form

$$H(\omega) = R(\omega) + jX(\omega) \quad (47)$$

so that in the given specification

$$H(\omega) = |H(\omega)| e^{j\phi(\omega)} \quad (48)$$

that  $|H(\omega)| = \sqrt{R^2(\omega) + X^2(\omega)}$  (49)

and  $\phi(\omega) = \tan^{-1} \left[ \frac{X(\omega)}{R(\omega)} \right]$  (50)

In using this programme for use in surface-wave bandpass filters, it is most useful to be aware of the fact that the filter is a member of the non-minimum phase class of filter.<sup>(16)</sup> This allows one to specify independently the magnitude and phase information of the filter. In synthesizing the response from this point the procedure used is as listed below.

- (1) Input into the programme the ideal rectangular bandpass of a filter, supplying the proper bandwidth, and constant group delay, as is shown in Figure#20.

- (2) Perform the inverse transform.
- (3) Truncate the transform.
- (4) Input the phase data as determined by the group delay information.
- (5) Multiply the magnitude of the truncated transform by an appropriate weighting function.
- (6) Determine the Fourier transform of the above manipulated response.
- (7) Determine the frequency response of the output transducer.
- (8) Multiply the frequency response obtained in (6) by (7) to determine the overall frequency response of the transducers.
- (9) Plot the overall frequency response, and the magnitude and imaginary part of the corresponding time response.

As is evident by the procedure outline the designer is faced with the use of an iterative procedure in determining the required time response for the frequency domain specifications. Listed in appendix #2 is a copy of the programme which performs the above procedure. The Fast Fourier Transform Subroutine used is listed as HARM. It is available in the SSPLIB library of subroutines. The use is quite straightforward, and only two points need be clarified. The first concerns the use of the weighting function in optimizing the response. The second deals with the particular method used in this programme for arriving at the phase information from the group delay specifications. These two points will now be dealt with.

#### Optimization through Weighting functions (1,14)

It was mentioned at the beginning of this section that since the limits of the Fourier transform are infinity, truncation of the time

response was necessary. This truncation in turn creates the Gibb's phenomena manifesting itself in out-of-band sidelobes and in-band ripples, when the Fourier transform to the frequency domain is taken. The comparison between the interdigital transducer and the transversal filter lead people to realize that one could look upon the transducer as having frequency properties quite similar to those of the "end-fire array" found in antenna theory<sup>(14)</sup> Men in this field had determined weighting functions which if multiplied by some function describing the basic element layout in an antenna, could result in considerable improvement in the obtained frequency response. Basically, the functions altered the manner in which one tapered off the elements in the array. It was found that by proper manipulation one could completely remove the inband ripples associated with the Gibb's phenomena. These weighting functions were used in the programme to try to optimize the response. The particular weighting function used is the Kaiser Function<sup>(14)</sup> defined by the equation

$$\begin{aligned}
 W(t) &= I_0 \omega_a \tau (1 - t^2/\tau^2)^{1/2} & |t| < \tau \\
 W(t) &= 0 & |t| > \tau
 \end{aligned}
 \tag{51}$$

for a time impulse of total length  $2\tau$ .  $I_0$  is the modified Bessel function of the first kind. Figure#20 and Table#1 refer to this function. The figure gives the shape of  $W(t)$  for the variable parameter  $\omega_a \tau = 6$ . Table# 1 gives the transition width and ripple for frequency response as a function of  $\omega_a \tau$ . The table indicates the decrease of both sideband level and in-band ripple. One other major affect of the function is to increase the

transition width of the response for a given  $\tau$  over that of the response obtained by direct truncation. In using this function, the first decision to be made is in the length  $\tau$ . An approximation to the minimum length was determined computationally by taking the Fourier transform of a square pulse. The bandwidth associated with this pulse was 13.5% as required by specifications. The resultant  $(\sin x/x)$  time response was then truncated at various zeros. Figures #21) and #22) show the resultant for truncations after the fifth zero and second zero respectively. From #22) we see the rounding out of the response and the approximate bandwidth necessary. As a result of this, the corresponding time interval was chosen as a starting point. For a centre frequency of 44.25 MHz the value of  $\tau$  is to be .3616 ysec. Now, the transition width required was  $\sim 2.50$  MHz, so the resultant  $TW \times \tau$  product became 1.08. Using table #1, the corresponding peak to peak ripple at band edge is given as  $\sim 0.21$  db and the peak out-of-band sidelobe as -37 db. The corresponding  $\omega_a \tau$  parameter is 3. Computer tests ran at  $\omega_a \tau = 3$  proved to give too wide of a transition width. Thus, the parameter  $\omega_a \tau$  was increased to 4. This proved to be a good value in that the required traps fell at the right frequencies, and the appropriate haystack response obtained. In the programme listed in this report the argument of the function  $I_0$  is found on the line following the "DO 37" statement of the main programme. The actual weighting is placed in using the subroutine  $I_0$ . This programme was developed from expansion formulae given for the modified Bessel function of the 0<sup>th</sup> order in the Handbook of Mathematical Functions page 378, edited by Milton Abramowitz and Irene Stegun. In implementing it on the computer one simply realizes that since

the data is in the form of real and imaginary data arrays being adjacent to each other (i.e. A(1), A(2) in the array A(512) of the programme corresponds to the first real and imaginary pair at  $t=0$ ), then the procedure to be taken is as follows

$$\text{Weighted response} = W(t) [A_{\text{real}}(t) + j A_{\text{imag}}(t)] \quad (52)$$

$= W(t) A_{\text{real}}(t) + jW(t) A_{\text{imag}}(t)$ . The magnitude of this is simply  $[W^2(t) A_{\text{real}}^2(t) + W^2(t) A_{\text{imag}}^2(t)]^{1/2} = W(t) [A_{\text{real}}^2 + A_{\text{imag}}^2]^{1/2} = \text{magnitude of weighting function multiplied by the magnitude of the Fourier transform.}$

The next step to be made in determining the time response is to include the effects of the non-uniform group delay in the passband. The procedure here follows directly from the definition of the group delay.

$$\tau_g = - \frac{\partial \phi(\omega)}{\partial \omega} \quad (53)$$

Our starting point is to consider a transmission system of properties

$$H(\omega) = A \text{ and } \phi(\omega) = g\omega \quad (54)$$

Then  $\tau_g = - \frac{\partial \phi(\omega)}{\partial \omega} = -g$ . Such a system is shown graphically in Figure#23. Those characteristics represent the ideal for a bandpass filter. The gain is constant across the passband, as is the group delay. This type of system represents a distortionless transmission system. If we wished to reconstruct the phase characteristics from the group delay we could choose the point of view that this system does not destroy the relative

phase relationships of the frequency components of the signal (i.e. a constant group delay over frequency simply relates that no dispersion is created by the system). Then if a transducer is non-dispersive, then an impulse applied to its input will result in signals in its passband to be transmitted with their original phase relationships left unchanged.

Now, if we have non-linear group delay we will interpret this as stating that the relative phases in the frequency of the passband will be changed according to the group delay characteristics. In non-linear phase devices one chooses a reference group delay and frequency and sets the resultant product equal to  $0_{\text{rads}}$ . Thus, one may arbitrarily choose the phase at the lowest frequency in the passband as being  $0^{\circ}$ . It is usual in electronic circuits to find that the group delay is usually constant for the large percentage of the frequencies in the passband. This value of group delay is then chosen as  $tg_{\text{ref}}$ . For the filter considered here this value is 660 nanoseconds. Then one constructs on the graph the linear phase shift line given by  $\phi = tg_{\text{ref}} \omega$  subject to the restriction that  $\phi = 0_{\text{rads}}$  at the lowest frequency in the passband. Then one determines the actual phase response given by the  $tg$  versus  $\omega$  graph. Since by definition

$tg = - \frac{\partial \phi(\omega)}{\partial \omega}$  then we know that

$$\phi(\omega) = - \int tg(\omega) d\omega \quad (55)$$

If there is no analytic functional form for  $tg(\omega)$ , (as is the case here) then one can proceed as follows. The passband is divided into a number of sub-divisions, depending on the complexity of the non-linear group delay. Then, each section is written in the functional form

$$\text{tg}(\omega) = A + B\omega + C\omega^2 + D\omega^3 + \dots \quad (56)$$

One chooses the point of truncation as desired by accuracy requirements. Then, a number of points in the subinterval equal to the number of desired coefficients are read from the graph. This procedure is carried out for each interval in the passband. The coefficients for each section are determined by use of a computer subroutine set up to solve simultaneous linear equations. Once the coefficients for each interval is determined, then one has an analytic form for  $\text{tg}(\omega)$ . This form is directly integrated. Then, in the computer programme for evaluating the time response, the phase difference between the linear value and non-linear value for a given frequency is inputted. That is

$$\phi = \int (\text{tg}(\omega) - \text{tg}_{\text{ref}}) d\omega \quad (57)$$

in the programme. In the programme, the original input data forced the linear phase characteristics. After the initial transform was carried out and the desired time truncation was performed, a second transform was done. This carried the information back into the frequency domain. Truncation does not affect the original phase. At this point the subroutine is called upon to introduce the required phase response. Then, another transform back into the time domain is carried out and manipulations based upon the weighting function  $W(t)$  as mentioned previously is carried out to determine the resultant frequency spectrum. This is then multiplied by the Fourier transform of the output transducers time domain specification to provide the overall response. The output transducers specifications is related to the programme by the subroutine OUTTRANS.

One point on the use of PHASE1 is to be mentioned. Since the major subroutine HARM requires the input information is real and imaginary strings, it is necessary, upon determining the phase angle from the group delay to connect the information into this form.

Since  $\tan \theta(\omega) = X(\omega)/R(\omega)$  then

$$X(\omega) = R(\omega) \tan \phi(\omega) \quad (58)$$

The  $R(\omega)$  used are the ones obtained from the first transform back from the time domain to the frequency domain after the truncation is performed. Figures #24 and #25 represent computer simulations using this programme. Figure #24 shows the results for a long impulse response and small tapering by the weighting function. Figure #25 which closely approximates the required response results from a stronger taper ( $\omega_a \tau = 4.0$ ) on a  $\sin x/x$  time response truncated after the second zero.

The next step is the determination of the admittances associated with the transducers. As outlined in section on modelling the surface wave transducer using the impulse response, <sup>(1,4)</sup> the determination for  $G_a(\omega)$  and  $B_a(\omega)$  for apodized transducers is in general quite complex. Due to the large number of Fourier Transforms required to determine it accurately, the cost on a computer becomes significant. However, alternate expressions which are simple to calculate have been derived by workers in the field. <sup>(1.4)</sup> Although they are not as accurate as the strip analysis would yield, they provide values which are correct to within  $\pm 10\%$ . These expressions are derived from the general method described earlier for determining the impulse response from the geometry. The impulse response stated was

$$h(t) = f_0^{3/2} 4k \sqrt{C} \sin \omega_0 t \quad \text{中} \quad (25)$$

From Parsavalls theorem

$$\int_{-\infty}^{+\infty} |h(t)|^2 dt = \int_{-\infty}^{+\infty} |H(\omega)|^2 d\omega \quad (28)$$

$$\therefore \int_{-\infty}^{+\infty} |H(\omega)|^2 = \frac{(4k\sqrt{C} f_0^{3/2})^2}{2} \tau_{\text{impulse}} \quad (59)$$

where  $\tau_{\text{impulse}}$  is the total length of the time response and determined by the Fourier transform of the required frequency response. Then, since the frequency domain also has finite limits we may say that

$$\int_{-\infty}^{+\infty} |H(\omega)|^2 d\omega = |H(\omega_0)|^2 2\Delta f \quad (60)$$

if the frequency response is the ideal rectangular response of a bandpass filter. This results since for this case  $|H(\omega_0)|$  is a constant across the bandwidth. Then, combining this with the above yields

$$G_a(\omega_0) = \frac{8f_0^3 k^2 C \tau_{\text{impulse}}}{\Delta f} \quad (4) \quad (61)$$

$$\text{since } G_a(\omega) = 2|H(\omega)|^2$$

Note, that strictly speaking this result is true only for rectangular bandpasses. However, many required bandpass filters are of this nature to a very good approximation. The quantity  $\Delta f$  is the bandwidth of the filter.

中 Determination of  $B_a(\omega), G_a(\omega)$  follows that of reference (4).

The corresponding value of  $B_a(\omega)$  is given in the literature as

$$B(\omega) \equiv 2\pi f \left(\frac{f_0}{\Delta f}\right) C \quad (4) \quad (62)$$

The ratio of  $B(\omega)/G(\omega)$  is the electrical  $Q$  of the device

$$\therefore B_a(\omega)/G_a(\omega) = \frac{\pi}{4k^2} \frac{\Delta f}{f_0} \quad (4) \quad (63)$$

But  $\frac{\Delta f}{f_0}$  is recognized as the fractional bandwidth of the filter. From this result one sees that if one knows the input admittance on a particular substrate, for a particular bandwidth then one can scale the result by the beamwidth used. Also, since the results of the above calculations of  $G_a(\omega)$  did not depend on the function  $H(\omega)$  being dispersionless, then the dispersive filters input admittance can also be determined by multiplication by the time-bandwidth product ( $\tau_{\text{impulse}} \Delta f$ ) of the non-dispersive filter (non-dispersive filters  $\tau_{\text{impulse}} \Delta f = 1.0$ ). Thus, universal admittance curves have been developed. The curves for two substrates, ST QUARTZ and YZ LITHIUM NIOBATE are indicated in Figure#26<sup>(1)</sup> for an assumed beamwidth of  $100\lambda_0$  where  $\lambda_0$  is the wavelength of the centre frequency of the filter. These curves were used to determine the approximate admittances for my filters.

One must next determine the substrate choice. At the moment, this choice is usually restricted to either ST QUARTZ or  $\text{LiNbO}_3$ . Parameters which must be considered are 1) velocity of propagation 2) beam-spreading and beam-steering effects 3) temperature coefficients 4) coupling constant. Lithium Niobate has a surface-wave velocity of 3.488 kilometers/sec. For

a filter of centre frequency  $\sim 44\text{MHz}$ , this means centre-to-centre finger spacings of  $\sim 40$  microns. This value is a very reasonable size to reproduce using conventional photo-lithographic techniques. Lithium Niobate has a high coupling constant ( $k^2 = 4.5\%$ ) yielding extremely good electric-to acoustic conversion. Also, since the Y cut-Z propagating  $\text{LiNbO}_3$  represents a puremode, it is auto-collimating. Thus beamspreading problems should be reduced to a minimum and controllable by assuring high purity at the growth level. The one draw-back of  $\text{LiNbO}_3$  is its temperature coefficient, which is amongst the highest of the possible substrate choices. It's value is  $-90 \text{ ppm}/^\circ\text{C}$  where the temperature coefficient is related through the expression

$$\frac{1}{\tau} \frac{\partial \tau}{\partial T} = \frac{1}{\ell} - \frac{\partial \ell}{\partial T} - \frac{1}{v} \frac{\partial v}{\partial T} \quad (1) \quad (64)$$

where  $\tau = \frac{1}{v}$ ;  $v$  = velocity of acoustic wave,  $\ell$  = distance between two points on surface and  $T$  is temperature. The term  $\partial \ell / \partial T$  is the thermal expansion coefficient, and  $\partial v / \partial T$  is the temperature component of velocity. Another important consideration to be included in choosing the substrate is the fractional bandwidth achievable. Since in the filter considered here the criterion was that the output transducer be as broadband as possible, then one must choose a substrate capable of supporting large fractional bandwidths. It was stated earlier that the fractional bandwidth was related through the expression

$$\frac{\Delta f}{f_0} \leq \sqrt{\frac{4k^2}{\pi}} \quad (1) \quad (65)$$

For Lithium Niobate this means that fractional bandwidths of up to 24% are possible. Since  $f_0/\Delta f$  = Number of finger pairs for this fractional bandwidth = 4, then one would use four finger pairs in an output transducer for this bandwidth. Also, it is important to note that for bandwidths up to this limit it is possible to match the transducer across its entire bandwidth. Other subsidiary considerations to be considered in connection with the substrate are fractional surface velocity changes associated with placing a thin metallic film on the free surface (caused by a shorting of the piezoelectric effect), and wave attenuation on the surface. The velocity change caused by shorting the piezoelectric effect is given by

$$K^2 = -2\Delta v/v \quad (1) \quad (66)$$

and for  $\text{LiNbO}_3$  is .0241. In surface wave transducers, it is this effect which is mainly responsible for phase error problems. The attenuation on  $\text{LiNbO}_3$  is given empirically as

$$\text{ATTENUATION} = 0.88 f^{1.9} + 0.19f \quad \text{dB}/\mu \text{ sec} \quad (1) \quad (67)$$

This effect would be most important for filters requiring a long delay between input and output signals. Lithium Niobate provides the least attenuation of any of the currently available substrates. For frequencies in the 40 MHz range, losses are completely negligible. These considerations clearly demonstrate the superiority of  $\text{LiNbO}_3$  for surface wave devices.

Two more design considerations are necessary to be made. They are 1) determination of insertion loss and 2) triple-transit effects.

Consideration 1) involves inherent losses due to the bidirectionality

of the surface-wave transducer, losses due to impedance mismatch between the characteristic impedances of the transducers and the source and load impedances, and losses associated with the finite resistances of the fingers of the transducers. Triple transit effects are caused by the above mentioned mismatches. The mismatches cause reflected waves to be produced, which bounce back and forth between input and output transducers. Again, we see the strong analogy between the interdigital transducer and the transmission line.

In Figure#(7) an equivalent circuit for a complete transducer was given. Consider an acoustic wave incident upon the transducer from the left. The power reflected from one input port and the power delivered to the other two ports is expressed by the power scattering matrix with coefficients

$$p_{ij} = \frac{p_i}{p_{\text{AVAIL } j}} \quad (1) \quad (68)$$

where  $p_i$  is the power transmitted or reflected from port  $i$  and  $p_{\text{AVAIL } j}$  is the power available from a matched generator at port  $j$ . For the case of the uniform transducer if the electrical port is loaded by an admittance  $Y_L = G_L - j\omega_0 C_T$  (i.e. cancels the interelectrode capacitance effect  $\omega_0 C_T$ ) then

$$p_{11} = \frac{1}{(1+b)^2} \quad (1) \quad p_{12} = \frac{b^2}{(1+b)^2} \quad (1) \quad p_{13} = \frac{2b}{(1+b)^2} \quad (1)$$

where  $b \equiv G_L / 8N^2 G_0$ . Maximum acoustic to electrical power occurs for

$$G_L = 8N^2 G_0$$

Then  $b = 1$  and

$$P_{11} = \frac{1}{4}, \quad P_{12} = \frac{1}{4}, \quad P_{13} = \frac{1}{2}$$

Then one sees that since  $p_{13}$  is the fraction of available power at port 1 delivered to port 3, then one half of the acoustic power is converted into electrical power. Also,  $\frac{1}{4}$  of the power is reflected from port 1, and  $\frac{1}{4}$  is radiated to port 2.

If  $G_L = \infty$  then  $p_{12} = 1$  and  $p_{13} = 0$ . This reflects the physical fact that if the electrical port is shorted then all acoustic power at port 1 is transmitted to port 2 without loss. Note that this is assured in the Mason equivalent circuit by the use of a transformer to couple the electrical power to the transducer. Also, if we set  $G_L = 0$  then  $p_{11} = 1$  and all of the power is reflected.

Another consideration is the effect of electrical loading on the input transducer. The transfer function given for a complete transducer pair configuration was

$$\frac{V_2}{V_1} = H_1(\omega)H_2(\omega)\exp(-j\omega T) \quad (23)$$

This is strictly true only for the case of 0 source resistance from the generator. Since all generators will have a finite source resistance, then the voltage applied to the input transducer will not equal the source voltage. The effects of this electrical loading can be determined by solving for the actual voltage appearing on the transducer terminals,

determining the ratio  $\frac{V_{\text{input terminal}}}{V_{\text{source}}} = \alpha(\omega)$  and then writing the new transfer function as

$$\frac{V_2}{V_s} = \alpha(\omega) H_1(\omega) H_2(\omega) \exp(-j\omega\tau) \quad (69)$$

The effects can be evaluated by considering the circuit of Figure#27. (4)

In this circuit an inductor is placed in parallel with the static capacitance and a source resistance of  $R_s$  is included. The value of the inductor is chosen to resonate with  $C_T$  and  $B_a(\omega_0)$  at the centre frequency of the filter. At that frequency then the admittance presented by this combination will be 0. Then by node analysis at node 1 the actual transfer function for the input transducer is

$$\frac{V_1(\omega)}{V_s(\omega)} \cdot H_1(\omega) = \frac{G_s H_1(\omega)}{G_s + \frac{1}{j\omega L} + j\omega C_T + jB_a(\omega) + G_a(\omega)} \quad (70)$$

where  $G_s = R_s^{-1}$ . At the centre frequency  $\omega_0$  this expression reduces to

$$\frac{V_1(\omega_0)}{V_s(\omega_0)} \cdot H_1(\omega_0) = \frac{G_s H_1(\omega_0)}{G_s + G_a(\omega_0)} = \frac{H_1(\omega_0)}{1 + \frac{G_a(\omega_0)}{G_s}} \quad (71)$$

If  $G_a(\omega_0) = G_s$  then  $\frac{V_1(\omega_0)}{V_s(\omega_0)} = \frac{1}{2}$  and only half of the generator voltage is delivered to the input transducer. At off-centre frequencies neither  $\frac{1}{j\omega L}$ ,  $j\omega C_T$  nor  $jB_a(\omega)$  will disappear. The response of the parallel capacitor-inductor- $B_a(\omega)$  will cause rounding of the filter bandpass as well as introducing a phase-distortion term. The term  $B_a(\omega)$  will introduce additional phase error. However, the most important effect is the

degradation of the sidelobe level. If the parallel L-C-B<sub>a</sub> combination is of low Q value, then we can set

$$j\left(\frac{1}{\omega L} + j\omega C_T + B_a(\omega)\right) \approx 0 \quad (72)$$

As indicated above at  $\omega_0$ , if  $G_a(\omega_0) = G_s$  the device will be matched. However, due to the required frequency characteristics of  $G_a(\omega)$ , at the sidelobe levels  $G_a(\omega_{\text{sidelobes}}) \ll G_s$  and the resultant transfer function will be twice as great as would be expected. This means an increase of 6 db in the resultant sidelobe levels. Since one must also consider the effect of the output transducer, it is seen that as much as a 12 db degradation of sidelobe level from the expected may occur. It is encouraging to note though, that significant strides being made in integrated-circuit technology may make the electrical matching problem virtually non-existent. Specifically, high-frequency-high gain operational amplifiers are appearing which offer very low ( $\ll 1$  ohm) output impedance. Their incorporation as source to transducer couplers should allow the calculated transfer functions based directly on the transducer design to be quite accurately realized.

The power output to the power input at a given frequency is referred to as the insertion loss at that frequency. Insertion loss are caused principally by 1) bidirectionality loss and 2) electrical mismatch loss. The later effect was described above. Bidirectionality loss is an inherent result of the nature of the surface wave device. Since power is generated in both directions from the transducer, then the input transducer must introduce a 3 db loss. Since the maximum power convertible to electric power from a perfectly matched output transducer is  $\frac{1}{2}$ , then this also

introduces a 3 db loss. Therefore the minimum insertion loss is 6 db. Losses due to electrical mismatch can have an even more pronounced effect as explained earlier. Often, transducers are intentionally mismatched. Reasons for this are 1) to lower the electrical  $Q$  of the input to eliminate bandwidth restrictions and 2) to reduce the scattering coefficient  $p_{11}$  which represents the reflected power from a transducer. It is the parameter  $p_{11}$  which represents the seriousness of the triple-transit phenomena.

One can view the triple transit phenomena in terms of the regenerated acoustic waves caused by the voltage induced upon the fingers by the incoming wave. If the receiving transducer is mismatched by placing an admittance  $Y_L \gg 8N^2G_0$  then the effect will be to reduce the voltage across a given set of finger pairs, and thus reduce the reflections. However, this also increases the insertion loss as described above. Thus, one must determine how much insertion loss and triple transit is allowable and make a suitable design compromise.

The last major effect to be considered in design is that associated with the acoustic reflections at electrode edges. In describing substrate properties it was pointed out that velocity changes occur when the surface of a piezoelectric is shorted out by placing a metallic film on it. The plating also causes mechanical loading of the surface which changes the velocity of the surface waves. Mechanical loading can be minimized by using as thin a plating as possible for the fingers. The thickness is restricted by the fact that decreasing the plating thickness increases the resistance of the fingers. In Figure#28<sup>(1)</sup> is a plot of transducer efficiency versus beamwidth. The efficiency quoted here is defined by

$$\text{Efficiency} = \frac{\text{ACOUSTIC POWER RADIATED}}{\text{ELECTRIC POWER INPUT}}$$

It is noted that the efficiency decreases for decreasing metallization thickness (i.e. larger  $\rho$ ) and for larger beamwidths. This result can be expected since in fact adjacent fingers actually act like a distributed RC line. The acoustic impedance mismatch is more pronounced than the finger resistance problem in Lithium Niobate. This is so because of the high coupling constant. The characteristic impedance was given for the Mason equivalent circuit as

$$R_0 = \pi/\omega_0 C_L K^2 = L/VC_L K^2$$

For a change in velocity  $\Delta V$  then

$$R_0' = L/(V+\Delta V)C_L K^2$$

$$\therefore \frac{R_0'}{R_0} = \frac{VC_L K^2}{VC_L K^2 + \Delta VC_L K^2} = \frac{1}{1 + \Delta V/V}$$

But, we know that  $\Delta V/V = K^2/2$

$$\therefore \frac{R_0'}{R_0} = \frac{1}{1 + K^2/2} \quad (1) \quad (73)$$

Therefore we clearly see that high-coupling substrates will have large finger edge reflections. For Lithium Niobate this effect can be quite strong. Finger edge reflection usually manifests itself as a shift in the centre frequency of the filter. This can be clearly seen since instead of a constant velocity of propagation along the surface, one should really consider an average surface velocity. Since  $V = \lambda f$ , then  $f = \frac{V}{\lambda}$

and since  $V$  decreases on average then the shift should be towards a lower centre frequency. The effect of these reflections is illustrated in Figure#29.<sup>(1)</sup> One solution<sup>(1)</sup> to the problem of edge reflections is the use of the split finger transducer as illustrated in Figure#30. Note in Figure#29, the sum at leftmost edge of the first finger is

$$\text{SUM} = R+R+R+R+R = 5R \quad (74)$$

In the case of the split geometry the sum is

$$\text{SUM} = R-jR-R+jR = 0 \quad (75)$$

thus demonstrating the benefits of the split-finger geometry. Another point to be considered in connection with the varying characteristic impedance along the surface is the average metallization. This factor comes into play when one deals with apodized transducers. In this case, the beamwidth of the acoustic radiation is a function of position on the substrate. This results in waves generated from small beamwidth areas to encounter more metallization(i.e. crossing more fingers) than large beamwidth areas. In the large beamwidth areas the main effect of the non-uniform metallization would be to cause wave-front distortion as the part of the beam generated nearer the buss-bars would see less metalization than sections along the central axis of the transducer. Thus, the outer sections of the wavefront would be delayed less in travelling along the surface, causing the wavefront distortion. The usual solution to the problem is the use of dummy fingers as illustrated in Figure#31.<sup>(1)</sup> This arrangement allows for uniform metallization.

A last point to be mentioned concerns harmonic operation. As was mentioned in the impulse model, one assumes a half-sine wave to be generated

between centres of adjacent fingers of opposite polarity. One can then see that the harmonic operation of the transducer will depend on the ratio of finger width-to-gap. This is the  $a/L$  ratio. For an  $a/L$  ratio of 0.5, the finger pairs will resonate at  $f_0$ ,  $5 f_0$ ,  $9 f_0$ , etc. Figure#(32)<sup>(1)</sup> shows the amplitude of the fundamental, 3rd and fifth harmonic as a function of the ratio  $a/L$ . Note for  $a/L = 0.5$ , no third harmonic is generated and the fifth harmonic amplitude is  $\sim \frac{1}{4}$  of the fundamental. For this reason, in design one usually uses an  $a/L$  ratio of 0.5.

This concludes the necessary design steps and information necessary to design a given filter. Below is a summary of the necessary design steps, listed in an orderly manner to achieve reliable results.

#### SUMMARY OF DESIGN PROCEDURES

- 1) Choose the method of division of the required response between the input and output transducer.
- 2) Determine the minimum required impulse length for each transducer. This can be done either analytically or by computer depending upon the complexities of the required response.
- 3) Determine the required finger placements for the transducers. This is done through the iterative procedure using the required phase response, and attempts at tapering the truncation through the optimization function.
- 4) Choose a substrate based on surface wave velocity, temperature coefficient, coupling coefficient, etc.
- 5) Determine the approximate input and output admittances of the transducers. This information is used to determine the matching circuits

for the input transducer and load for the output transducer.

- 6) Evaluate the effects of the various second order characteristics.

The two important considerations are triple-transit and electrode-edge distortions. These will indicate the need for either split fingers, dummy fingers or both.

### Experimental Procedures

As a first attempt at building surface-wave filters, it was decided to try and reproduce the responses observed in Figures #21 and #22. The responses are those of simple truncation of the ideal time response for the rectangular bandpass filter. The expected phase is linear. Figure #21 is for symmetrical truncation of the time response after the 5th zero. In Figure #22 the truncation is after the second zero. The out-of-band sidelobes and Gibb's phenomena is clearly evident. In both cases the bandwidth expected is 5 MHz, with the traps falling at 41.75 and 46.75 respectively. The curves indicate a high degree of rejection at the trap positions. In #22 the traps are approximately 60 db down from the 3 db points. In Figure 21, the traps are down  $\sim$  50 db from the 3 db point.

The procedure to be followed in fabricating a surface-wave filter for an expected response is as follows.

#### A. Development of Mask on Rubylith

- 1) From the computed time response plot the magnitude and imaginary part. This information is used to determine the finger spacings and magnitude of the overlap of adjacent fingers as discussed earlier.
- 2) Determine the beamwidth of the transducers. Frequency and substrate size restrictions will play a role in this determination.

- 3) Choose the substrate to be used.
- 4) Calculate the approximate input admittances  $B_a(\omega)$  and  $G_a(\omega)$ . This information will be used in determining the matching circuits for the input and output transducers.
- 5) From knowledge of the surface-wave velocity and centre frequency of the filter compute the wavelength of the acoustic disturbance.  
Choose either full or split fingers based on expected edge-distortion effects.
- 6) From desired values of group delay determine the centre-to-centre spacings of transducers.
- 7) Determine a magnification factor desired for the mask. From this information, the centre-to-centre spacing of adjacent fingers, and desired beamwidth one can then determine the necessary geometry for the mask. This is done by multiplying the normalized response computed in step #1 by the values determined above. Also, at this stage one can compute the interelectrode capacitance of the transducers.
- 8) Choose the size of the buss bars to be placed on the transducers. Draft appropriate drawings as a guide.
- 9) Using Rubylith sheeting and an appropriate cutting table reproduce the magnified model of the required filter geometry.

#### B. The Photo-reduction

- 1) The Rubylith mask is placed on the screen of the reduction camera. The mask is illuminated from behind. The camera is set up to the required reduction necessary to produce an image, on a high resolution plate, of the mask. The image on the plate is the actual size

the device will be. The plate is then exposed, developed and washed. It is carefully dried and stored in a dust-free atmosphere.

#### C. Substrate Preparation

- 1) Clean the surface of all organic contaminants. This is accomplished using an acetone bath in an ultrasonic cleaner, followed by a acetone vapour cleaning and drying process.
- 2) Determine the metal to be used for production of the fingers. This metal must be of very high purity (99.9% or better). The metal must also be cleaned to make it free of organic substances. The method used in step #1 above is usually sufficient for the metal also.
- 3) Place the substrate and metal in a vacuum evaporator unit. Evaporate the metal onto the substrate, carefully controlling the film thickness to its desired value.
- 4) Remove the substrate with its metal film and place it in an annealing oven to assure bonding of the metal to the substrate.

#### D. Photolithographic Reproduction

- 1) Using a positive-working photo-resist such as Shipleys AZ-1350B, place a small drop on the centre of the substrate.
- 2) Immediately spin the substrate. The initial speed is the key factor. The resist thickness should be uniform across the substrate and approximately  $3000\text{\AA}$ .
- 3) Prebake the resist in an oven at  $76^{\circ}\text{C}$  for  $\sim 15$  minutes. Remove and let cool for  $\sim 5$  minutes.
- 4) Place the photographic image of the mask face down on the substrate. The mask must be carefully oriented on the substrate, according to the propagation direction on the chosen substrate.

- 5) Expose the mask and substrate to an intense white light source directly above the substrate. The time is  $\sim 30$  seconds.
- 6) Develop the resulting photo resist image of the mask which is on the metal. Use a weak ( $\sim 0.5\%$  KCL solution) or Shipleys Positive-Working Photo-resist developer.
- 7) Wash the substrate in distilled water and dry using a refrigerant (i.e. Freon spray).
- 8) Post-bake the substrate for  $\sim 10$  minutes. Let cool for  $\sim 2 - 5$  minutes.
- 9) Place the substrate in a slightly temperature elevated acid solution to etch the exposed metal away. This process requires approximately 10 minutes and should be accompanied by a continual steady agitation of the acid solution.
- 10) Remove the substrate, now free of all metal except for the required circuit, from the acid. Wash carefully using distilled water. Spray acetone on the substrate to remove the photo-resist covering the fingers and buss bars. Wash a second time and dry with Freon Spray. At this point the circuit is prepared, but wires are still to be attached.
- 11) Attach wires using an ultrasonic bonder, or hydrogen bonder equipped with a pre-heater stage.

D. Package Development

- 1) Design a substrate holder to accommodate the filter. Attach the necessary coupling jacks to the holder as dictated by the test device to be used.

The foregoing describes the basic procedure to be followed in realizing the filter. In the next section specific information pertaining to the filters developed here will be given.

#### Specific Filter Geometry - Mask Dimensions

Filter #1 was nominally designed for a centre frequency of 44.25 MHz and a transition width of 5 MHz. It represented direct truncation after the 5th zero of a  $\sin x/x$  type of time response. The delay between centres of input and output transducers was set at 1.0  $\mu$ sec. The output was made as broadband as possible for a Lithium Niobate substrate (24% bandwidth using 4 finger pairs). This information sets the longitudinal extent of the filter.

From the velocity of surface waves on Lithium Niobate ( $V = 1.373 \times 10^5$  inches/second), then for  $V = \lambda_0 f_0$  and  $f_0 = 44.25 \times 10^6$ , the wavelength is given as  $\lambda_0 = .0031028$ ". The finger width for an  $a/L$  ratio of 0.5 is then  $.0007757$ ". In the input transducer array there are 80 finger pairs with  $\lambda_0/2 = .0015514$ " between centres of adjacent fingers. Thus, the length of the input transducer is  $.2490318$ ". The output transducer has four finger pairs. Thus its length is  $.005815$ ". The 1.0  $\mu$ sec time delay gives a centre-to-centre spacing of  $.13733$ ". Beamwidths are usually dictated by the tendency of beamspreading. However, on Lithium Niobate this effect is quite small and for a 1.0  $\mu$ sec delay negligible. The beamwidth was thus set by convenience of mask production. The beamwidth was chosen as  $50\lambda_0 = .15514$ ". The magnification factor of the mask was made large. Its value was set at 100x. Buss bar connections were then added. Figure #33 shows the dimensional outline for the transducer array for a

100x magnification factor. These sizes are specifically for a  $\lambda_0/4$  of .00078". This slight change is necessary to allow accurate cutting on the table which can cut lines to the nearest .001" (table used Haag-Streit, Bern Swiss Made Model 733 ). The corresponding centre frequency then becomes 44.014 MHz. Figures#34 and#35 show the Rubylith masks at a magnification factor of 5. A mask co-ordinate programme is given in Appendix#2.

#### Photo-Reduction Detail

An initial x5 reduction was carried out by the audio-visual department of the university. This left a necessary x20 reduction. The camera used for this reduction was a Microkon 1700, HCL Manufacturing, Willow Grove P.A. It comes equipped with a travelling microscope which mounts on the photographic plate holder. This holder in turn is attached to a camera bed in such a manner that the photographic plate or travelling microscope is parallel to the illuminated screen which holds the required mask. The holder position is variable on the bed, allowing reductions between 10x and 20x. Calibration is carried out in the following manner

- 1) The travelling microscope is mounted on the holder.
- 2) The mask is then placed on the fluorescent illuminated screen, covered by a plastic sheet and held in place by vacuum action.
- 3) The camera comes equipped with a digital shutter control. This control is set for maximum time opening.
- 4) The F-stop and focus settings for the camera lens are then adjusted by viewing the illuminated mask through the telescope.
- 5) The mask is then replaced by a simple geometric pattern cut in a piece of rubylith. Usually, it is of the form of a rectangle. The strip

is usually quite long, in the range of 5 to 10 inches, cut to a tolerance of  $1/1000$  of an inch. This is accomplished on the above mentioned cutting table.

- 6) The position of the holder on the camera bed is adjusted to approximately give the required reduction.
- 7) The travelling microscope then scans the length of the rectangle. The microscope is equipped with a vernier accurate to  $1/10000$ ". The beginning and end points of the strip are measured. The difference is compared with the required width. For the example of the strip being 10" wide  $\pm .001$ ", then for a reduction of 20, the difference on the vernier scale should be  $0.5 \pm .00005$ ". The vernier is accurate to  $0.0001$ ". The holder comes with adjustable stop screws. These screws are adjusted until the measured difference is the required distance to within  $.0001$ ".
- 8) The camera is then set for use. The strip calibrator is then replaced by the mask. The photographic plate holder is then loaded with a "2x2" high resolution photographic glass plate (Kodak #            ). This must be done in red light.
- 9) The photographic plate is then mounted on the camera. The shutter opening time is then adjusted, and the picture taken. The F-stop value used was F-4, and the shutter opening time was 14.5 seconds.
- 10) Develop the plate under red light. The required time is approximately 1 minute. Wash for an additional 30 seconds in distilled water and place the plate in a fixer for an additional 4 minutes. Wash, dry and store the plates in a dust-free atmosphere.

### The Substrate

The substrate used was a rectangular 1" × 1/2" piece of Lithium Niobate. It's surface is optically polished (using the Neutons Ring method) at the manufacturing level. The Z-propagation axis is the long axis of this rectangle. Substrate preparation is divided into two sections. The first is the cleaning of the substrate. The second involves the placing of the metal layer on the piezoelectric surface.

The most successful cleaning method discovered was of acetone cleaning in an ultrasonic bath - followed by an acetone vapour cleaning and drying process. This latter process simply involves placing a half-filled beaker of acetone on a hot plate. It is heated under low heat until a vapour appears. The substrate is removed from the ultrasonic bath using tweezers. It is then dipped into the heated acetone. By slowly raising the substrate up through the vapour one achieves a contaminant-free-cleaning plus an extremely dry substrate. The substrate is then placed in a very clean petrie dish and sealed shut.

Placing the metal surface on the substrate requires the use of a vacuum evaporator unit. The one used was a (Speedi-Vac Model #12E3/1670). The unit consists of a combination roughing-oil diffusion vacuum system and metal evaporator system. The unit also comes equipped with a crystal-calibrator attached to a frequency meter. This unit allows for determination of the metal-film thickness. The procedure to be followed here is as follows.

- 1) Close Roughing Line and High Vacuum valves. Slowly open chamber air admittance valve until chamber pressure is up to atmospheric. Remove glass bell jar from unit.

- 2) Install cleaned piezoelectric substrate, face down in substrate holder. Place the cleaned metal to be evaporated along the axis of the heater filament located directly below the substrate holder. Re-install the glass bell jar, making certain that the metal protective cage is placed over the bell jar.
- 3) Close chamber air admittance valve. Slowly open the roughing line valve. Turn on the penning guage. Pump down the approximately 50 Ton pressure. Close roughing valve, and very slowly open the high vacuum valve, ascertaining the pressure does not rise above 100 Ton. Turn on the Pirani guage below approximately 50 Ton pressure. Run the high vacuum diffusion pump until the chamber pressure has fallen to approximately  $1.0 \times 10^{-5}$  Ton. This usually requires about three hours.
- 4) When the pressure is sufficiently low, the evaporation process can be carried out. Turn on the frequency counter and record the initial reading on the scale. The thickness monitor is calibrated to give a  $\sim 1.0$  Hz change in frequency for every angstrom of metal thickness. Subtract from the first reading the required number of Hertz as indicated above. For example, if the initial reading was 43 KHz, and the desired thickness was  $3000 \text{ \AA}$ , then using the  $1.0 \text{ Hz/\AA}$  calibration, the required final reading on the frequency counter should be 40 KHz. Record the final required reading.
- 5) Turn on the low tension heater switch and adjust the rheostat control for a filament current of approximately 35 amps. As the filament heats up, the metal for plating begins to melt. The conduction through the filament rises and one must recompensate by reducing the rheostat

control. Just before the evaporation point there will be a sudden rise in current. At this point the rheostat control should be lower, and then raised again to its value of 35 amps after the main evaporation has occurred.

- 6) Watch the frequency counter. It will now be decreasing at a fast rate. As the frequency nears the desired end-point value slowly turn off the rheostat and filament control. Record the final counter value, and determine the thickness of the metal film.
- 7) Close the high vacuum valve and turn off the peranni gauge. Close the roughing valve and slowly open the air admittance valve. When the pressure is back to atmosphere remove the bell jar and the coated substrate.
- 8) Transfer the substrate to an annealing oven (Lindberg Heni-Duti, Watertown, Wisc.). For an aluminum coating set the temperature at 450<sup>o</sup>F and leave for 15 minutes. This step assures good bonding of the metal to the piezoelectric substrate.

#### Photo-lithographic Reproduction

The metal coated substrate is now ready to be formed into a circuit. The first step is to obtain positive-working photo-resist such as Shipleys AZ1350B. The viscosity should be approximately 40 centipoise and should be well filtered with 1-micron filter paper to remove any hard crystals which may have developed from air contamination. This must be done under yellow light, as must all photo-resist work.

- 2) The piezoelectric substrate should be placed on appropriate spinner (headway Research, Inc.). The important consideration in a spinner is the initial acceleration. The spinner should have reached its

maximum speed in under 1.0 seconds. This is a requirement necessary to assure even, thin coatings ( $\sim 3000\text{\AA}$ ) of photo-resist. The spinner used had variable speed control and variable time control. The substrate was held on the spinner by vacuum action.

- 3) Place one small drop of photo-resist on the centre of the substrate. Immediately start the spinner. If one observes the action from a glancing angle off the substrate one will note interference fringes. From these fringes one can judge the evenness and totality of covering obtained on the metal film. Experimental results indicate a time of 15 seconds at  $2700\text{\AA}$  to give optimum results using Shipleys AZ1350B photo-resist.
- 4) Pre-bake the photo-resist coated substrate in an oven at  $76^{\circ}\text{C}$  for 15 minutes. This hardens the photo-resist.
- 5) Remove the substrate from the oven and allow to cool for about 2 minutes.
- 6) Place the substrate, with the photo-reduced mask face down on it under an intense white light source ( $\sim 300$  watts). The source is at this point off. The orientation of the mask should comply with the propagation direction of the surface waves. Therefore, the fingers of the transducers should have their length perpendicular to the long-axis of the crystal (the Z-axis).
- 7) Turn on the intense light source for 30 seconds. The photo-resist should look a light green under intense light.
- 8) Remove the mask from the substrate, and place the exposed substrate in a photo-resist developer. Shipleys supplies the proper developer for its AZ1350B resist. Develop the pattern for approximately

- 1 minute. One will notice that all the photo-resist directly exposed to the light (i.e. those areas not covered by the mask pattern) will be removed in this step, leaving only a photo-resist pattern of the circuit on the metal surface. Dry the substrate.
- 9) Post-bake the substrate in an oven at  $76^{\circ}\text{C}$  for an additional 5 minutes. This is done since the developer tends to "soften" the photo-resist. This, if left would reduce the resolution of the final circuit.
- 10) Remove the substrate from the oven and place in the acid etchant proper for the aluminum metal (15 PARTS nitric acid, 5 PARTS phosphoric acid, 1 PART acetic acid). The etchant properties can be enhanced by raising the temperature to approximately  $35^{\circ}\text{C}$ . The etching process should be accompanied by continual, even agitation of the acid. The etch time is approximately 4 minutes.
- 11) Remove the circuit from the etchant, wash in distilled water, and carefully dry with Freon spray. Using acetone, spray the substrate to remove the photo-resist from metal pattern remaining. At this point the actual circuit is fabricated, and only wires and holding package remain to be added.

### Wire Bonding

The two most used industry methods are 1) ultrasonic bonders and 2) hydrogen bonders. Due to the acoustic nature of the devices, it is not known whether there would be shattering effects caused by the ultrasonic bonder. To use a hydrogen bonder, it is necessary to ascertain that the substrate is at the stage temperature of the bonder. Due to the anisotropic nature of the substrate, the Lithium Niobate with its high temperature

coefficient, is found to be subject to thermal shock<sup>†</sup>. Thus one cannot use hydrogen bonders with these devices unless the design is modified to allow a pre-heater stage before the actual bonder stage. It was found necessary for test purposes to use a paste solder mix called Eccobond solder. This solder requires approximately 7 hours to harden to a low resistance state.

#### Test Package

A simple test package consisting of a 2" square aluminum base equipped with the Omni Products O5M 204CC captivated contact microwave connectors was fashioned. Two such connectors are needed for each package. The centre contacts of each connector are separated by 1". This is the same length as the substrate. This allows the contacts to be used for two purposes. The first use is the usual electrical contact to the wires. The second is the use of the contacts as acoustic absorbers for surface waves travelling past the transducers. A two-layer protective covering of plexiglass was formed. The first layer consists of a square annulus of 1/2" on a side and 1/16" thick. Mounted on top of this is a covering layer of plexiglass. It is a 2"x2" square 1/16" thick. The package is held together by 4 1/2" bolts at the corners of the package.

#### Matching Networks

The filters we operated without matching networks.

<sup>†</sup> BASED ON EXPERIMENTS CARRIED OUT AT LINEAR TECHNOLOGY INC., BURLINGTON, ONTARIO IN MAY, 1975.

## RESULTS AND CONCLUSIONS

Results

The following theoretical parameters are predicted for the filters based on the design procedures used.

Filter #I

|                  |   |                       |
|------------------|---|-----------------------|
| Centre frequency | - | 44.014 MHz            |
| Bandwidth        | - | 5.0 MHz               |
| Transition Width | - | 1.25 MHz, symmetrical |
| Trap Depth       | - | 50 db                 |
| Phase            | - | Linear                |
| Group Delay      | - | 1.0 $\mu$ sec         |

Input Transducer

$$G_a(\omega_0) = 3 \times 10^{-3} \text{ mhos}$$

$$B_a(\omega)_{\text{AVERAGE}} = 2 \times 10^{-2} \text{ mhos}$$

$$C_T = 23.50 \text{ pf}$$

Output Transducer

$$G_a(\omega_0) = 9.2 \times 10^{-3} \text{ mhos}$$

$$B_a(\omega_0) = 0.0$$

$$C_T = 7.3 \text{ pf}$$

Insertion Loss > 12 db

Filter #II

|                  |   |               |
|------------------|---|---------------|
| Centre Frequency | - | 44.014 MHz    |
| Bandwidth        | - | 5.0 MHz       |
| Transition Width | - | 1.35 MHz      |
| Trap Depth       | - | 60 db         |
| Phase            | - | Linear        |
| Group Delay      | - | 1.0 $\mu$ sec |

Input Transducer

$$G_a(\omega_0) = 1.8 \times 10^{-3} \text{ mhos}$$

$$B_a(\omega) = 3 \times 10^{-2} \text{ mhos}$$

AVERAGE

$$C_T = 17.0 \text{ pf}$$

Output Transducer

$$G_a(\omega_0) = 9.2 \times 10^{-3} \text{ mhos}$$

$$B_a(\omega_0) = 0.0$$

$$C_T = 7.30 \text{ pf}$$

Insertion Loss > 12 db

Theoretical-Experimental Comparison

The magnitude responses of the filters were tested using a Hewlett-Packard 8601A Generator/Sweeper and an Alfred Oscilloscope Model 8000 equipped with the Model 7051 Sweep Network Analyser. The phase spectrum was measured using the Hewlett-Packard Phase-Magnitude Analyser. The static capacitance was measured using a Wayne-Kerr Auto Balance Bridge equipped with special low-capacity leads for accurate pf range.

The following characteristics were found.

Filter I

|                  |   |                                   |
|------------------|---|-----------------------------------|
| Centre Frequency | - | 44.00 MHz                         |
| Bandwidth        | - | 4.2 MHz                           |
| Transition Width | - | 1.0 MHz                           |
| Trap Depth       | - | 23 db                             |
| Phase - Periodic |   | variations of $\sim \pm 10^\circ$ |
|                  |   | superimposed on linear phase.     |
| Group Delay      | - | $1.0 \pm .1 \mu\text{sec}$        |

Input Transducer

$$G_a(\omega_0) \quad -$$

$$B_a(\omega_0) \quad -$$

$$C_T = 22.0 \text{ pf} \pm 1 \text{ pf}$$

Output Transducer

$$G_a(\omega_0) \quad -$$

$$B_a(\omega_0) \quad -$$

$$C_T = 7.0 \pm .5 \text{ pf}$$

Insertion Loss 28.1 db

Filter II

|   |   |                              |
|---|---|------------------------------|
| Centre Frequency                          | - | 44.1 MHz                     |
| Bandwidth                                 | - | 5.25 MHz                     |
| Transition Width                          | - | 1.30 MHz                     |
| Trap Depth                                | - | 20 db                        |
| Phase - Linear                            | - | except near centre frequency |
| where $\sim 5^\circ$ nonlinearity occurs. |   |                              |
| Group Delay                               | - | $1.0 \pm .1 \mu\text{sec}$   |

Input Transducer

$$G_a(\omega_0) \quad -$$

$$B_a(\omega_0) \quad -$$

$$C_T = 17.5 \pm 1 \text{ pf}$$

Output Transducer

$$G_a(\omega_0) \quad -$$

$$B_a(\omega_0) \quad -$$

$$C_T = 7.0 \pm .5 \text{ pf}$$

Insertion Loss - 25.8 db

### Discussion of Results

Filter #I suffered from feedthrough from the capacitance from the input to the output transducer. The apodized array was too long in time extent for the 1  $\mu$ second delay of the filter. This can clearly be seen from an examination of Figure #34. The feedthrough increased the ripple in the passband to such an extent that the Gibb's phenomena was completely masked out. The phase response was linear with  $\sim \pm 10\%$  periodic variations superimposed upon it. The phase variations followed the magnitude variations throughout the passband as would be expected from the phase-magnitude relationship through the Hilbert transform. The centre frequency was correct to the measuring accuracy. The bandwidth was 4.2 MHz, compared to the expected 5.0 MHz which is a 20% error. The trap depth was but -23 db, compared to the expected -50 db. Clearly, a matching network would be needed. The corresponding insertion loss was also high, being measured at 28.1 db. From the magnitude response though, one can clearly see the intended square bandpass. This certainly reflects the strong surface wave coupling of the Lithium Niobate surface. The corresponding phase errors associated with high coupling substrates is not analyzable from this filter. The measured static capacitances of the transducers was as predicted by theory to within the measurement accuracy. The group delay was also correct.

Filter #II represented a considerable improvement over #I. By reducing the feedthrough, one clearly sees much greater agreement between theory and experiment. The predicted bandpass response is quite nearly followed in both magnitude and phase responses. The centre frequency was off by only 0.2% with a bandwidth error of 5%. The transition width error

was 3.7%. The phase was linear, except for a small deviation near the centre frequency as would be expected from the dip in the magnitude response there. This dip is predicted by the computer simulations as being the Gibb's phenomena. However, its magnitude is greater than predicted. It is a -5 db level, whereas, it was predicted to be  $\sim$  -1.5 db. However, a certain amount would be added due to the triple-transit error.

From the results on this filter, one can see that the edge reflection problem predicted by the change in characteristic impedance from metalized to non-metalized areas was not serious. In fact, it cannot be seen in the phase response. The trap depth, again was not nearly as great as expected, and insertion losses were high at 25.8 db. Again, one clearly sees the need for the development of good matching circuits.

CONCLUSIONS

From the experimental results, it is quite clear that the sampled Fourier Transform technique used in the synthesis is a powerful and essentially correct engineering approach. Second order effects do not appear as serious as predictions. Based on the results, it is clear that these filters are extremely reliable. Filtering action was apparent in Filter #1, even though it was operated under very unfavourable conditions, such as high feedthrough, and poor electric contact methods. Filter #2 shows the degree of agreement between theory and experiment which can be achieved with a minimum of component parts to the filter. The fabrication techniques are simple for the frequency range used, and with properly maintained facilities high reproductibility should be easy to achieve. Surface wave filters should certainly be considered as a serious competitor, and eventually a replacement for the high frequency filter market in electronics.

APPENDIX 1

SLOW TRANSMISSION LINE ANALOGY

## APPENDIX 1

Slow Transmission Line Analogy <sup>(15)‡</sup>

In this appendix I would like to show an alternative characterization of the surface-wave transducer, based directly on the concept of it being a uniform transmission line with periodically spaced excitation potentials. In figure A1(1)a <sup>(15)</sup> is shown such a line of characteristic impedance  $Z_0$ . In A1(1)b <sup>(15)</sup> is shown the lumped equivalent.

We can write the following 3-port admittance characterization

$$i_1 = Y_{11}e_1 + Y_{12}e_2 + Y_{13}e_3 \quad (1)$$

$$i_2 = Y_{12}e_1 + Y_{11}e_2 + Y_{23}e_3 \quad (2)$$

$$i_3 = Y_{13}e_1 + Y_{23}e_2 + Y_{33}e_3 \quad (3)$$

where the acoustic and electric symmetries have been substituted in. If we consider the electric port shorted, then we expect a wave incident on port 1 to travel along the transmission line unaffected. By transmission line theory then

$$i_1 = \frac{e_1}{Z_0}, \quad i_2 = -\frac{e_2}{Z_0} \quad \text{where } i_2 = i_1 \exp(-j\beta x)$$

Letting  $e_3 = 0$  in the above matrix we get

$$\frac{e_1}{Z_0} = Y_{11}e_1 + Y_{12}e_2 \quad (1')$$

‡ Approach based on work presented in reference (15).

$$-\frac{e_1}{Z_0} \exp(-j\beta x) = Y_{12}e_1 + Y_{11}e_2 \quad (2')$$

from which we can solve for  $Y_{11}$  and  $Y_{12}$ . Solving, we get

$$Y_{11} = -j/Z_0 \cot(\beta x) \quad (4)$$

$$Y_{12} = j/Z_0 \operatorname{cosec}(\beta x) \quad (5)$$

Note that these results are exactly the same as those for a transmission line.  $Y_{11}$  is the input admittance of a shorted transmission line (i.e.  $Y_{11} = e_1/i_1$ ). Similarly  $Y_{12}$  is the transfer admittance, representing the short-circuit output current for a given input voltage (i.e.  $Y_{12} = e_1/i_2$ ).

Now, if we consider applying a potential  $e_3$  to the electric port, then from (1) and (2) we can write

$$\frac{e_1}{Z_0} = Y_{11}e_1 + Y_{12}e_2 + Y_{13}e_3 \quad (6)$$

$$-\frac{e_2}{Z_0} = Y_{12}e_1 + Y_{11}e_2 + Y_{23}e_3 \quad (7)$$

Then we have:

$$e_3 Y_{13} = \frac{e_1}{Z_0} - Y_{11}e_1 - Y_{12}e_2 \quad (8)$$

$$\therefore Y_{13} = \frac{1}{e_3} \left\{ e_1 \left( \frac{1}{Z_0} - Y_{11} \right) - Y_{12}e_2 \right\} \quad (9)$$

and also

$$e_3 Y_{23} = -\frac{e_2}{Z_0} - Y_{12} e_1 - Y_{11} e_2 \quad (10)$$

$$\therefore Y_{23} = -\frac{1}{e_3} \left\{ e_2 \left( \frac{1}{Z_0} + Y_{11} \right) + Y_{12} e_1 \right\} \quad (11)$$

which gives expressions for  $Y_{13}$  and  $Y_{23}$ .

Port 3 represents the input admittance of the transducer. Therefore we can write

$$i_3 = e_3 (G + jB) \quad (12)$$

$$\therefore e_3 (G + jB) = Y_{13} e_1 + Y_{23} e_2 + Y_{33} e_3 \quad (13)$$

Solving for  $Y_{33}$  we have

$$Y_{33} = G + jB - \frac{1}{e_3} (Y_{13} e_1 + Y_{23} e_2) \quad (14)$$

This gives expressions for all the independent parameters in the (Y) matrix.

Now, again in complete analogy with the transmission line, we write voltage in the form  $K \exp(j\beta x)$ . In the case of a transmission line with periodically spaced voltage source, we can write for the voltage at port 1 of the equivalent total transducer

$$e_1 = \sum_{i=1}^n K_i \exp(j\beta x) \quad (15)$$

and at port 2 we must then have  $e_2 = -e_1^*$  where  $*$  represents conjugation and the  $-$  sign comes from the convention used for current directions. The conjugation results from the waves travelling in the opposite direction.

Now, above, we stated that  $Y_{33}$  was the input admittance of the complete equivalent transducer. Therefore, the real part of  $Y_{33}$  must be the acoustic conductance term  $G$

$$\therefore G = \operatorname{Re} [Y_{33}] \quad (16)$$

We know that the power carried away by the waves at port 1 will be given by  $\frac{e_1^2}{Z_0} = \frac{e_1 e_1^*}{Z_0}$ . Similarly, the waves to the left will carry away  $\frac{e_2 e_2^*}{Z_0}$ .

This power is supplied by  $e_3$ . Therefore we have

$$G = \frac{e_1 e_1^* + e_2 e_2^*}{2Z_0 e_3^2} = \frac{e_1 e_2^*}{Z_0 e_3^2} \quad (17)$$

$$\text{Now } e_1 = \sum_{i=1}^n \cos(\beta x_{i1}) + j \sum_{i=1}^n \sin(\beta x_{i1}) \quad (18)$$

$$e_2^* = - \sum_{j=1}^n \cos(\beta x_{j1}) - j \sum_{j=1}^n \sin(\beta x_{j1}) \quad (19)$$

since  $e_2^* = -e_1$ . Carrying out the multiplication and after some manipulation we arrive at

$$G = \frac{1}{Z_0 e_3^2} \left[ \sum_{i=1}^n K_i^2 + 2 \sum_{i=1}^n \sum_{j=i+1}^n K_i K_j \cos\{\beta(x_i - x_j)\} \right] \quad (20)$$

Now, since the term B is known to be the Hilbert transform of G, then since the transform of  $\cos x$  is  $-\sin x$  (note similarity between Hilbert transform and differentiation for simple functions).

$$B = \omega C_T - 2 \sum_{i=1}^n \sum_{j=i+1}^n K_i K_j \sin \{ \beta(x_i - x_j) \} \quad (21)$$

where  $C_T = \sum_{i=1}^n C_n$  where  $C_n$  is the capacitance per section.

Therefore, we have a complete characterization of the surface wave filter based directly on a transmission line model. The single finger section of the transducer as modelled by the Mason equivalent circuit can be found here by the substitution

$$e_2 = \sum_{i=1}^2 K_i \exp(j\beta x) \quad (22)$$

$$e_1 = -e_2^* \quad (23)$$

etc. This direct identification may help one to understand in a simple manner the operation of surface wave transducers.

APPENDIX 2

COMPUTER PROGRAMMES

## APPENDIX 2

The following two programmes were used in the development of the filters. The first programme determines the time response required for a filter given a set of frequency domain specifications. Both linear and nonlinear phase types can be handled. The major subroutine used for the calculations is the HARM version of the Fast Fourier transform. Other subroutines used are the  $I_0$  subroutine for optimizing the response through weighting functions; OUTTRANS determines the frequency response of the output transducer from its time-domain specifications (this can be done since it is a uniform overlap transducer); PHASE 1 incorporates the effects of non-linear phase shifts and PLOT 1 is the subroutine used for printing the final time transform for inspection purposes. The function AMP(xx) is used to put in the initial idealized input data associated with the rectangular bandpass filter.

The second programme is the one used to give the length of fingers, position of fingers and polarity needed to realize a mask of a given magnification factor. The magnification factor is simply inputted into the programme. This programme was used for making the masks for filter #1 and filter #2.

HSAA,T200TMT1+

FTN.

ATTACH,PLOT1 IR.

ATTACH,SSPL IR.

LDSET,LIR=SSPL IR.

LDSET,LIR=PLOT1 IR.

LG0.

6400 END OF RECORD

PROGRAM TST(INPUT,OUTPUT,TAPE5=INPUT,TAPE6=OUTPUT,TAPE10)

C A PROGRAM TO TEST THE OPTIMIZATION ROUTINE

COMMON X(512), Y(512)

DIMENSION A(1024),M(3),INV(256),S(256)

M(1)=0

M(2)=M(3)=0

C GENERATE THE INPUT DATA

DO 10 I=1,512

X(I)=(I-1)\*0.2-51.2

10 Y(I)=AMP(X(I))

C TRANSFORM THE INPUT DATA

DO 15 I=257,512

A(2\*I-513)=Y(I)

15 A(2\*I-512)=0.0

DO 20 I=1,256

A(2\*I+511)=Y(I)

20 A(2\*I+512)=0.0

CALL HARM(A,M,INV,S,-1,IFERR)

DO 25 I=1,256

25 Y(I+256)=SQRT(A(2\*I-1)\*\*2+A(2\*I)\*\*2)

DO 30 I=1,256

30 Y(I)=SQRT(A(2\*I+511)\*\*2+A(2\*I+512)\*\*2)

CALL PLOT(0.0,0.0,-3)

CALL PLOT1

DO 36 I=321,512

A(I)=0.0

36 A(I+192)=0.0

36 CONTINUE

DO 37 I=1,160

XC=4.0\*SQRT(1.0-I\*\*2/160.0\*\*2)

CALL IO(XX,RI0)

A(2\*I-1)=A(2\*I-1)\*(RI0/11.301695)

A(2\*I)=A(2\*I)\*(RI0/11.301695)

A(1026-2\*I-1)=A(1026-2\*I-1)\*(RI0/11.301695)

A(1026-2\*I)=A(1026-2\*I)\*(RI0/11.301695)

37 CONTINUE

DO 38 I=1,256

Y(I)=SQRT(A(2\*I+511)\*\*2+A(2\*I+512)\*\*2)

38 Y(I+256)=SQRT(A(2\*I-1)\*\*2+A(2\*I)\*\*2)

CALL PLOT(17.5,-5.5,-3)

CALL PLOT1

DO 39 I=1,256

Y(I)=A(2\*I+512)

39 Y(I+256)=A(2\*I)

CALL PLOT(17.5,-5.5,-3)

CALL PLOT1

C THIS IS THE FOURIER TRANSFORM IN THE FREQUENCY DOMAIN

CALL HARM(A,M,INV,S,+1,IFERR)

DO 40 I=1,256

Y(I)=SQRT(A(2\*I+511)\*\*2+A(2\*I+512)\*\*2)

40 Y(I+256)=SQRT(A(2\*I-1)\*\*2+A(2\*I)\*\*2)

```

- SEARCH FOR YMAX
  YMAX=Y(1,0)
  DO 42 I=2,512
42  IF(Y(I).GT.YMAX)YMAX=Y(I)
  DO 45 I=1,512
45  Y(I)=10*ALOG(Y(I)/YMAX)
  YY(I)=Y(I)
  CALL PLOT(17.5,-5.5,-3)
  CALL PLOT1
C PLOT THE PHASE
  DO 58 I=1,256
  IF(A(2*I-1).NE.0.0)GO TO 51
  Y(I+256)=0.0
  GO TO 52
51  Y(I+256)=ATAN(A(2*I)/A(2*I-1))
52  IF(A(2*I+511).NE.0.0)GO TO 53
  Y(I)=0.0
  GO TO 58
53  Y(I)=ATAN(A(2*I+512)/A(2*I+511))
  YZ(I)=Y(I)
58  CONTINUE
  CALL PLOT(17.5,-5.5,-3)
  CALL PLOT1
  CALL LETTER (11,0.3,270.0,20.0,1.65,11)HEND OF PLOT)
  CALL PLOT (22.5,-5.5,-3)
  CALL PLOT(0.0,0.0,999)
  DO 60 I=1,1024
60  A(I)=0.0
  CALL OUTTRANS
  STOP
  FND
  SUBROUTINE PLOT1
  COMMON X(512), Y(512)
  CALL PLOT (3.0,1.0,-3)
C DRAW THE PLOT FRAME 9 X 25
  CALL PLOT (25.0,0.0,2)
  CALL PLOT (25.0,9.0,2)
  CALL PLOT (0.0,0.0,2)
  CALL PLOT (0.0,0.0,2)
C DRAW THE AXES 8 X 24
  CALL PLOT (0.5,4.5,3)
  CALL PLOT (24.5,4.5,2)
  CALL PLOT (12.5,0.5,3)
  CALL PLOT (12.5,8.5,2)
C RESET THE ORIGIN TO THE FRAME CENTRE
  CALL PLOT (12.5,4.5,-3)
C FIND THE PLOT SCALE
  XMAX=ABS(X(1))
  YMAX=ABS(Y(1))
  DO 10 I=2,512
  IF(ABS(X(I)).GT.XMAX) XMAX=ABS(X(I))
10  IF(ABS(Y(I)).GT.YMAX)YMAX=ABS(Y(I))
  XSCALE=12.0/XMAX
  YSCALE=4.0/YMAX
C SCALE AND PLOT THE DATA
  XS=X(1)*XSCALE
  YS=Y(1)*YSCALE
  CALL PLOT (XS,YS,3)

```

```

DO 20 I=2,512
XS=X(I)*XSCALE
YS=Y(I)*YSCALE
20 CALL PLOT (XS,YS,2)
ENCODE(10,100,V) YMAX
CALL LETTER(15,0.2,0.0,0.0,-5.0,14HMAX Y IN PLOT=)
CALL LETTER(10,0.2,0.0,4.5,-5.0,V)
100 FORMAT(G10.3)
RETURN
END
SUBROUTINE IO(X,PIO)
PIO=ABS(X)
IF(PIO-3.75)1,1,2
1 7=X*X*7.111111E-2
PIO((((4.5812E-2*Z+2.60768E-2)*Z+2.659732E-1)*7+1.206749E0)*7
1+2.089942E0)*Z+2.515623E0)*Z+1.
RETURN
2 Z=3.75/PIO
PIO=EXP(PIO)/SQRT(PIO)*((((((2.02377E-2*Z-1.647632E-2)*Z
1+2.635537E-2)*Z-2.057706E-2)*Z+9.16281E-3)*7-1.57565E-2)*Z
2+2.25319E-3)*7+1.328592E-2)*Z+3.989423E-1)
RETURN
END
SUBROUTINE OUTTRANS
COMMON A(1024),X(512),Y(512),YY(512),YZ(512)
C THIS IS A PLOT OF THE TIME DOMAIN SPECIFICATIONS OF THE OUTPUT TRANSDUCER
DO 5 I=1,256
Y(I)=A(2*I+511)
5 Y(I+256)=A(2*I-1)
CALL PLOT(17.5,-5.5,-3)
CALL PLOT1
DO 10 I=1,9
READ(2,12) A(2*I-1)
10 READ A(2*I+1005)
12 FORMAT(F10.3)
CALL HARM(A,M,INV,S,+1,IFERR)
DO 20 I=1,256
Y(I)=SQRT(A(2*I+511)**2+A(2*I+512)**2)
20 Y(I+256)=SQRT(A(2*I-1)**2+A(2*I)**2)
YMAX=Y(1.0)
DO 22 I=2,512
22 IF(Y(I).GT.YMAX)YMAX=Y(I)
DO 25 I=1,512
25 Y(I)=10*ALOG(Y(I)/YMAX)
CALL PLOT1
CALL PLOT(17.5,-5.5,-3)
DO 30 I=1,512
30 Y(I)=YY(I)*Y(I)
CALL PLOT(17.5,-5.5,-3)
CALL PLOT1
DO 38 I=1,256
IF(A(2*I-1).NE.0.0)GO TO 31
Y(I+256)=0.0
GO TO 32
31 Y(I+256)=ATAN(A(2*I)/A(2*I-1))
32 IF(A(2*I+511).NE.0.0)GO TO 33
Y(I)=0.0
GO TO 38

```

```

22 Y(I)=ATAN(A(2*I+512)/A(2*I+511))
28 CONTINUE
DO 40 I=1,512
40 Y(I)=Y7(I)+Y(I)
CALL PLOT(17.5,-5.5,-3)
CALL PLOT1
RETURN
END
SUBROUTINE PHASE1
COMMON A(1024),TG(16)
RWD=6.0E+6
DELTAW=RWD/16.0
TGTOT=6.60E-7
T+OUT=0.0E+0
DO 10 I=1,16
READ(2,15) TG(I)
15 FORMAT(E10.4)
10 CONTINUE
DO 20 I=1,16
PHI(I)=(TG(I)-TGRFF)*DELTAW
A(240+2*I)=A(220+2*I)*TAN(PHI(I))
20 A(786-2*I)=A(785-2*I)*TAN(PHI(I))
SUM=0.0
DO 30 I=1,16
SUM=SUM+TG(I)
30 CONTINUE
SEP=(TGTOT-SUM/16.0-TGOUT)*VF
WRITE(6,15)SEP
RETURN
END
FUNCTION AMP(XX)
IF(ABS(XX).LT.24.0)GO TO 10
IF(ABS(XX).GT.27.2)GO TO 10
IF(ABS(XX).EQ.24.0)GO TO 11
IF(ABS(XX).EQ.27.2)GO TO 11
AMP=1.0
GO TO 12
10 AMP=0.0
GO TO 12
11 AMP=0.5
12 RETURN
END
6400 END OF RECORD
END OF FILE

```

```

PROGRAM TST (INPUT,OUTPUT,TAPE5=INPUT,TAPE6=OUTPUT)
COMMON X(512), Y(512)
DIMENSION A(1024), M(3), INV(256), S(256)
M(1)=9
M(2)=M(3)=0
R=.156
Q=.9984
D=.078
MAGN=100
C GENERATE INPUT DATA
DO 10 I=1,512
X(I)=(I-1)*0.2-51.2
10 Y(I)=AMP(X(I))
C TRANSFORM THE INPUT DATA
DO 15 I=1,257,512
15 A(2*I-513)=Y(I)
DO 20 I=1,256
20 A(2*I+512)=0.0
CALL HARM (A,M,INV,S,-1,IFERR)
DO 30 I=705,1021,4
A(I+2)=SQRT(A(I)**2+A(I+1)**2)
IF(A(I).LE.0.0)GO TO 36
A(I+2)=(SQRT(A(I)**2+A(I+1)**2)*Q+R/2)*MAGN
GO TO 36
36 A(I+2)=- (SQRT(A(I)**2+A(I+1)**2)*Q+R/2)*MAGN
40 WRITE(6,100) A(I+2),A(I+1)
100 FORMAT(1H0,23HFINGER LENGTH IN INCHES,615.6,10X,4HIMAG,615.8)
DO 44 I=1,321,4
A(I+2)=SQRT(A(I)**2+A(I+1)**2)
IF(A(I).LE.0.0)GO TO 42
A(I+2)=(SQRT(A(I)**2+A(I+1)**2)*Q+R/2)*MAGN
GO TO 44
42 A(I+2)=- (SQRT(A(I)**2+A(I+1)**2)*Q+R/2)*MAGN
44 WRITE(6,100) A(I+2),A(I+1)
DO 50 I=1,1
Y(I)=0.0
Y(I+1)=0
50 WRITE(6,102) Y(I),Y(I+1)
102 FORMAT(1H0,12HSTART FINGER,615.8,10X,1CHEND FINGER,615.8)
DO 51 I=1,319,2
Y(I)=D*(I+1)
Y(I+1)=D*(I+2)
51 WRITE(6,102) Y(I),Y(I+1)
DO 55 I=1,1
Y(I)=25.74
Y(I+1)=25.74+D
55 WRITE(6,102) Y(I),Y(I+1)
DO 56 I=1,13,2
Y(I)=25.74+D*(I+1)
Y(I+1)=25.74+D*(I+2)
56 WRITE(6,102) Y(I),Y(I+1)
DO 60 I=1,7,2
Y(I)=.13965*MAGN
60 WRITE(6,104) Y(I)
104 FORMAT(1H0,27HLENGTH OF ODD UNAP FINGERS=,5X,615.8)

DO 61 I=2,8,2
Y(I)=-.13965*MAGN
61 WRITE(6,105) Y(I)
105 FORMAT(1H0,28HLENGTH OF EVEN UNAP FINGERS=,5X,615.8)
STOP
END

FUNCTION AMP(XX)
IF (ABS(XX).LT.2-.0)GO TO 10
IF (ABS(XX).GT.27.2)GO TO 10
IF (ABS(XX).EQ.24.5)GO TO 11
IF (ABS(XX).EQ.27.2)GO TO 11
AMP=1.0
GO TO 12
10 AMP=0.0
GO TO 12
11 AMP=0.5
12 RETURN
END

```

TRANSITION WIDTH (TW) AND RIPPLE FOR A  
BESSEL WEIGHTING FUNCTION

| PARAMETER<br>$\omega_a \tau$ | FILTER RESPONSE  |   |   |
|------------------------------|------------------|---|---|
|                              | $TW \times \tau$ | PEAK - PEAK<br>RIPPLE AT<br>BAND EDGE<br>(dB) | PEAK<br>OUT OF BAND<br>SIDELOBE<br>(dB) |
| 0                            | 0.50             | 1.4   | -21                                     |
| 1                            | 0.56             | 1.0   | -24                                     |
| 2                            | 0.80             | 0.52  | -30                                     |
| 3                            | 1.03             | 0.21  | -37                                     |
| 4                            | 1.32             | 0.076   | -45                                     |
| 5                            | 1.64             | 0.026   | -54                                     |
| 6                            | 2.00             | 0.0094  | -62                                     |
| 7                            | 2.23             | 0.0040  | -71                                     |

TABLE I: Transition Width and Ripple for a Bessel Weighting Function  
of time duration  $2\tau$ .

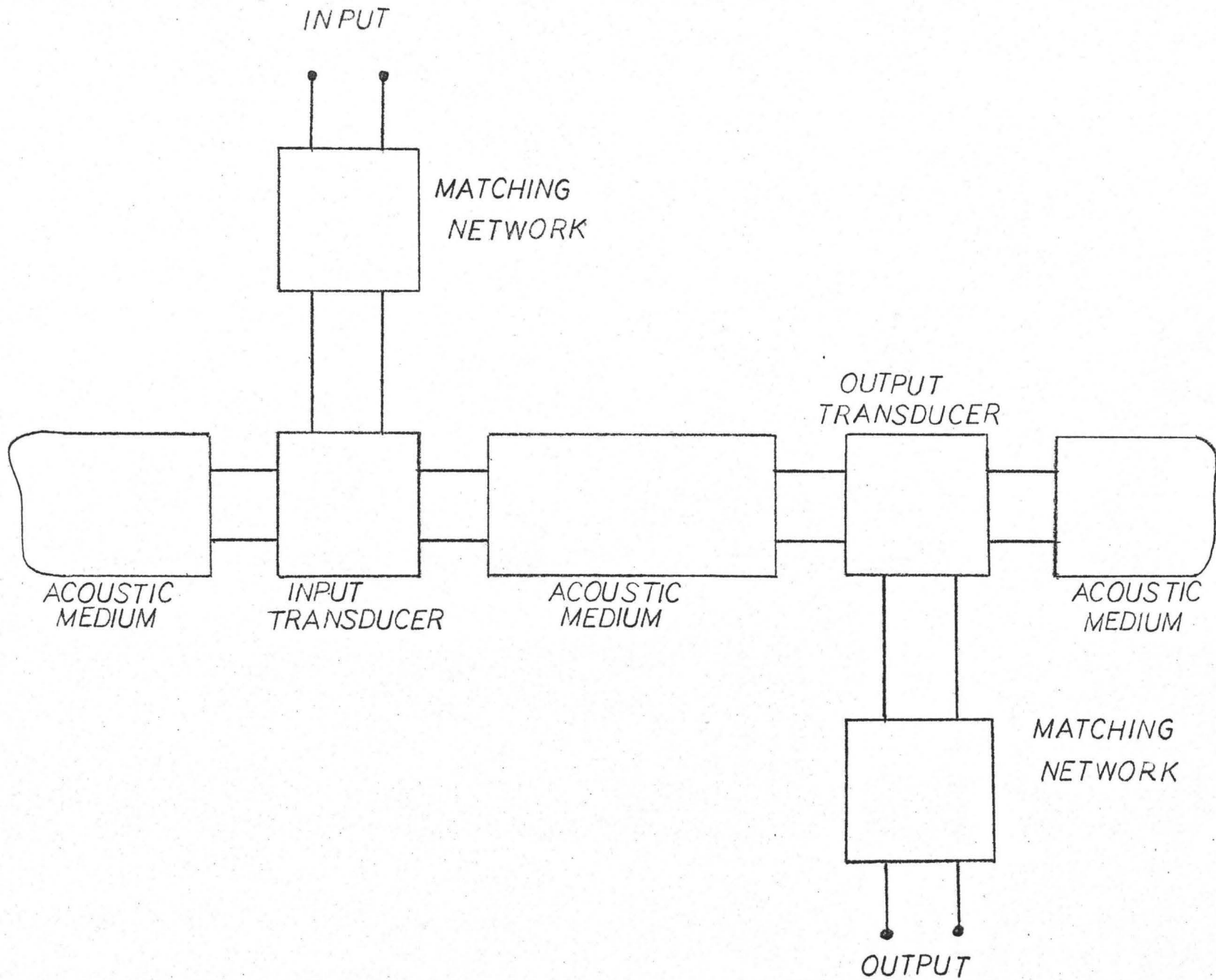


Figure 1: Block Diagram of a surface-wave device.

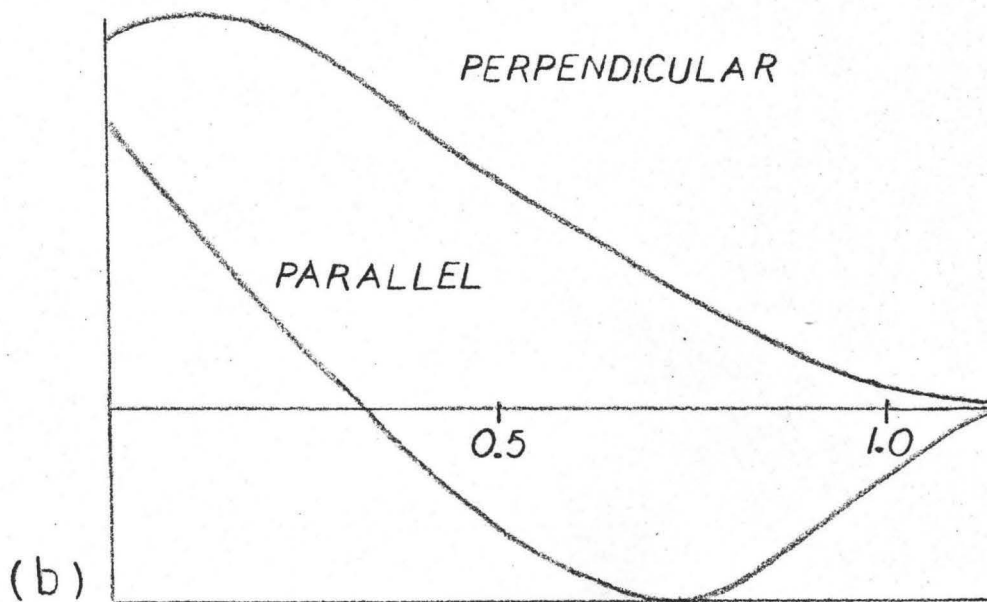
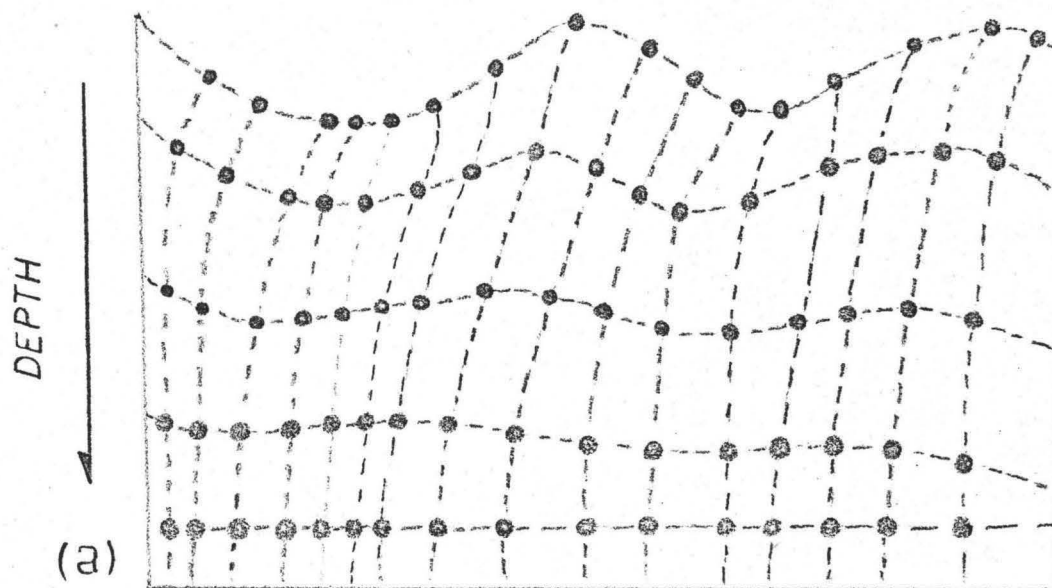


Figure 2: Displacement due to surface acoustic waves on an isotropic solid.

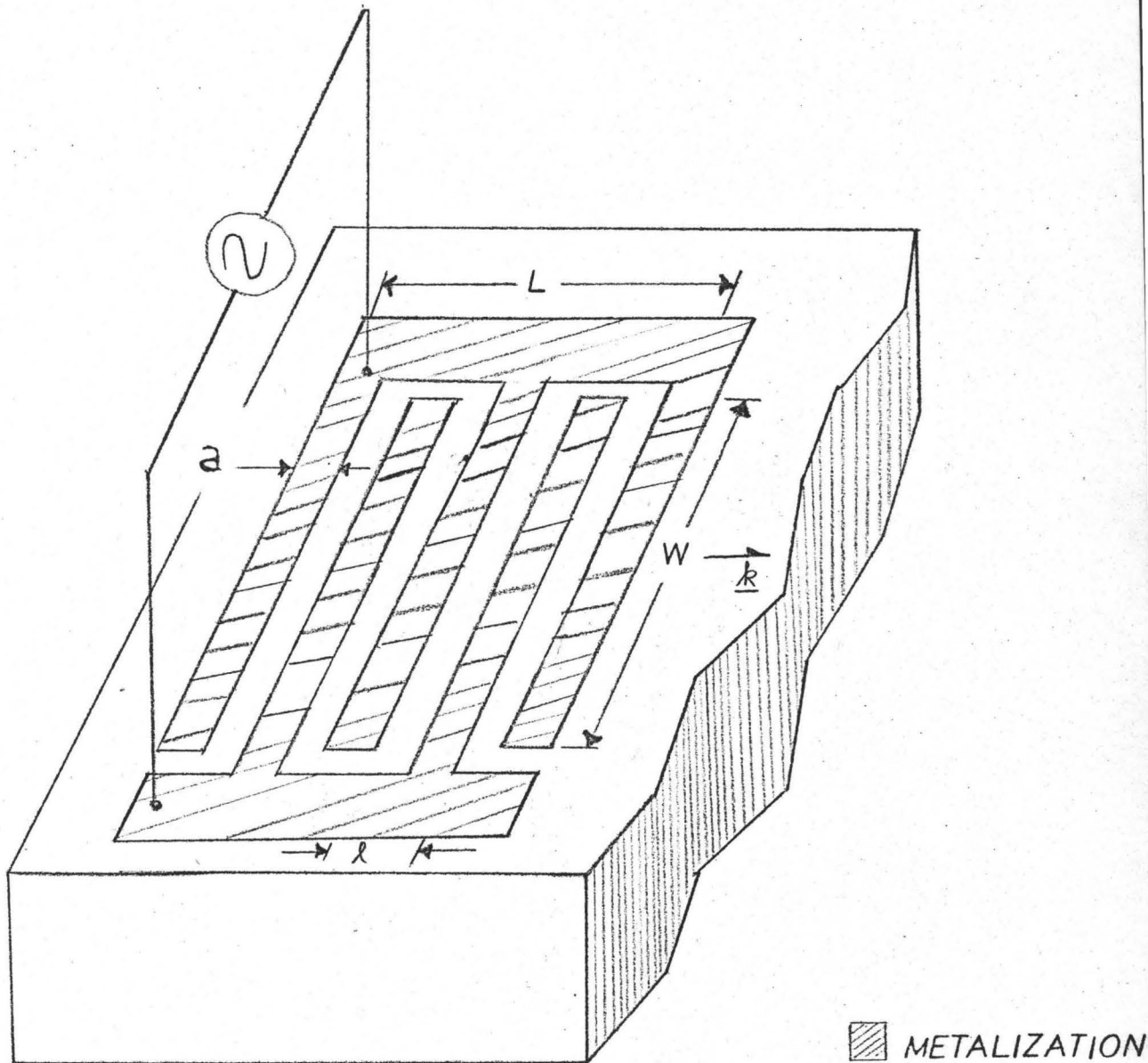


Figure 3: Basic structure of an interdigital transducer.

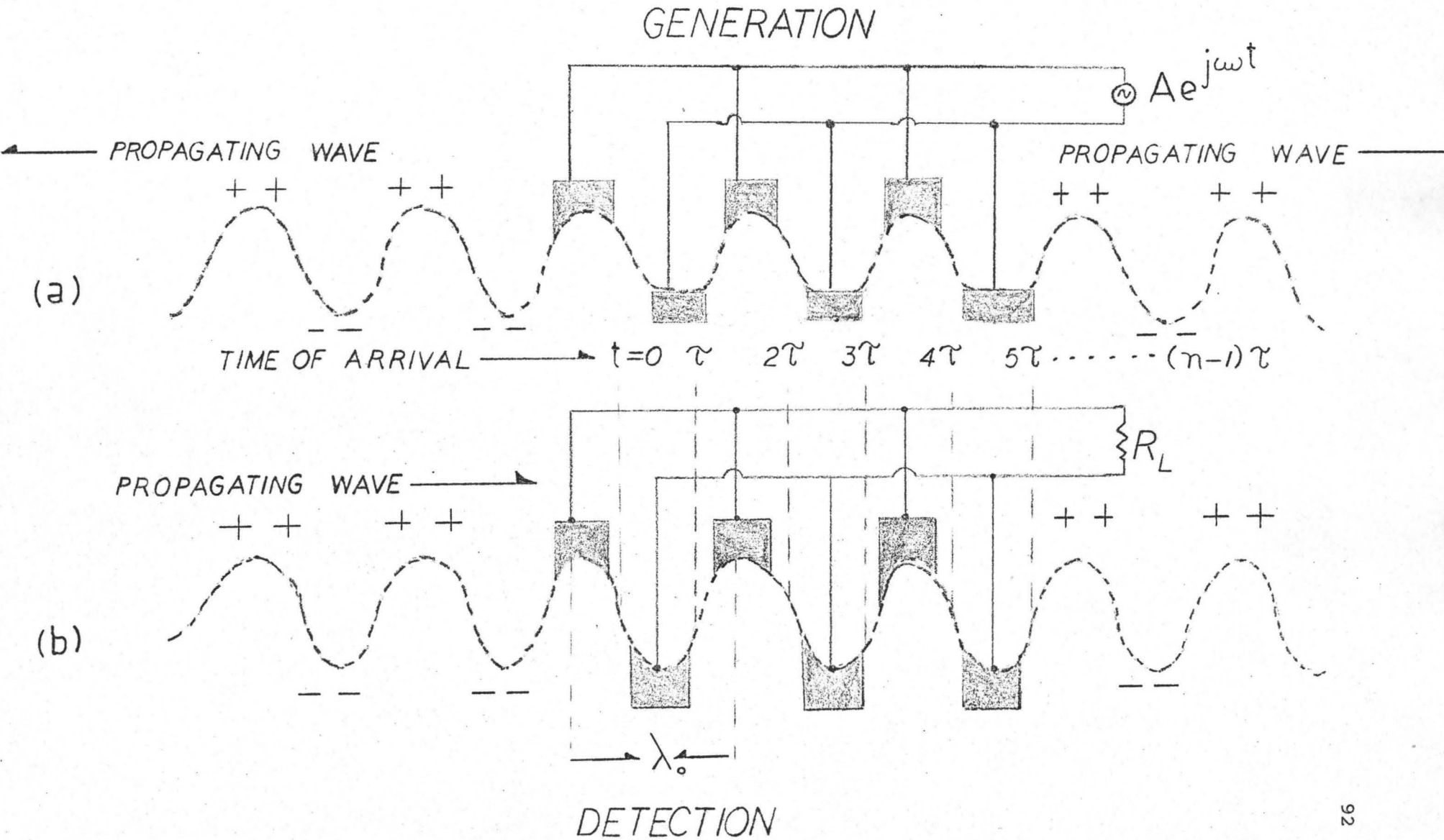


Figure 4: Side View of an Interdigital Transducer.

(a) Generation mode

(b) Detection mode

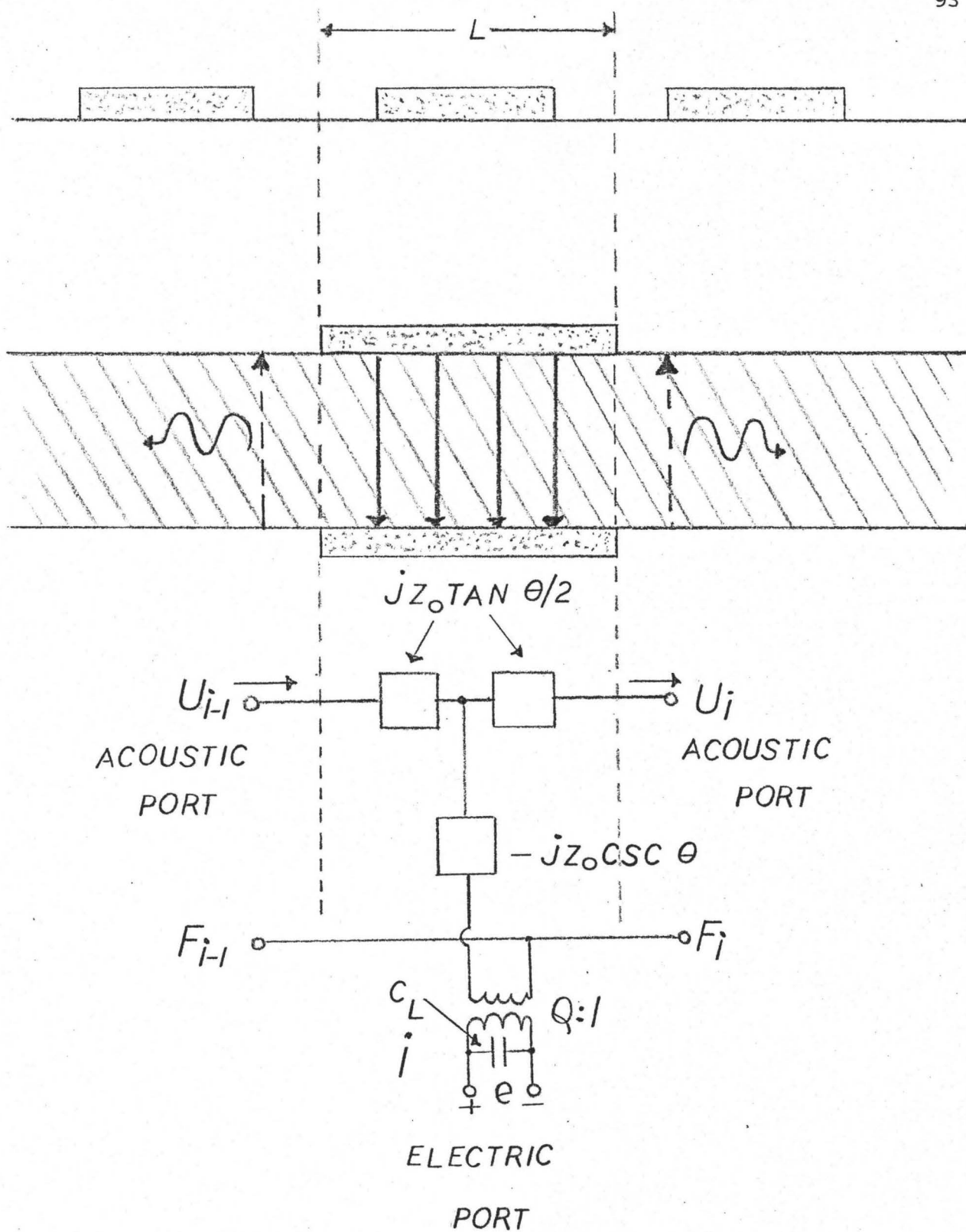


Figure 5: "Mason Equivalent Model" of a section of transducer.

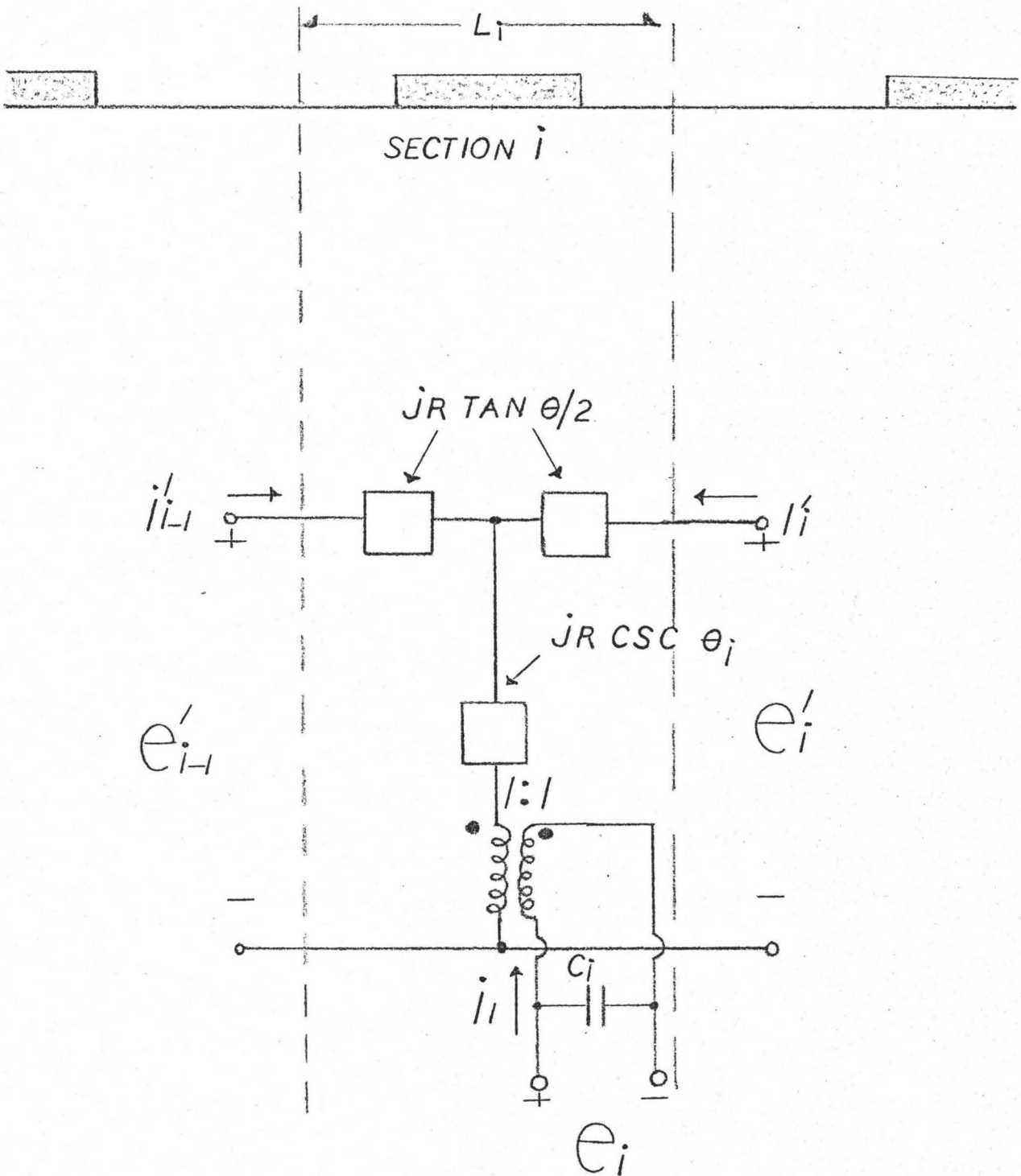


Figure 6: Complete electrical equivalent of a section of a transducer.

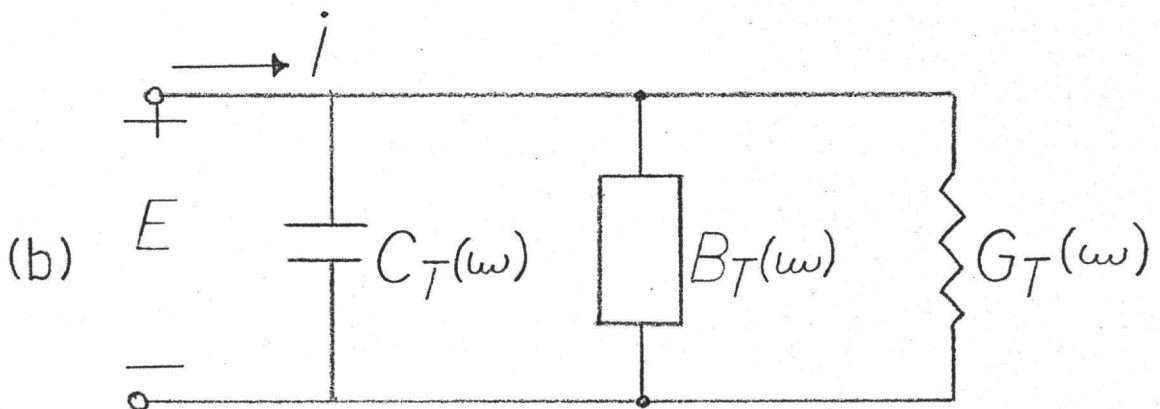
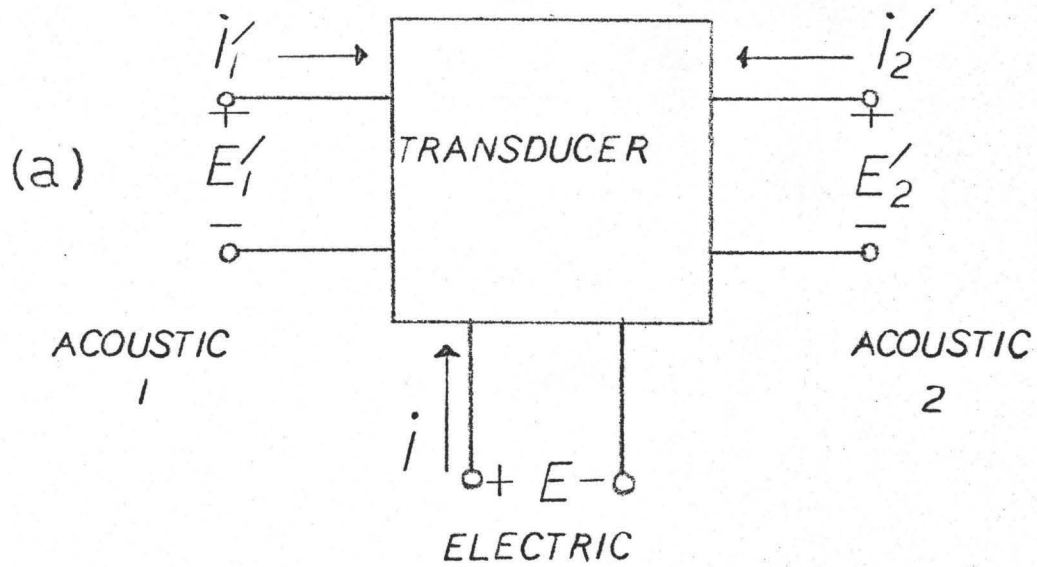


Figure 7: Models of Complete transducers.

(a) 3-Port model showing the two acoustic and one electrical ports

(b) Equivalent circuit as reviewed from the electrical port

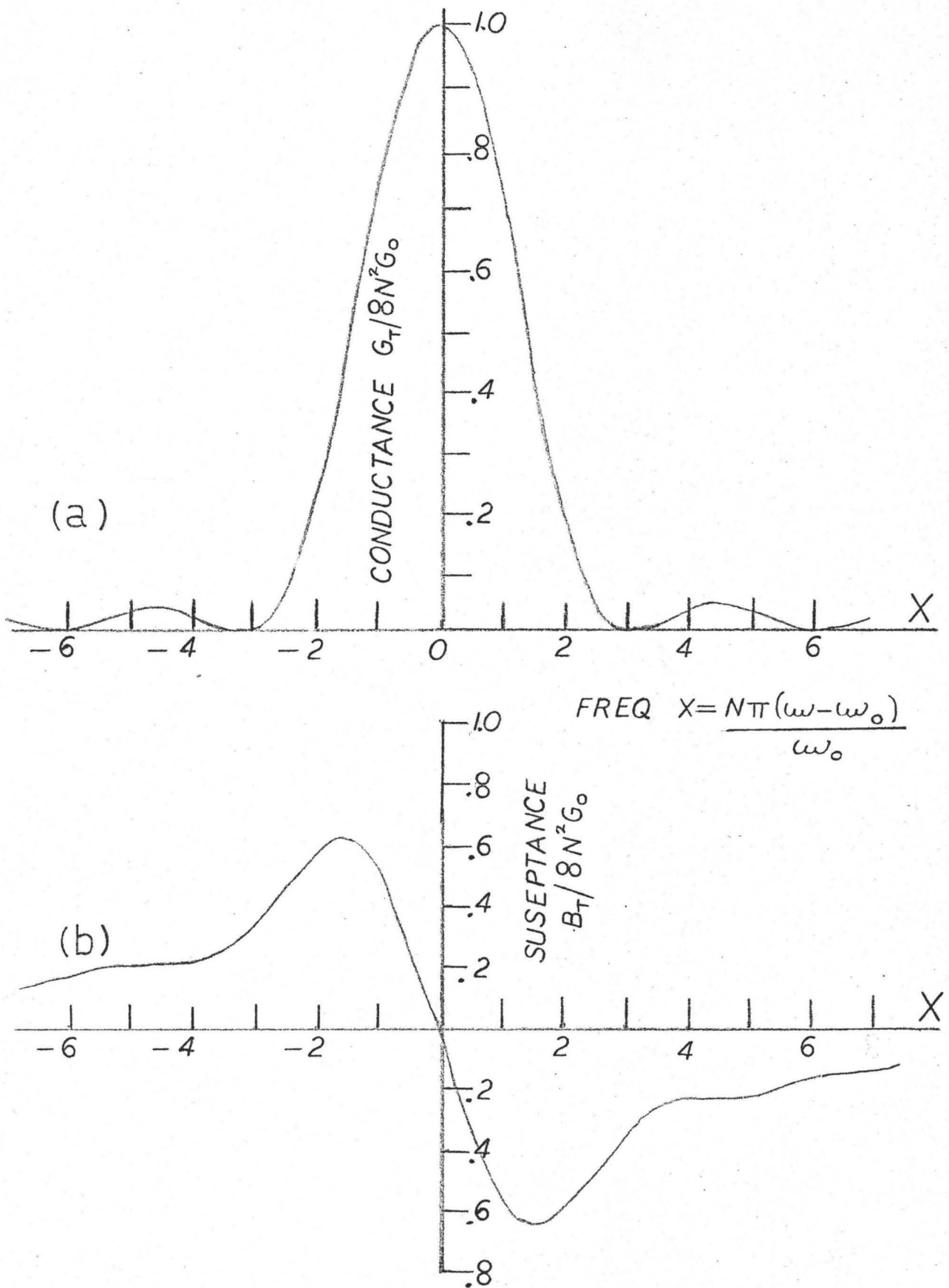
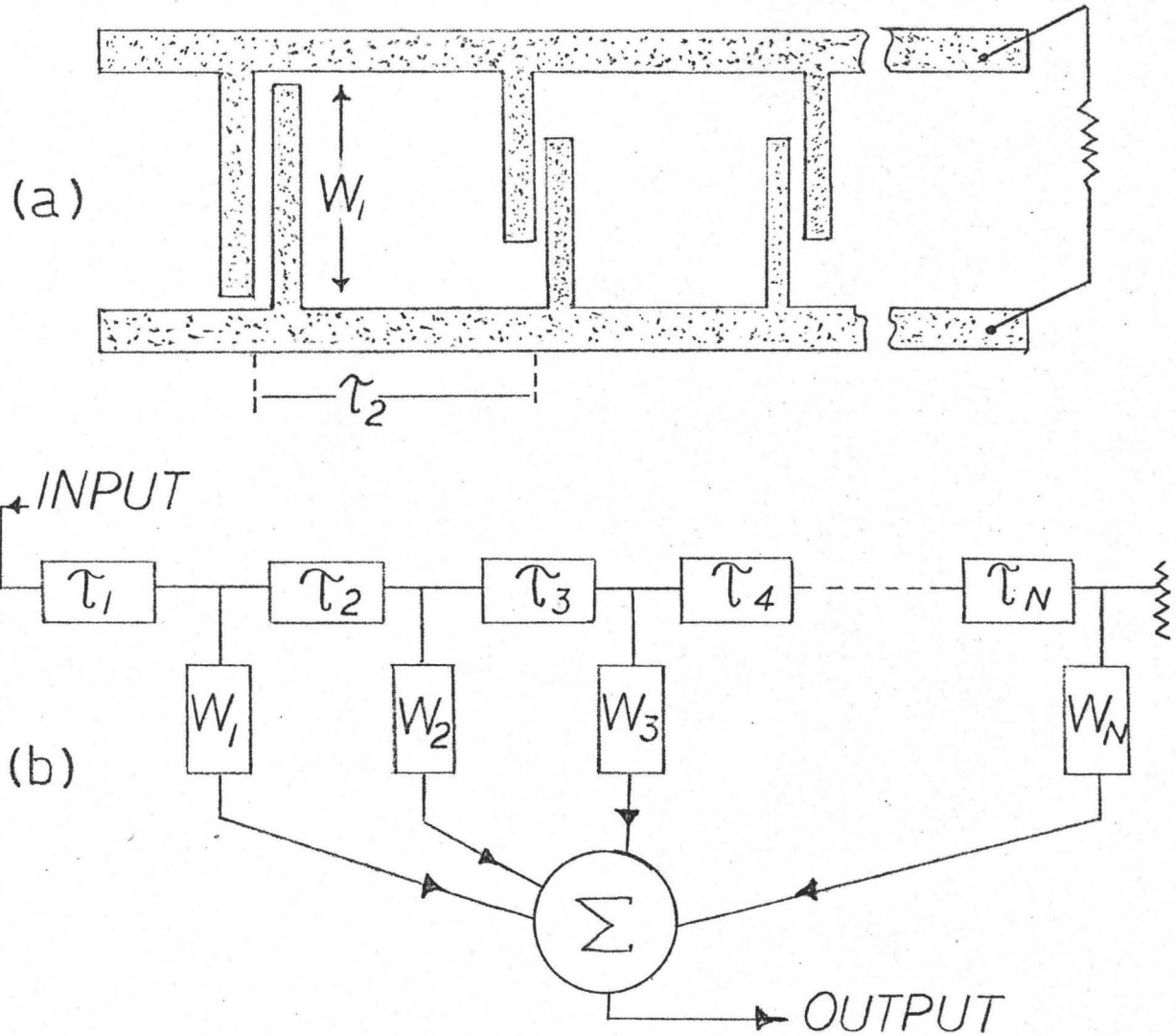


Figure 8: Acoustic elements associated with the transducer model.

(a) Acoustic conductance

(b) Acoustic susceptance



**Figure 9:** Comparison between surface-wave transducer and transversal filter.

- (a) Surface wave impinging upon the transducer from the left
- (b) Block representation of operation of a transversal filter

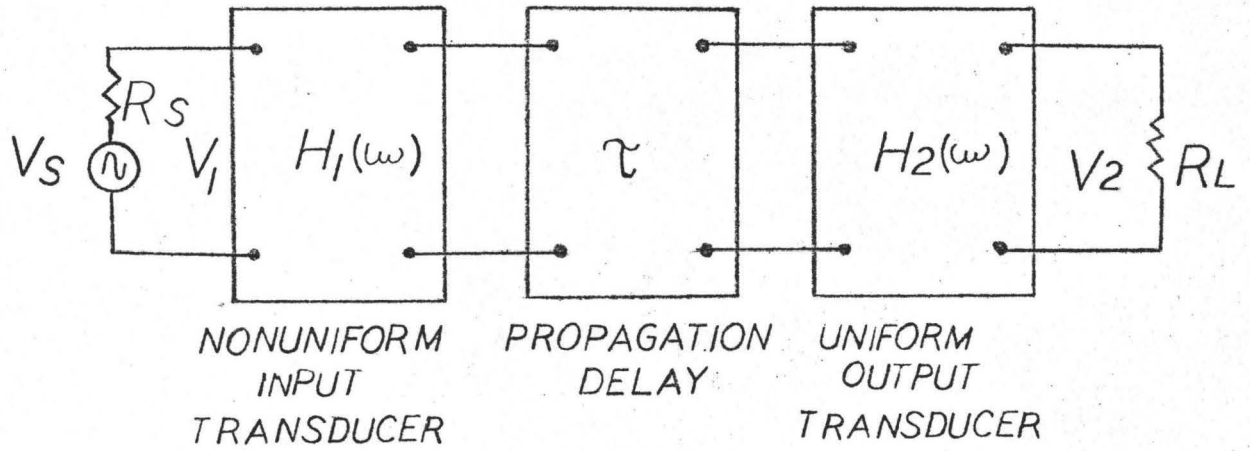


Figure 10: Typical arrangement for a surface wave device.

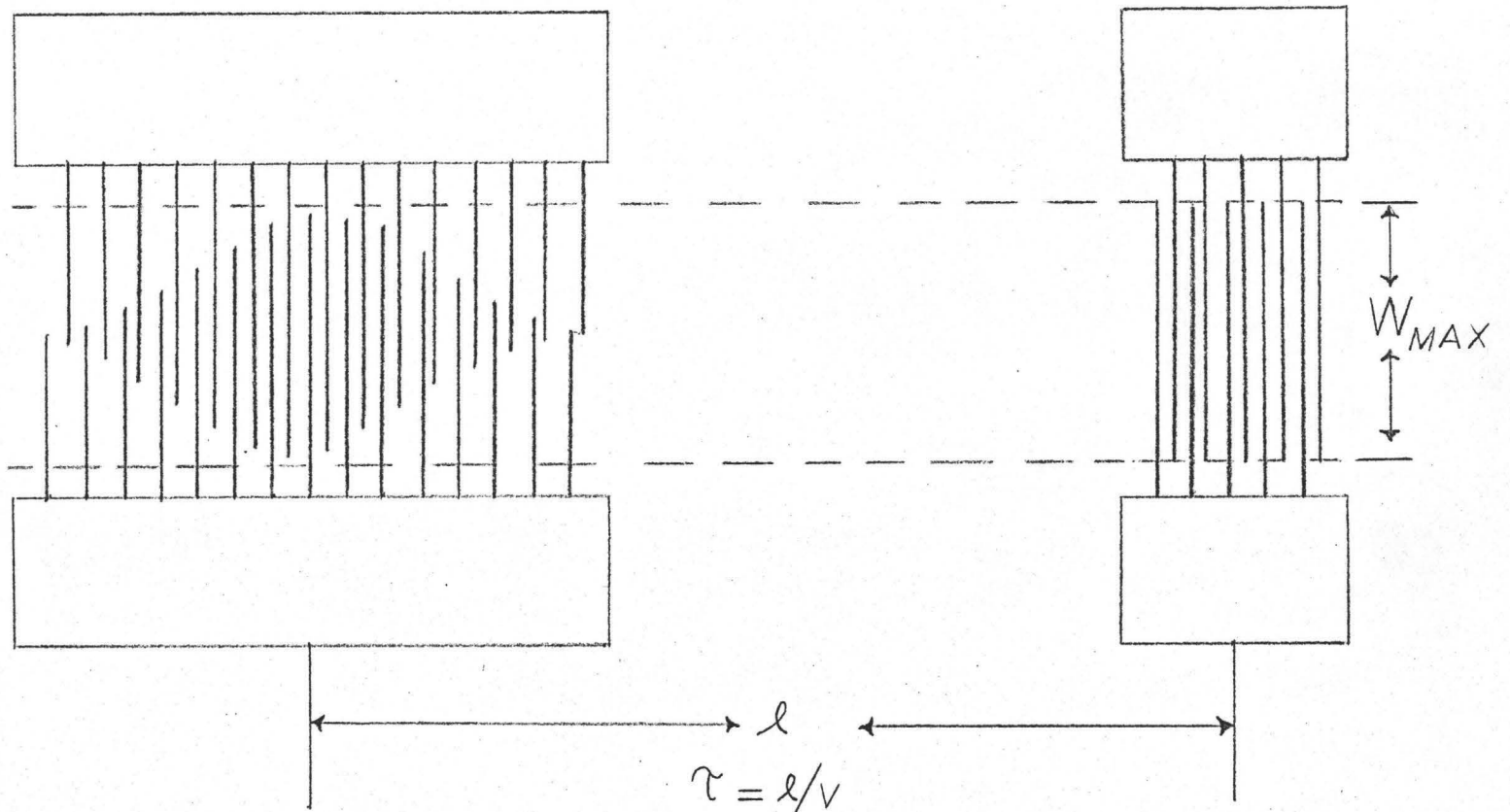


Figure 11: Two-transducer arrangement with the one on the left being of the apodized class.

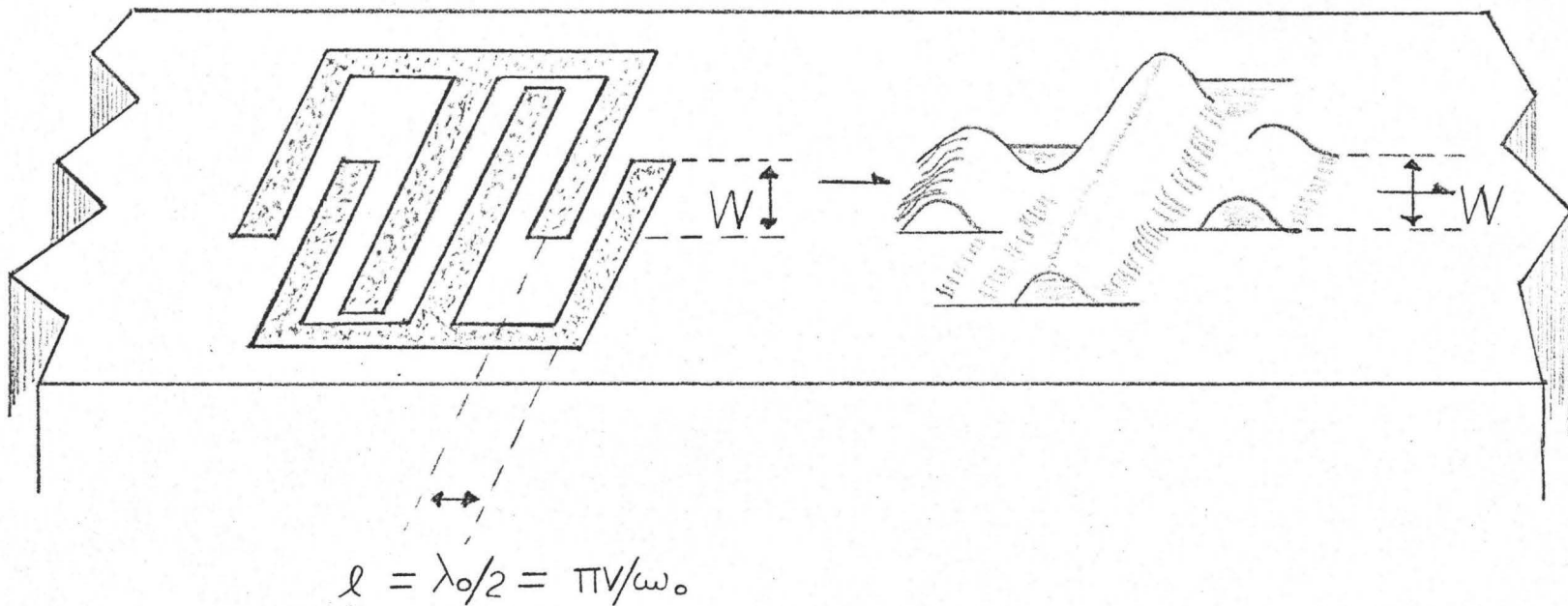


Figure 12: Acoustic field response of an apodized transducer.

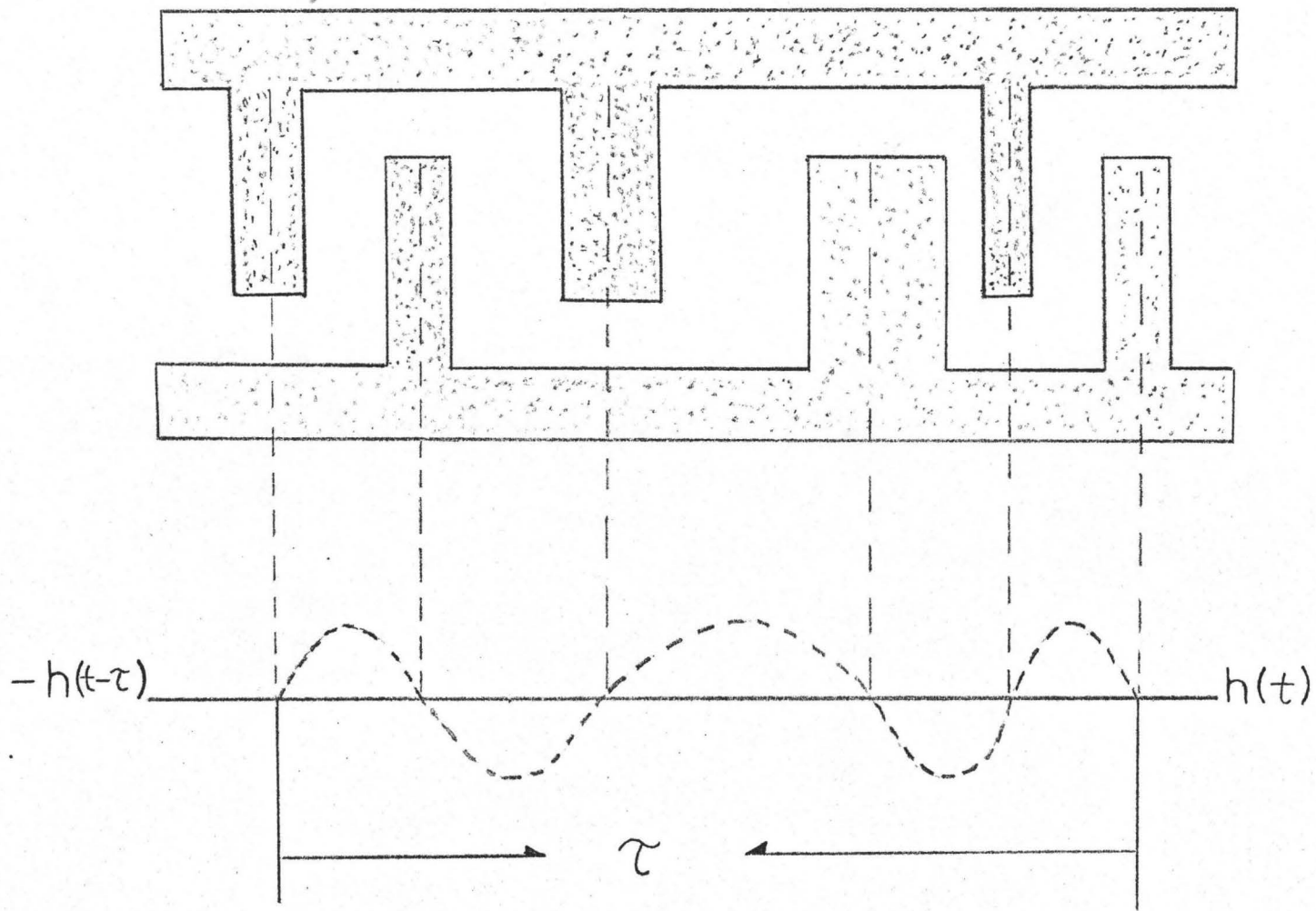


Figure 13: Schematic showing method of time response determination from the transducer geometry.

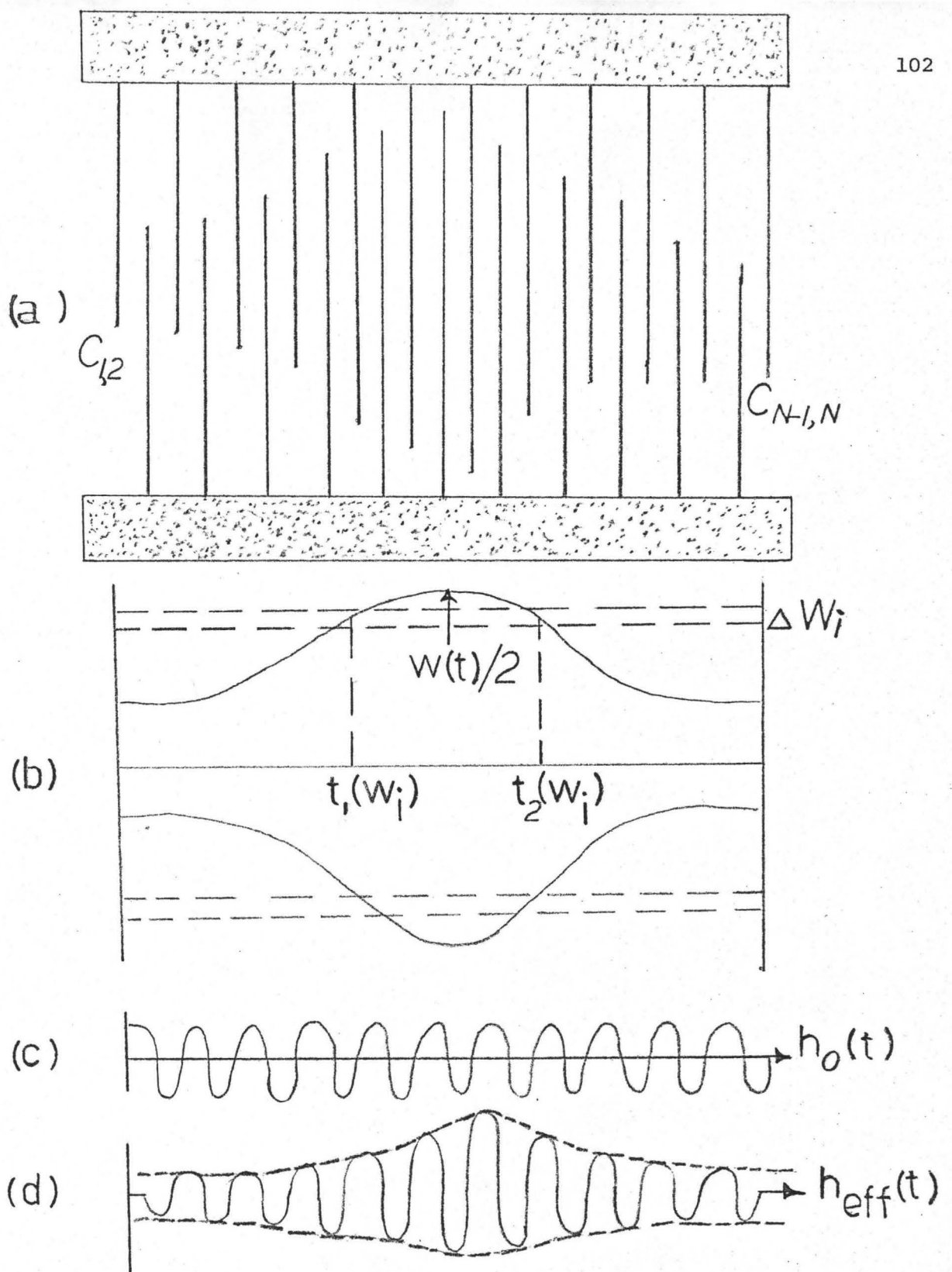


Figure 14: Determination of effective transducer time responses.

- (A) Apodized transducer with constant centre-to-centre finger spacings
- (B) Demonstration of strip analysis technique
- (C) Time response associated with the strip shown in (B)
- (D) Effective time response of the apodized transducer in (A)

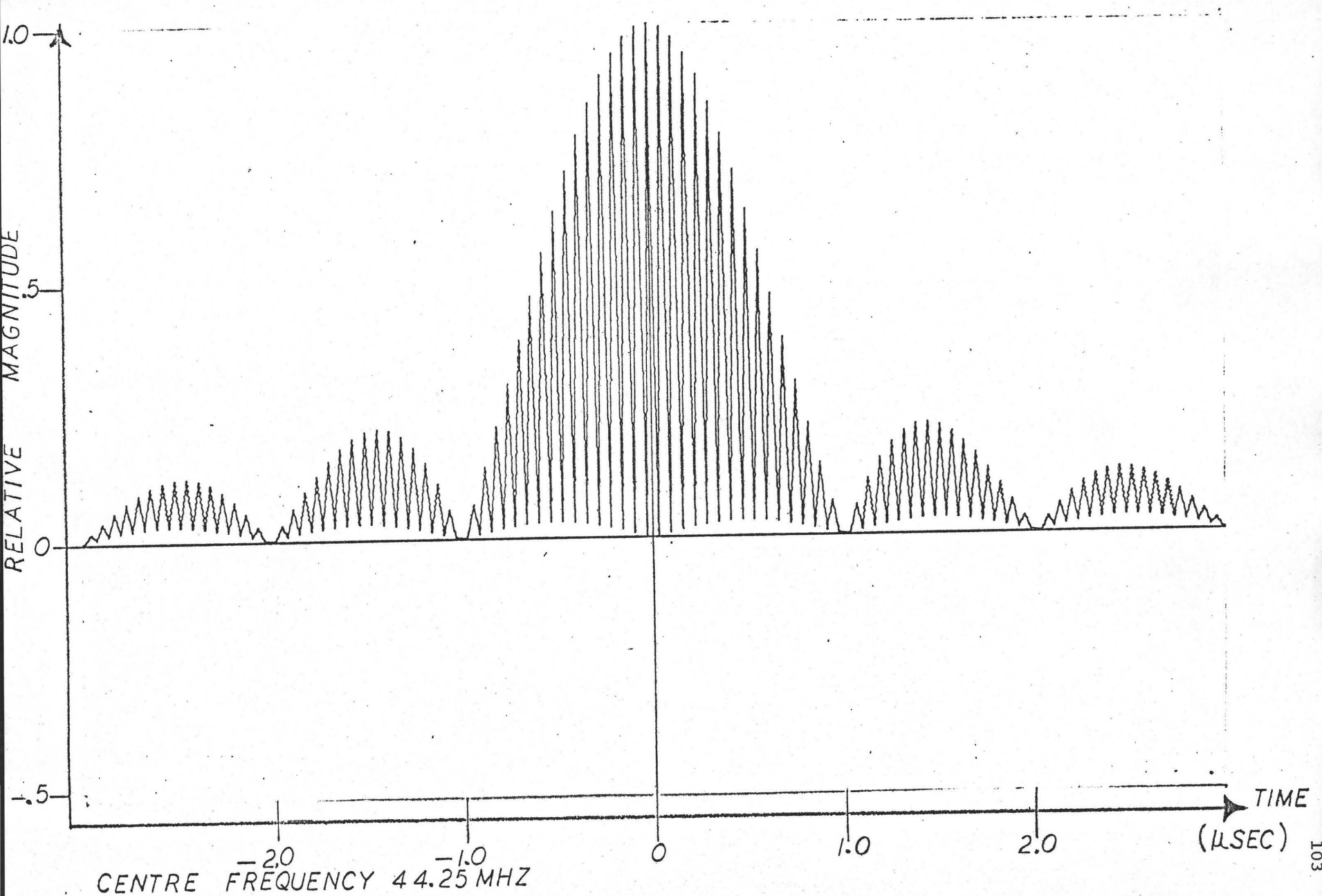


Figure 15: Magnitude of time response for a rectangular bandpass, linear phase filter.

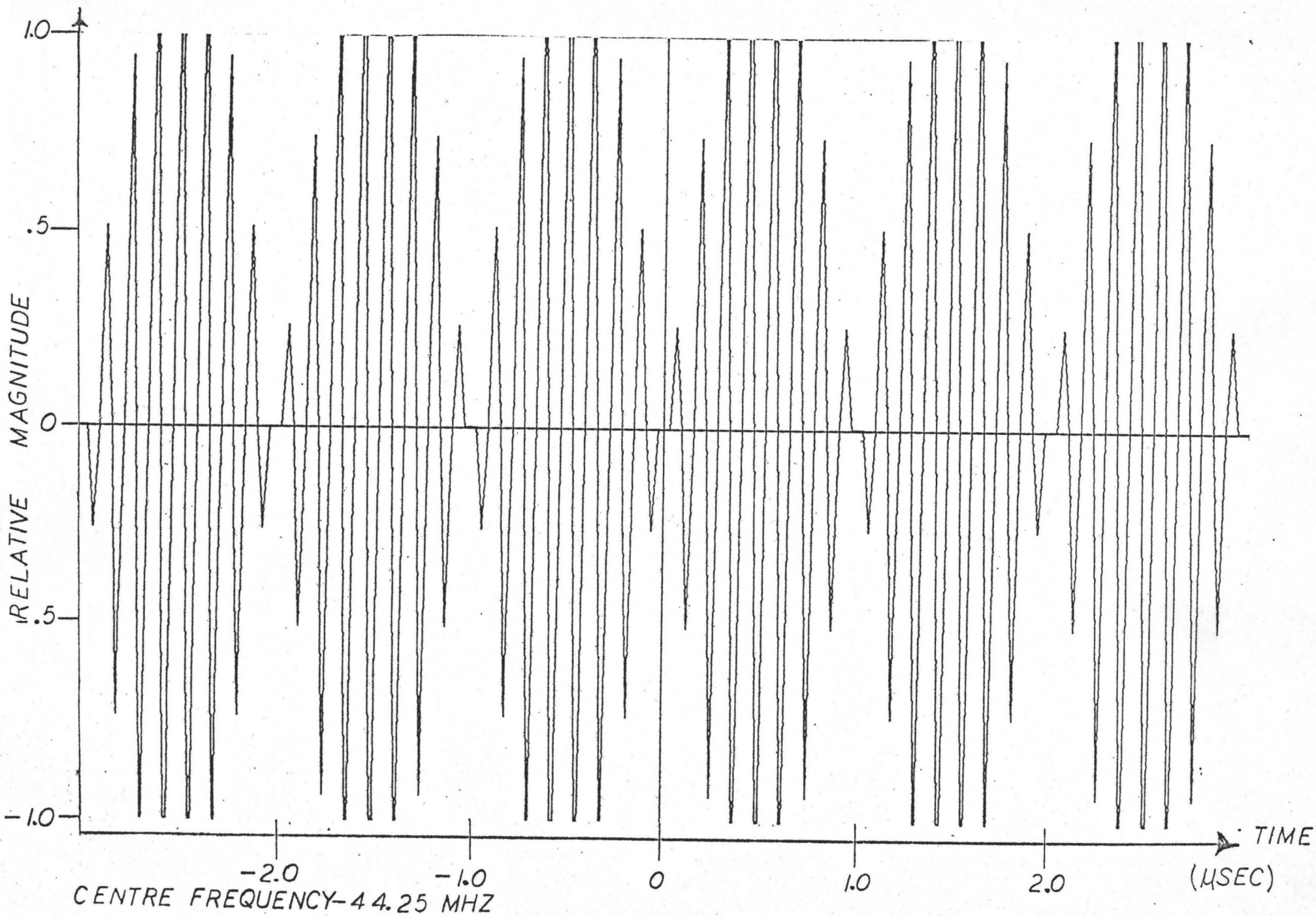


Figure 16: Imaginary component of time response for rectangular bandpass, linear phase filter.

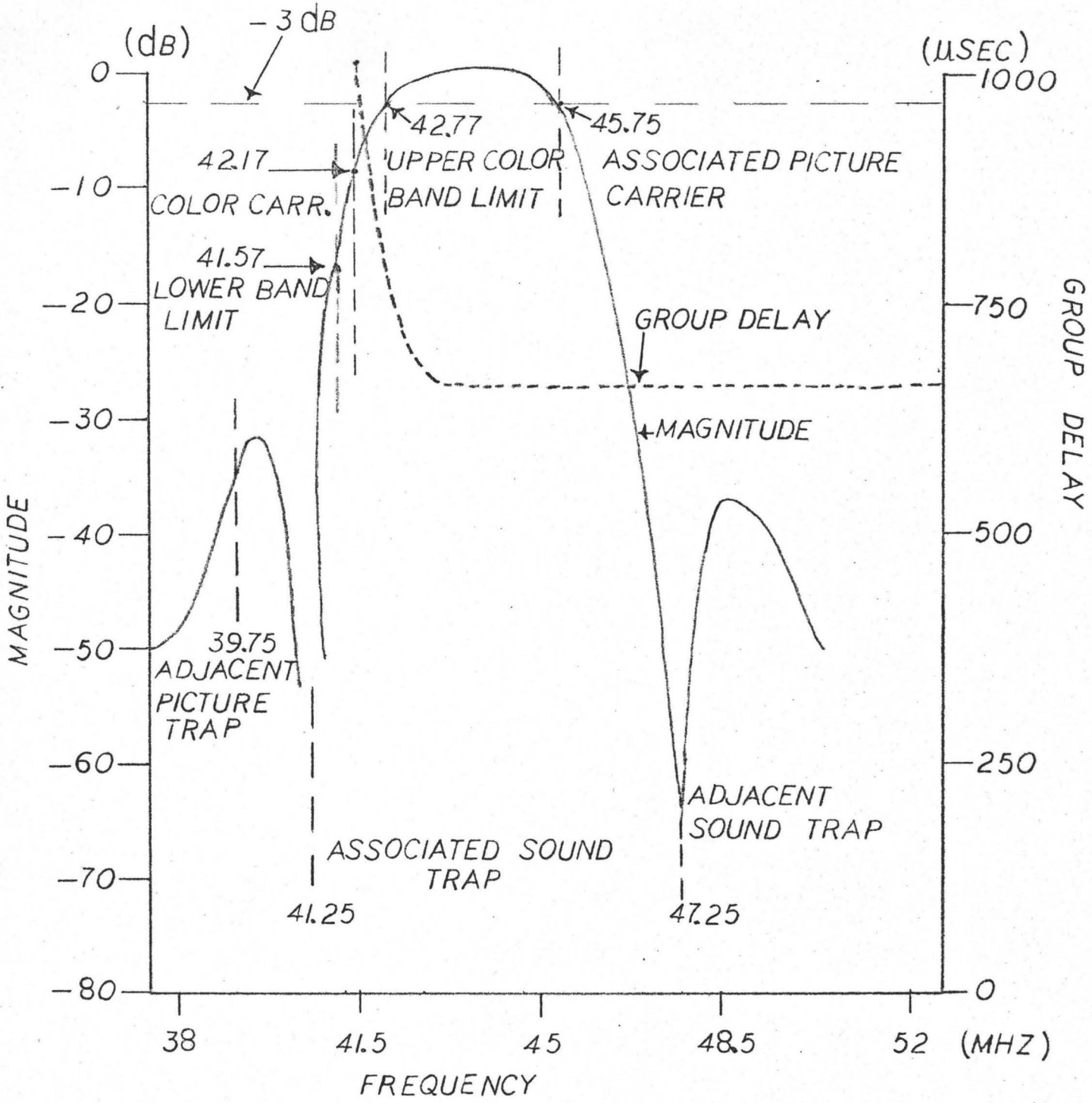
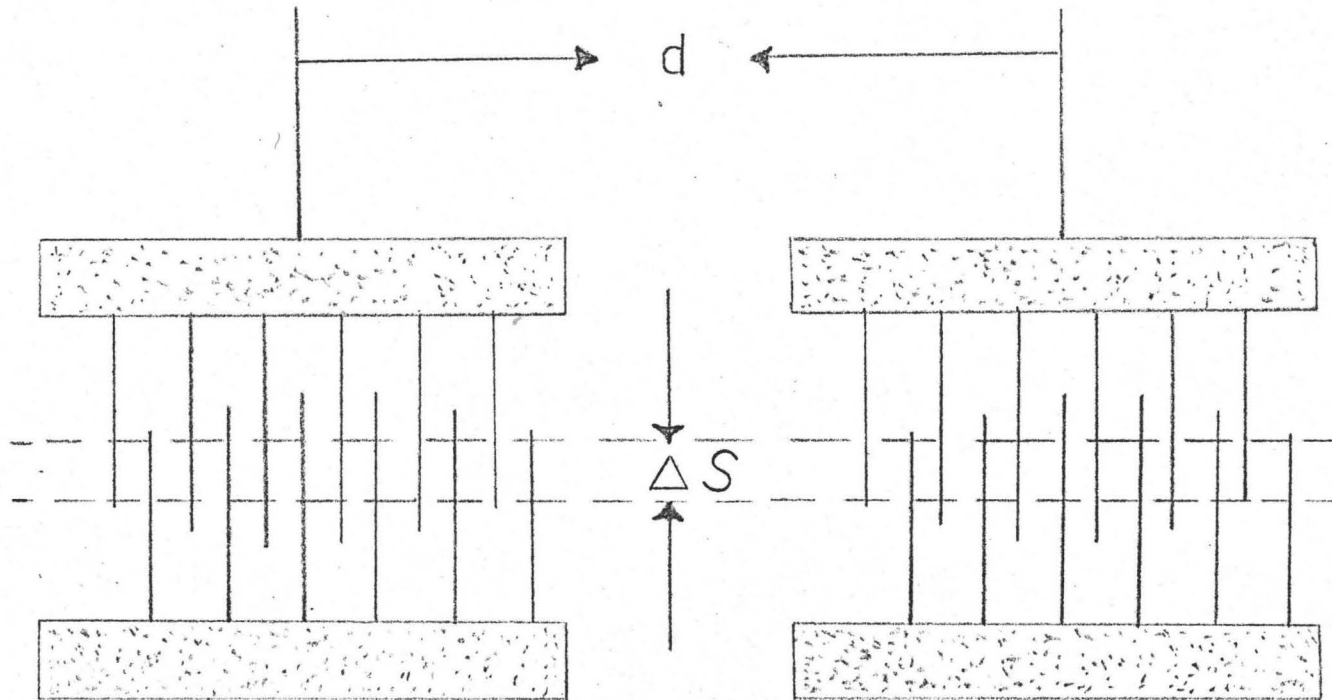


Figure 17: "Haystack" colour T.V. video I.F. response.  
 (reconstructed from information provided by  
 Electrohome Electronics Corporation)



$$H_{TOT}(\omega) = \sum_{S=1}^Q H_{1S}^{\star}(\omega) H_{2S}(\omega) \exp(-jkd)$$

Figure 18: Modeling the frequency response of two apodized transducers.

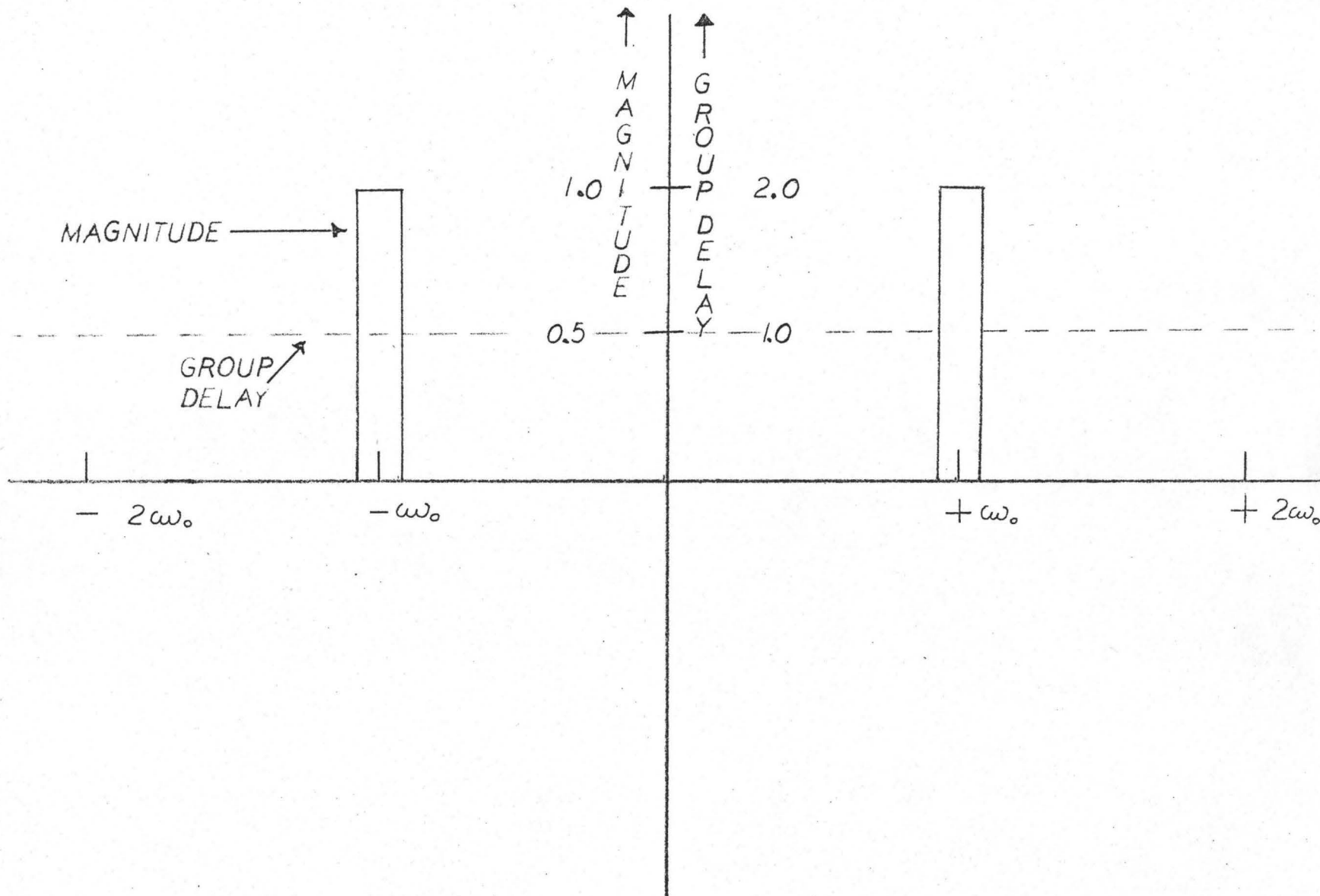
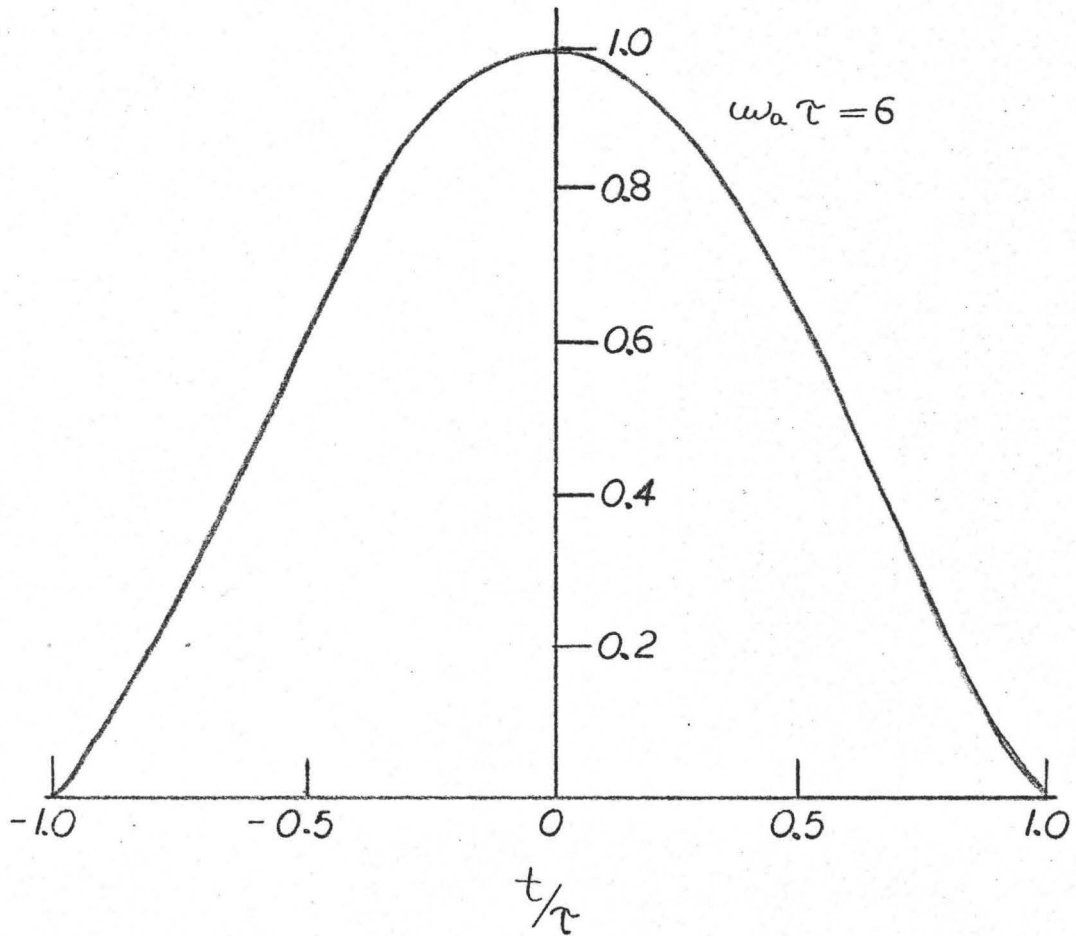


Figure 19: Form of the initial input data to the Fast Fourier Programme.



KAISER WEIGHTING FUNCTION  $W(t)$

Figure 20: The Kaiser Weighting Function.

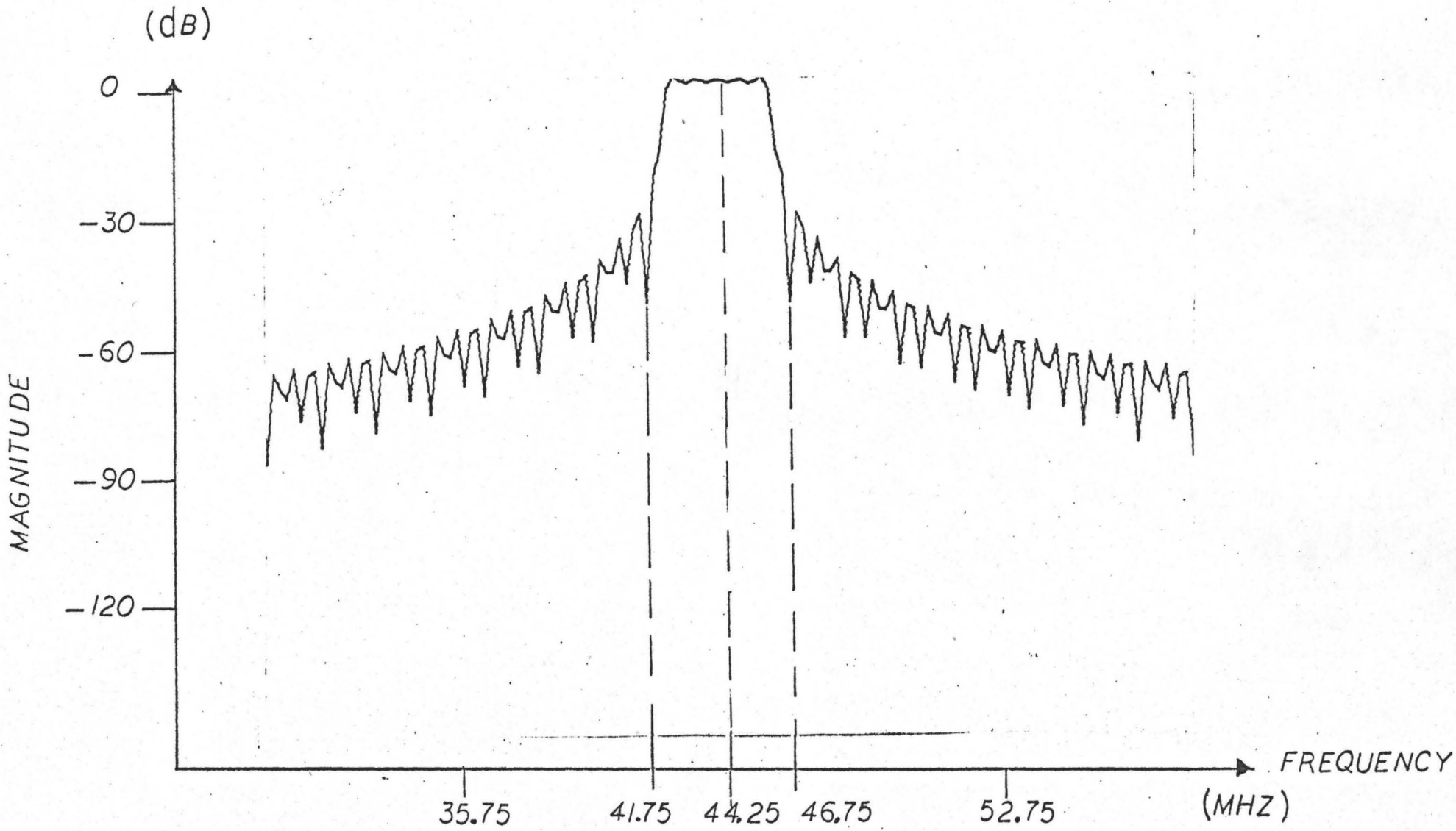


Figure 21: Effect on frequency response due to time response truncation after fifth zero.

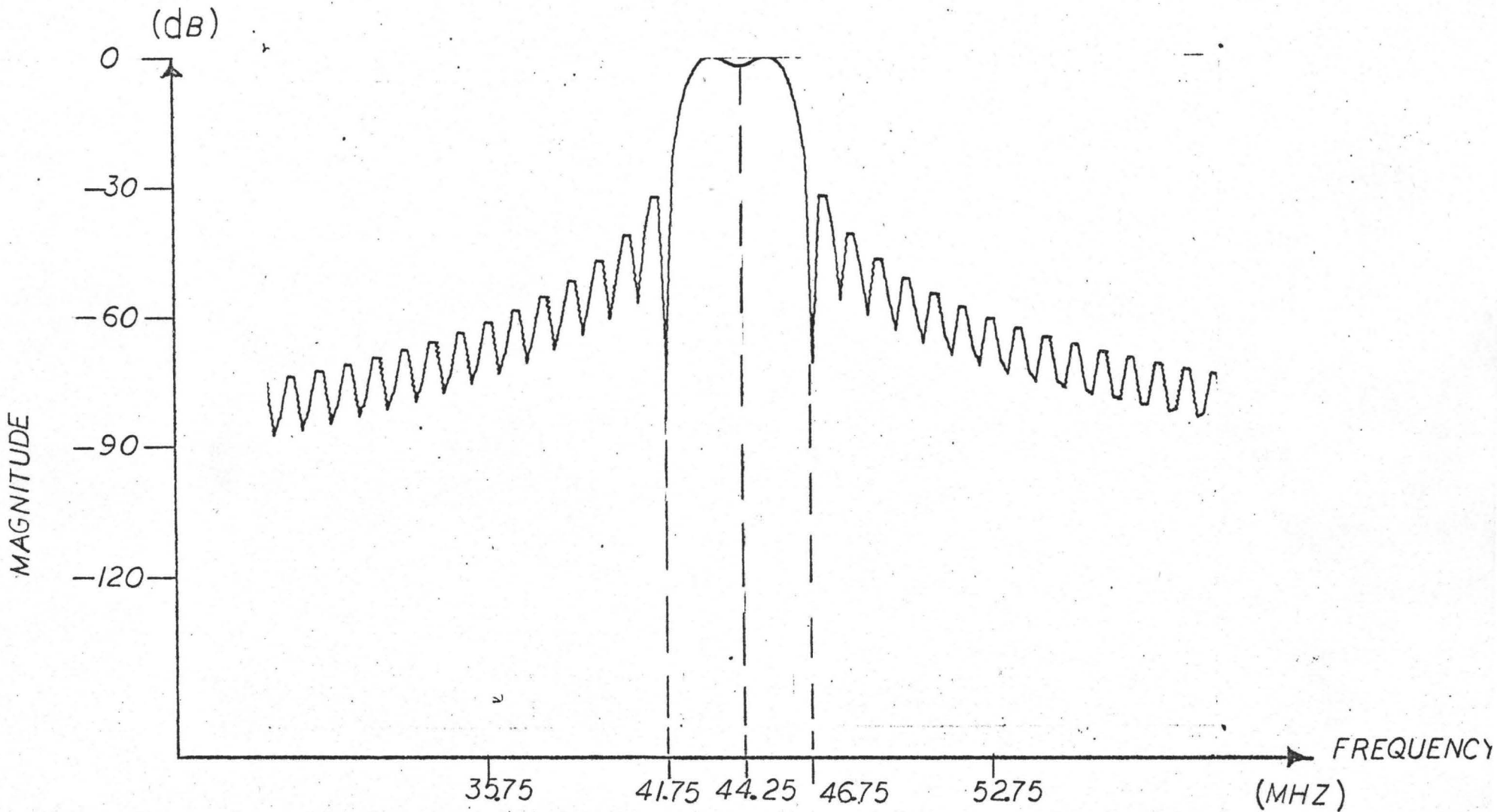


Figure 22: Effect on frequency response due to time response truncation after the second zero.

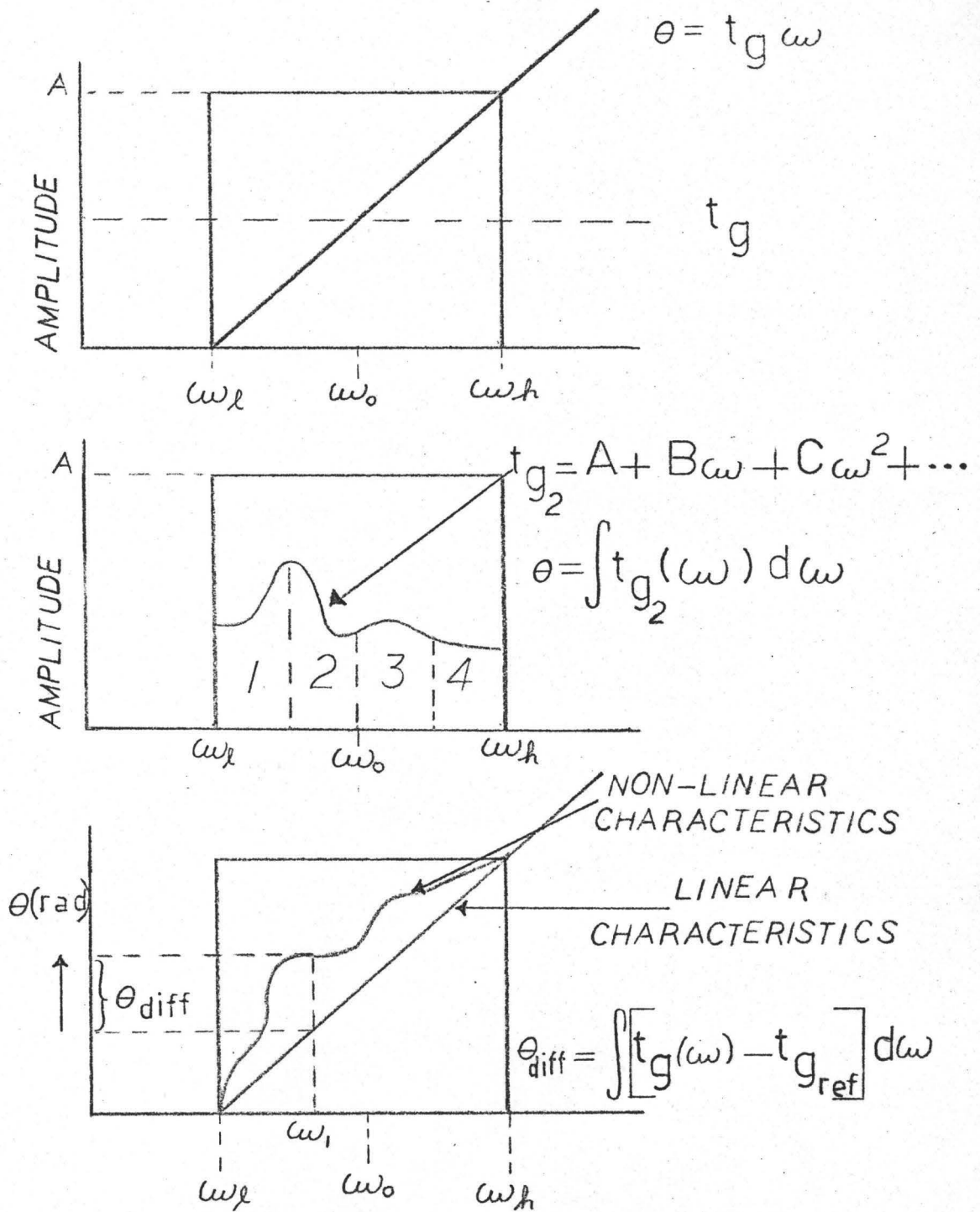


Figure 23: Determining the phase from the group delay.

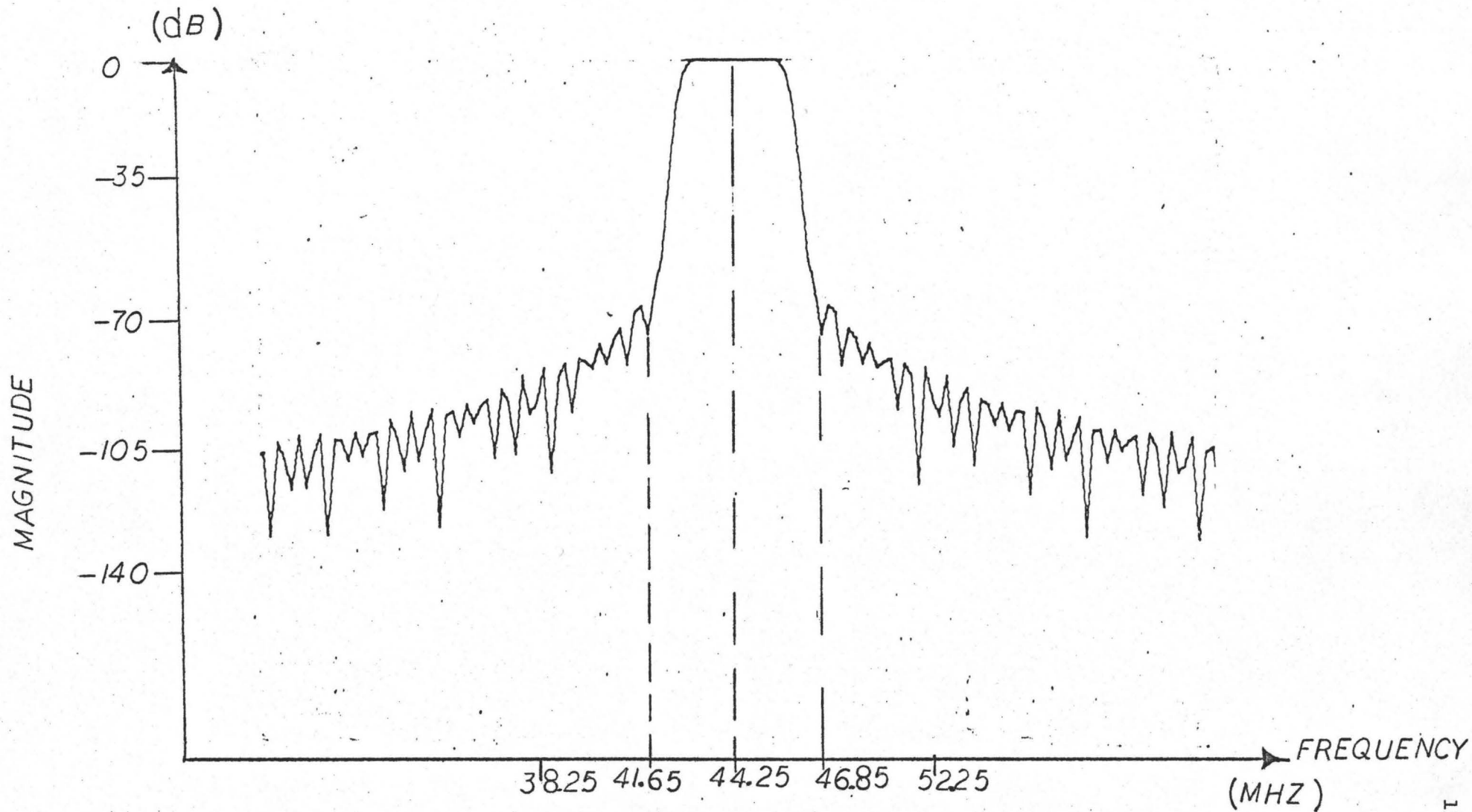


Figure 24: Kaiser-optimized frequency response for truncation after the fifth zero.

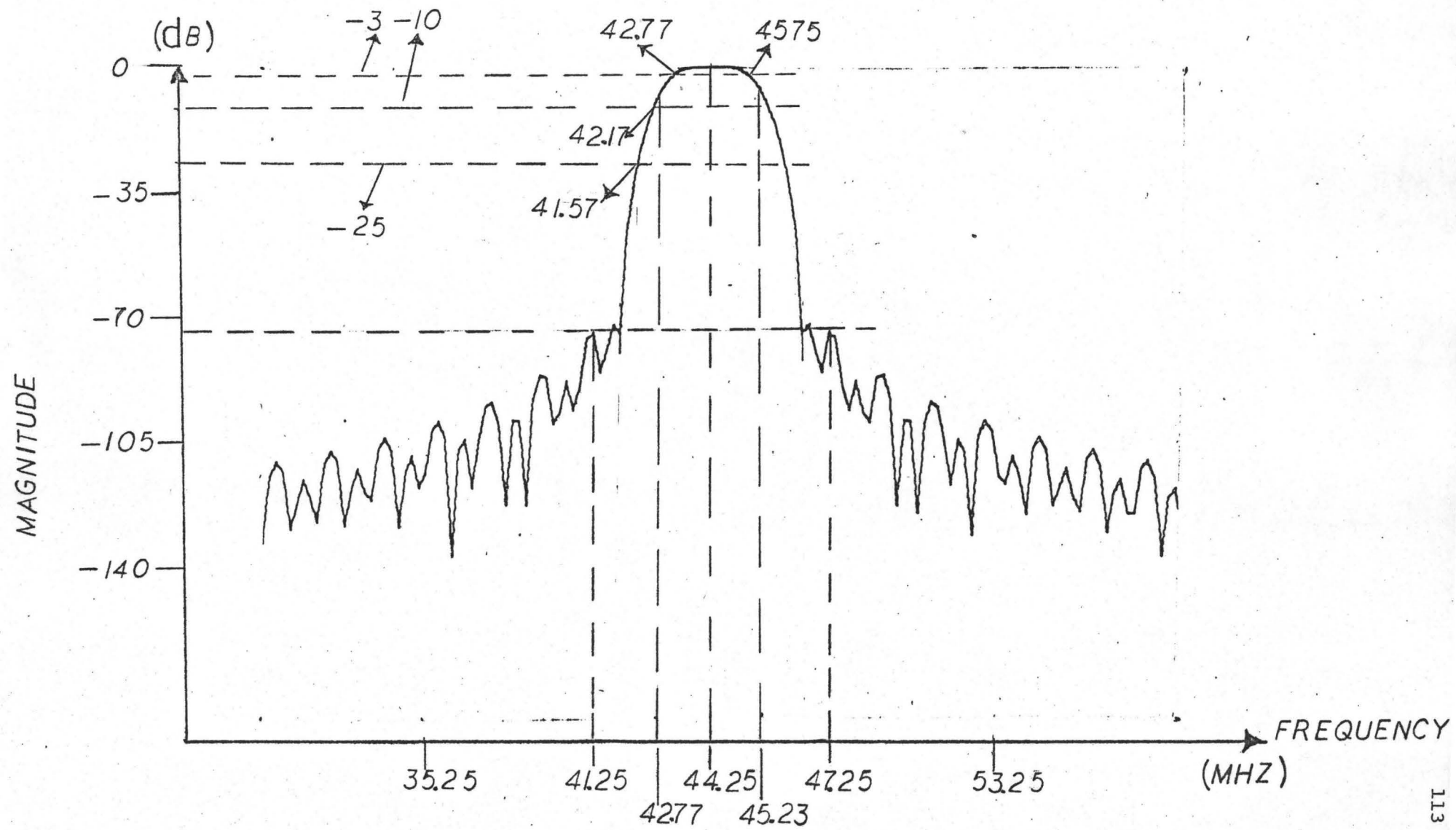


Figure 25: Kaiser-optimized frequency response for truncation after the second zero.

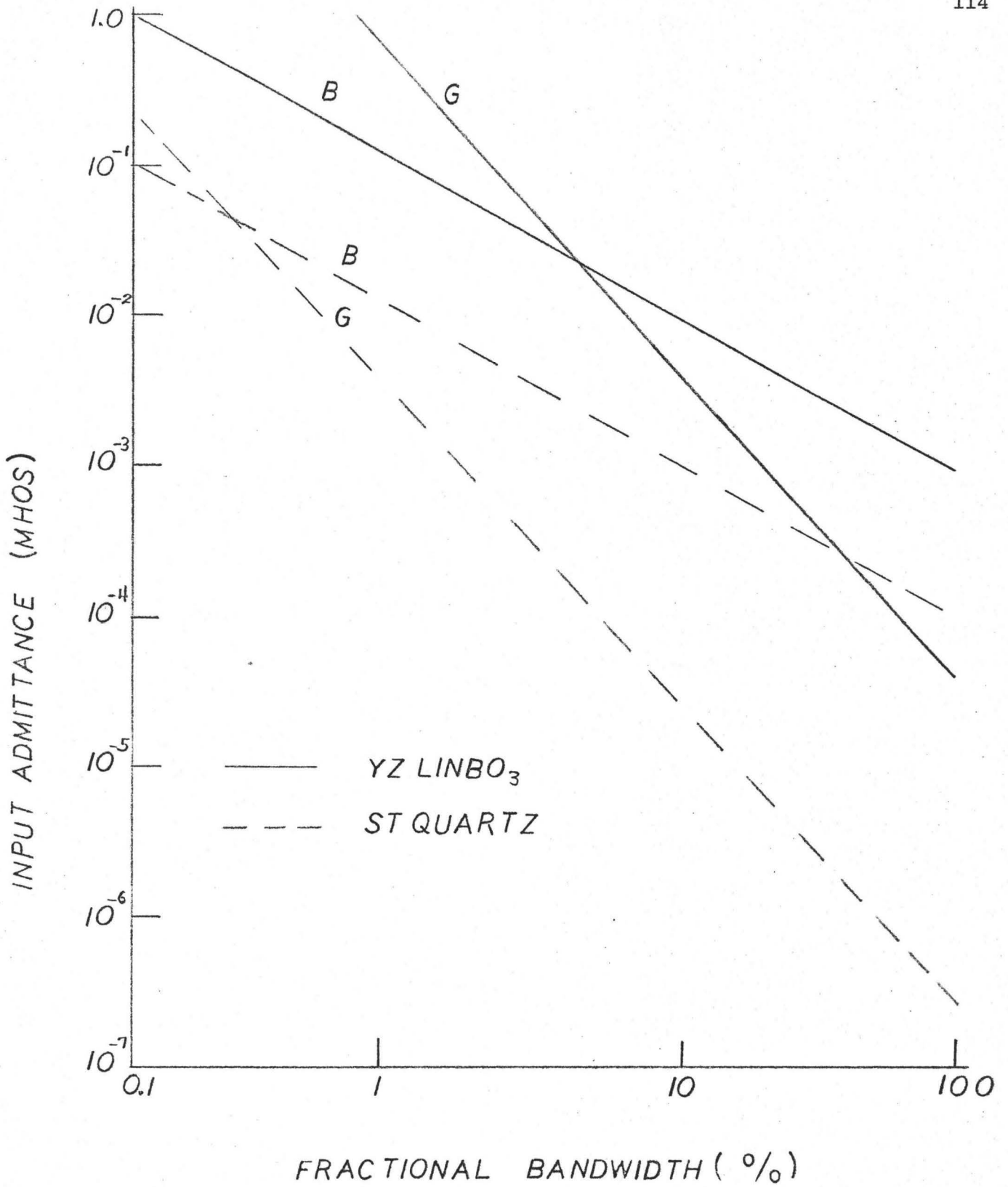
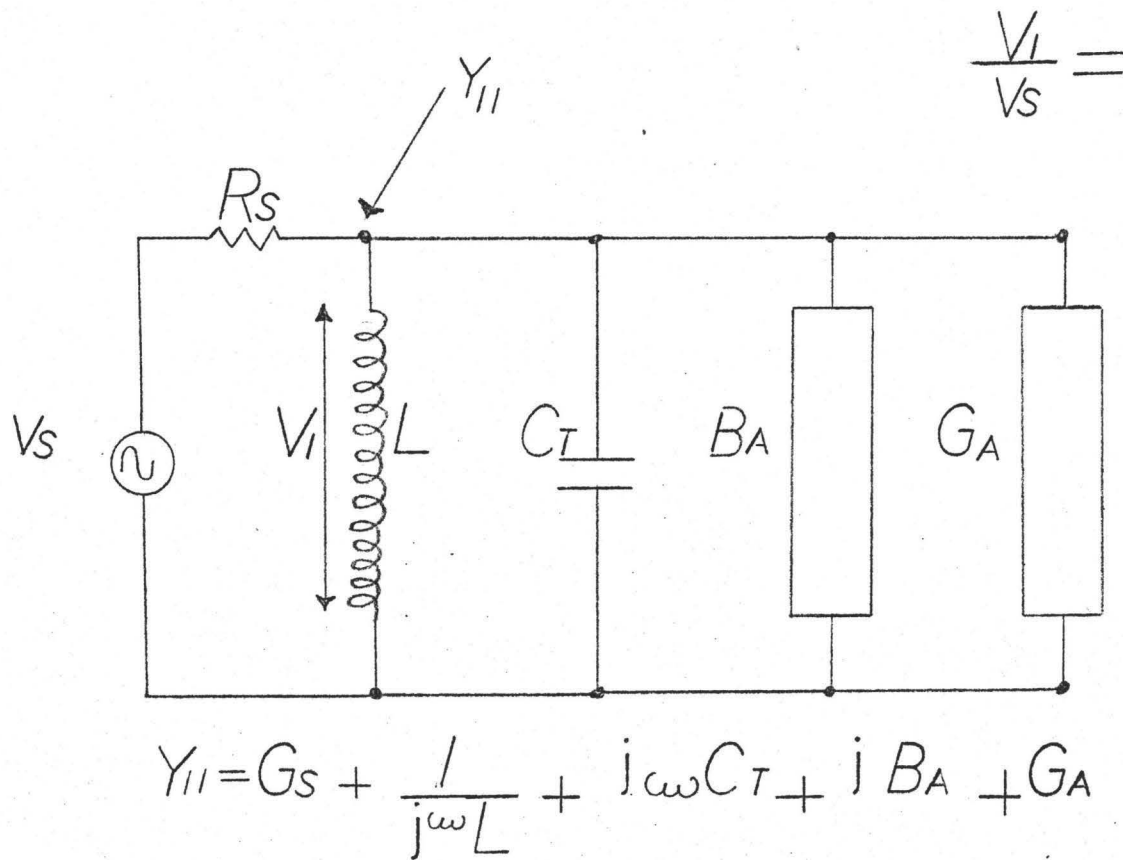


Figure 26: Universal admittance curves for surface-wave transducers on Lithium Niobate and Quartz substrates.



$$\frac{V_1}{V_s} = \frac{G_s}{G_s + \frac{1}{j\omega L} + j\omega C_T + jB_A + G_A}$$

$$Y_{11} = G_s + \frac{1}{j\omega L} + j\omega C_T + jB_A + G_A$$

Figure 27: Electrical Matching for Input Transducers.

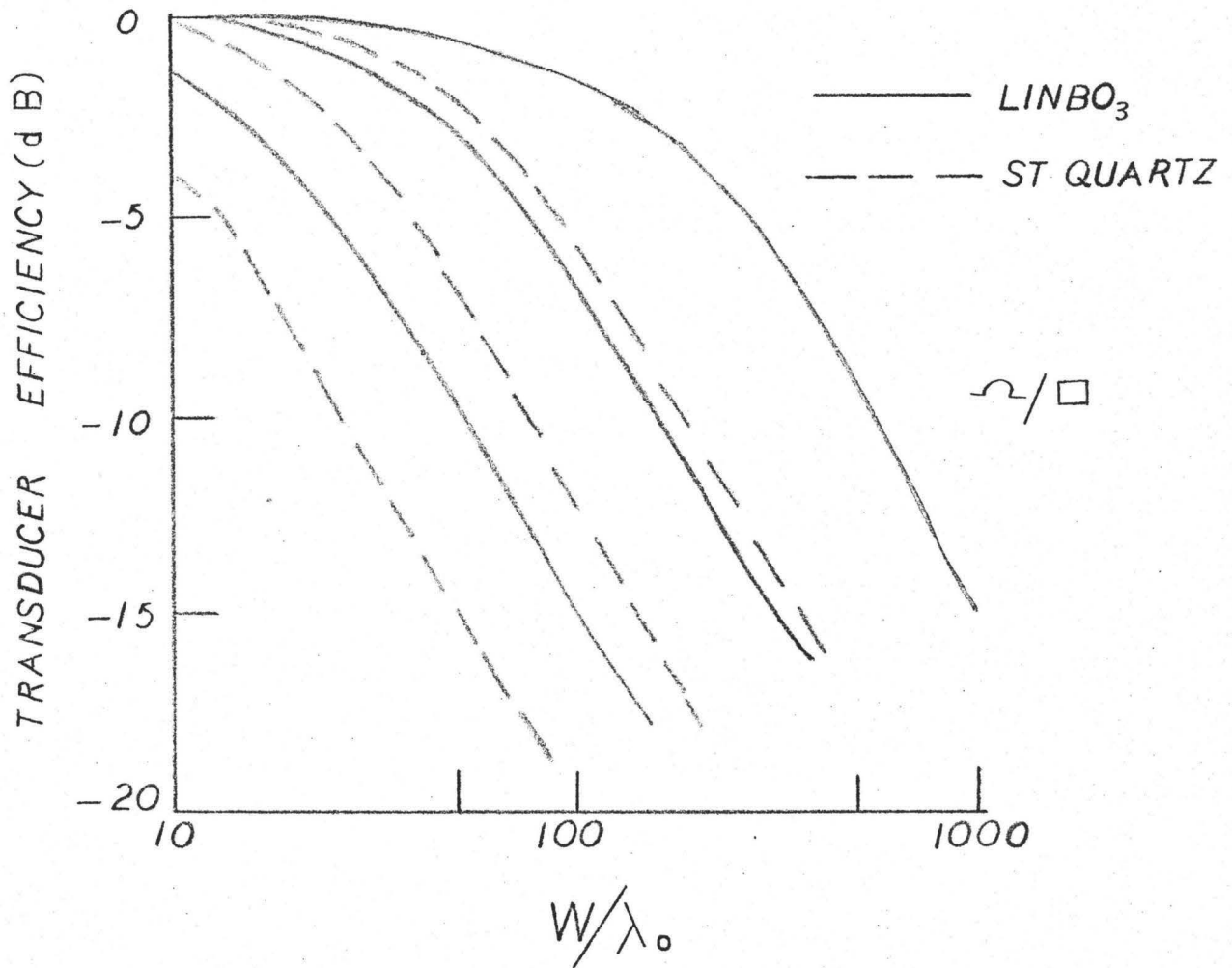


Figure 28: Transducer Efficiency versus Beamwidth.

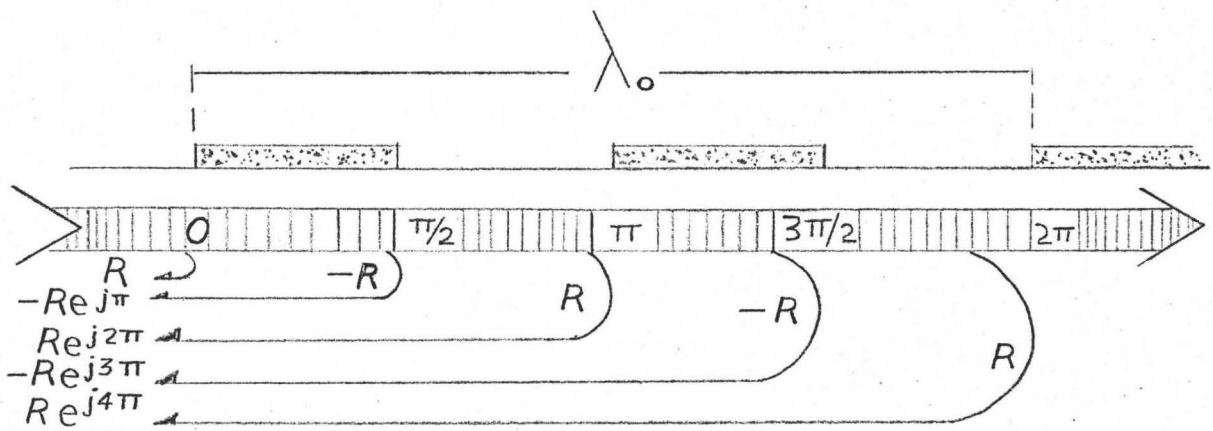


Figure 29: Finger-edge reflection from a surface wave transducer.

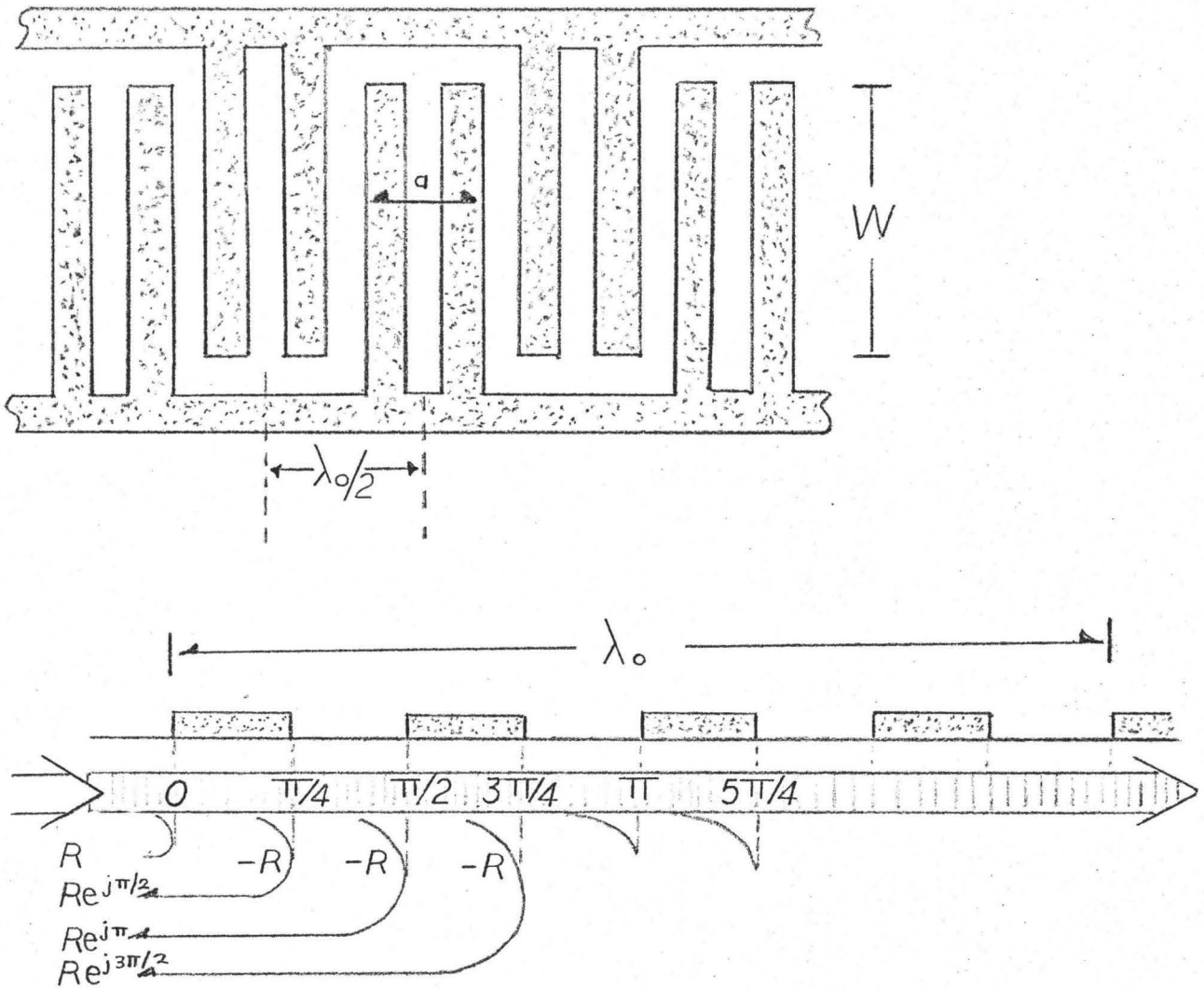


Figure 30: Use of split-finger transducer geometry to reduce effects of finger-edge reflections.

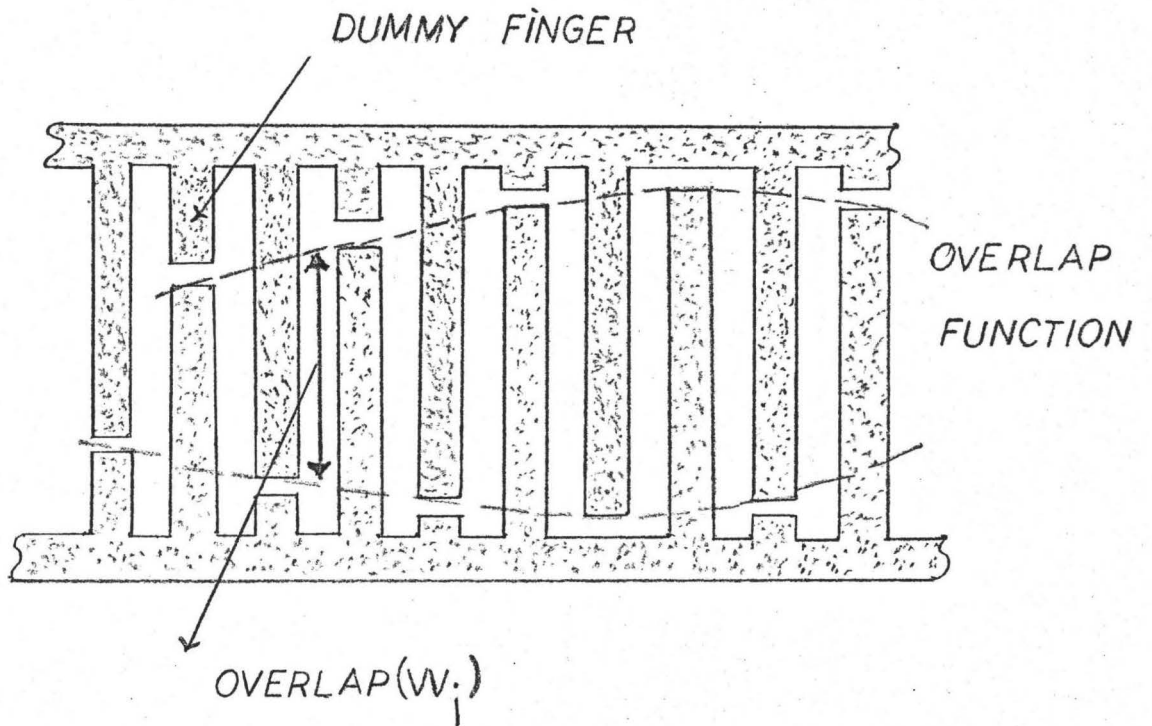


Figure 31: Dummy fingers used to reduce wavefront distortion.

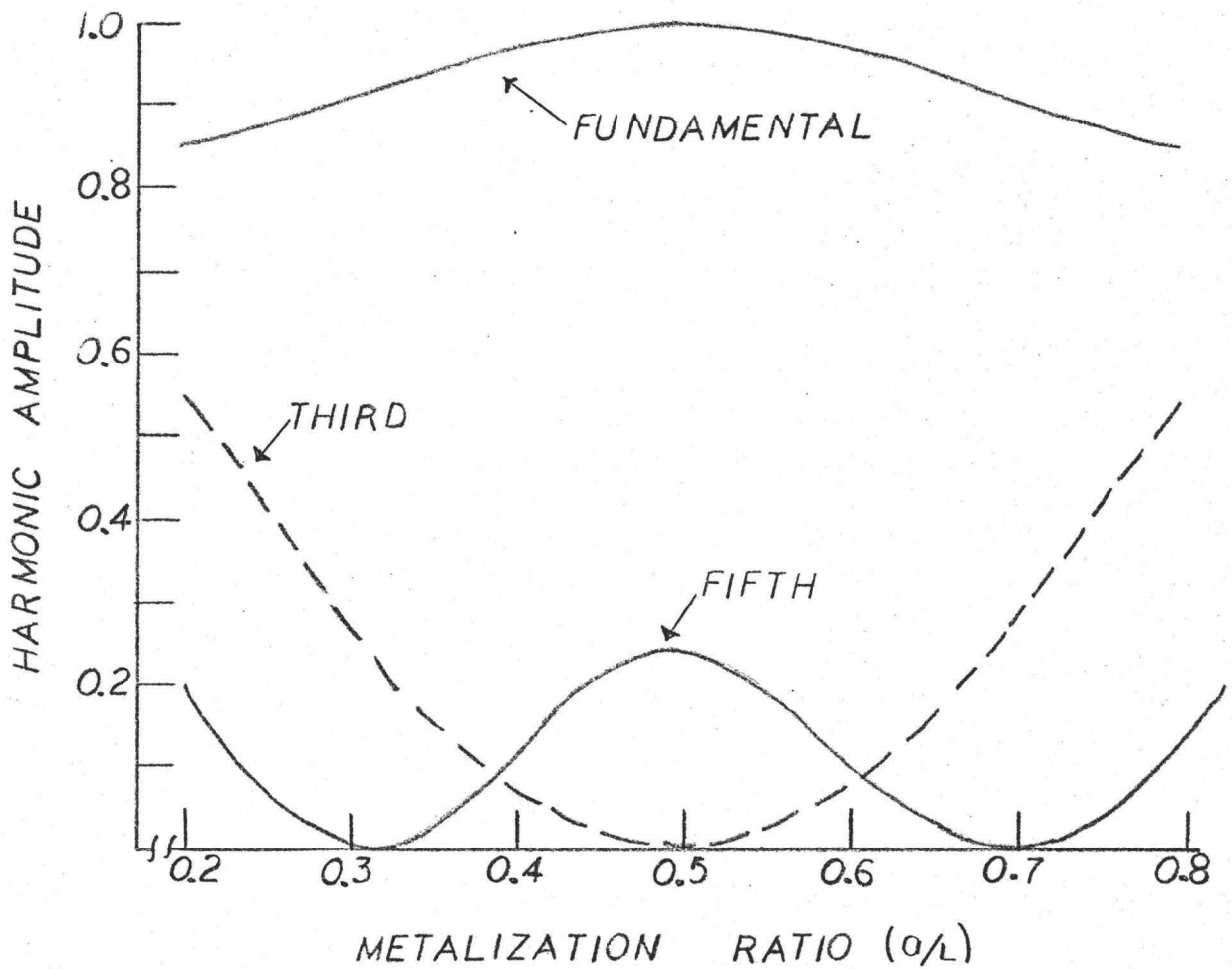


Figure 32: Harmonic amplitude versus metalization ratio for fundamental, third and fifth harmonic operation of the transducer.

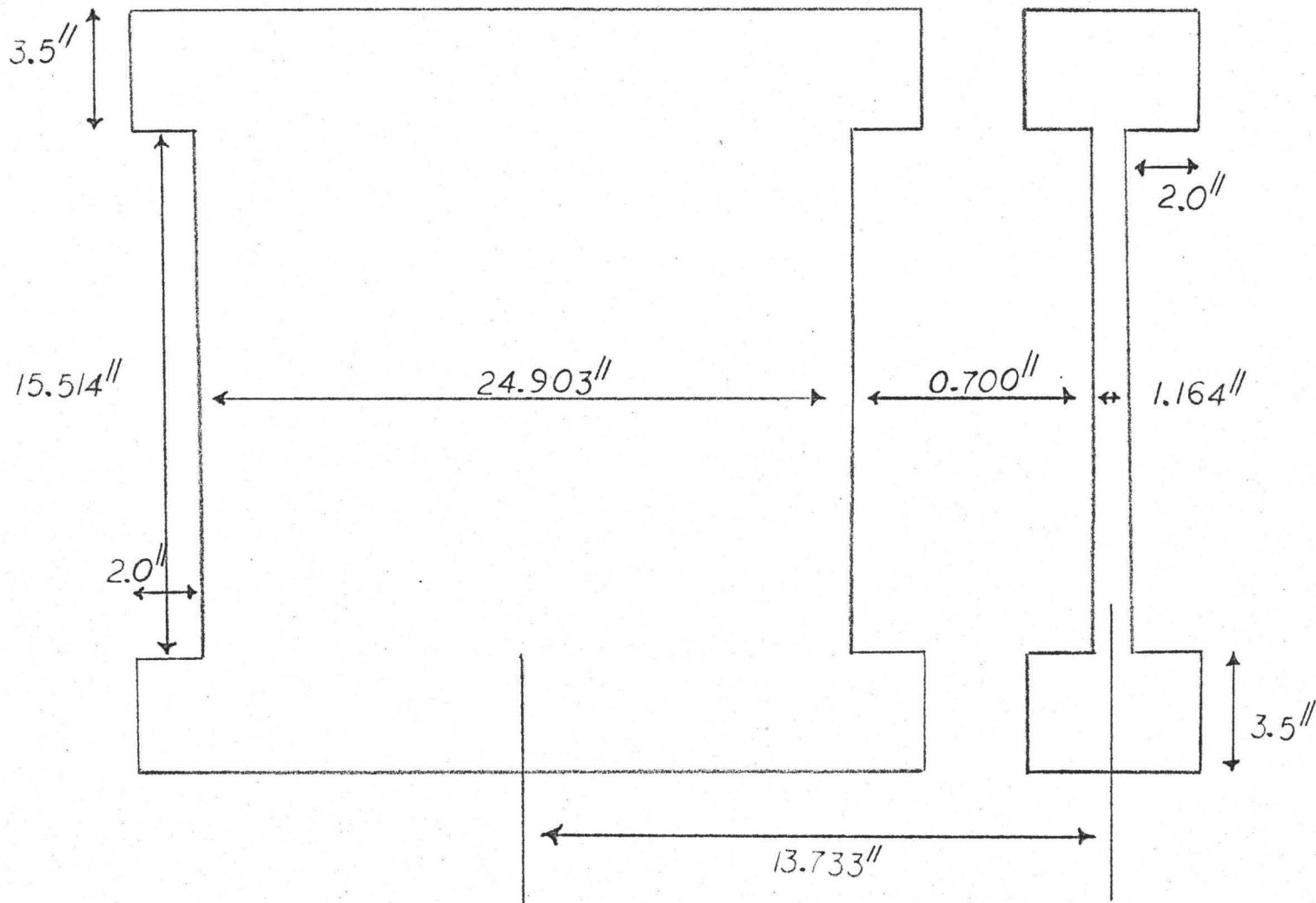


Figure 33: Geometrical outline for filter #1-100x.

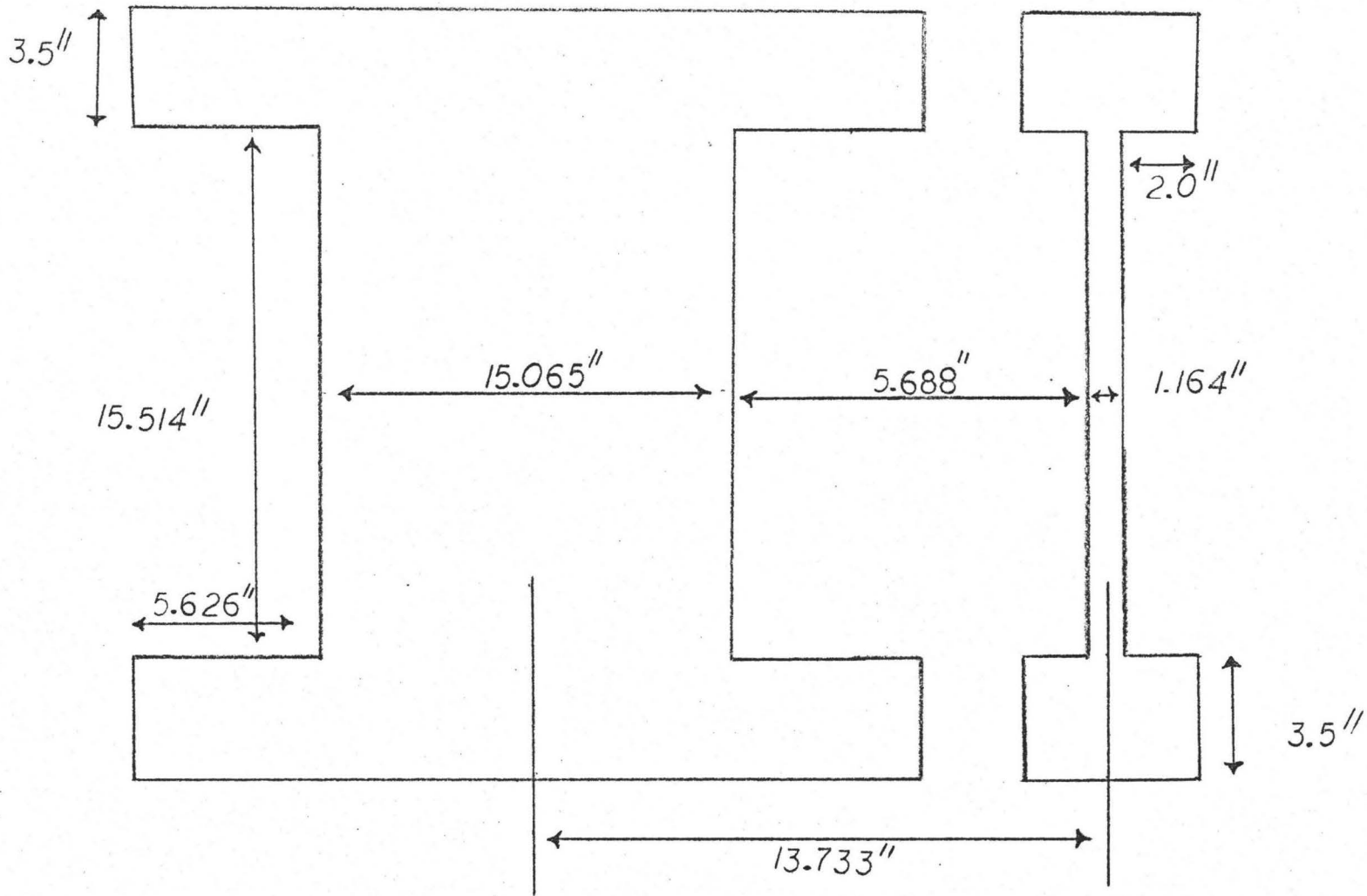


Figure 34: Geometrical outline for filter #2-100x.

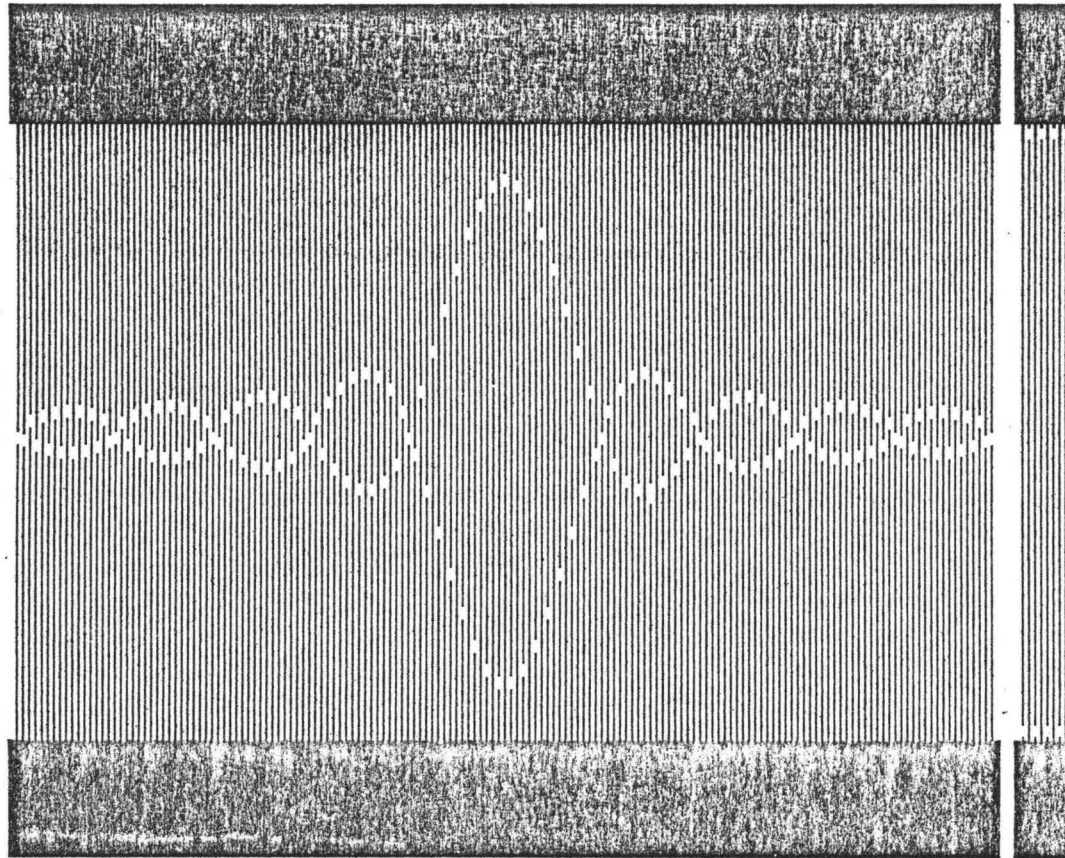


Figure 35: Mask for filter #1-5x.

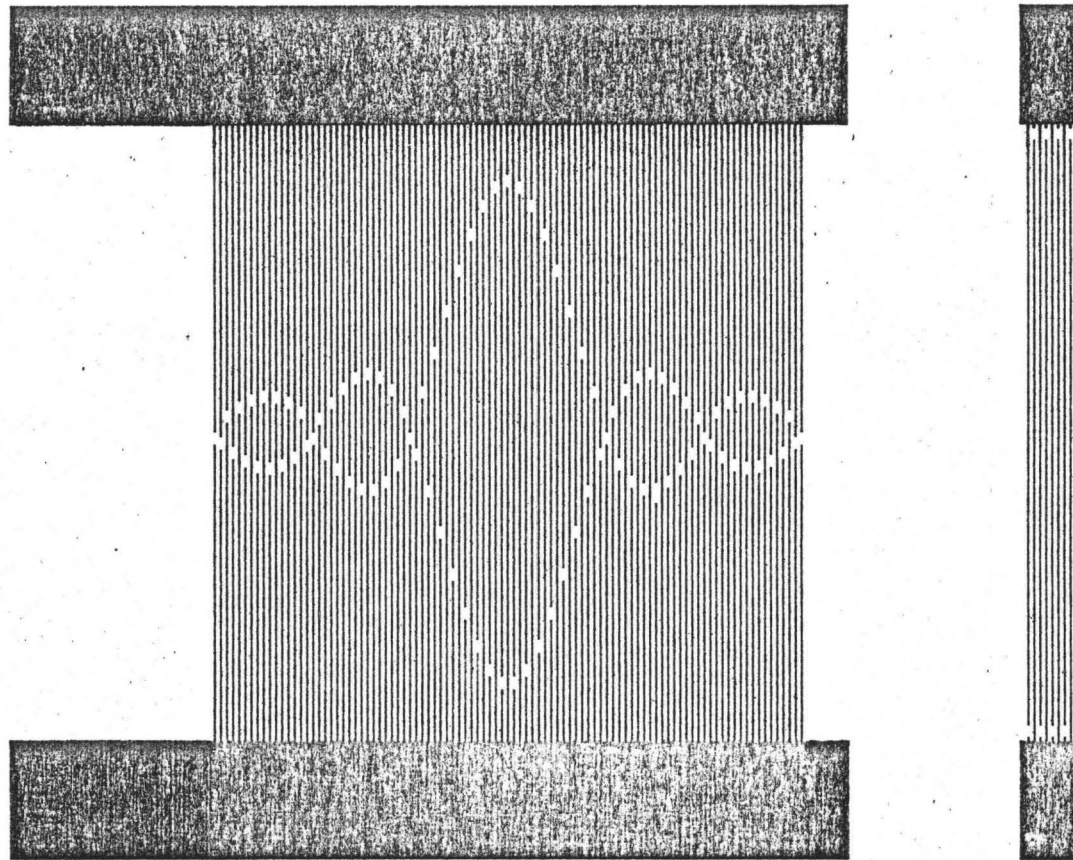


Figure 36: Mask for filter #2-5x.

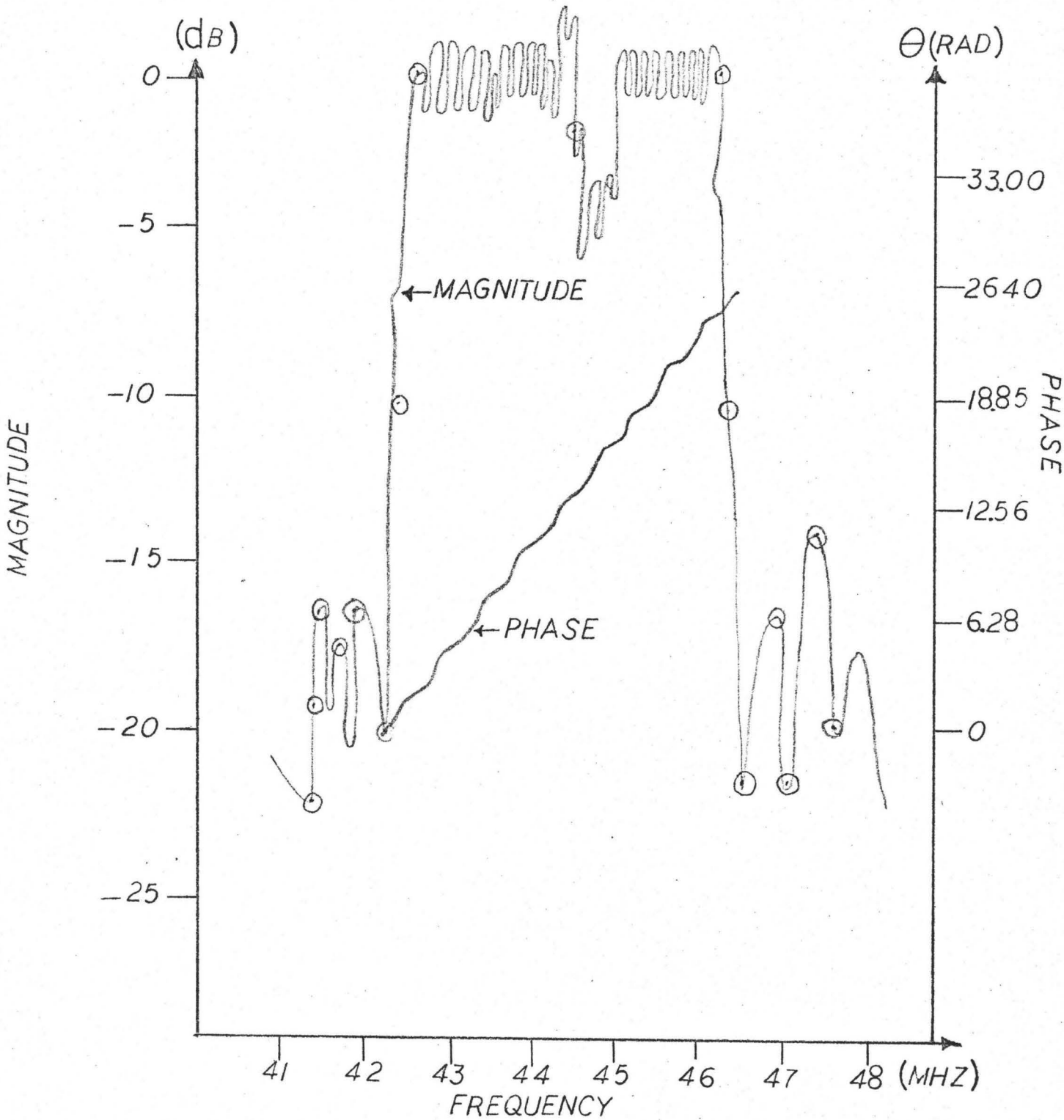


Figure 37: Observed response of filter #1.

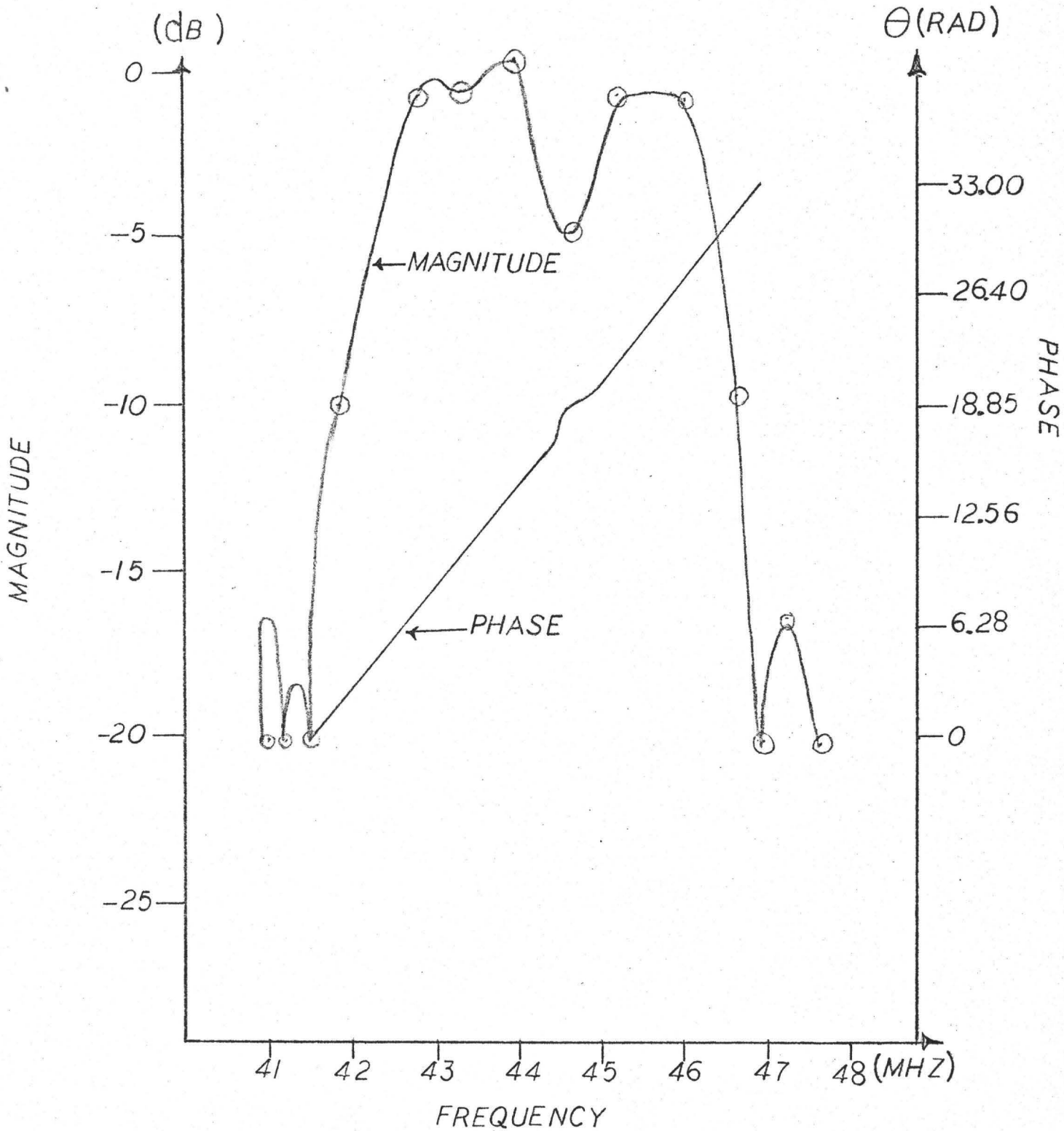
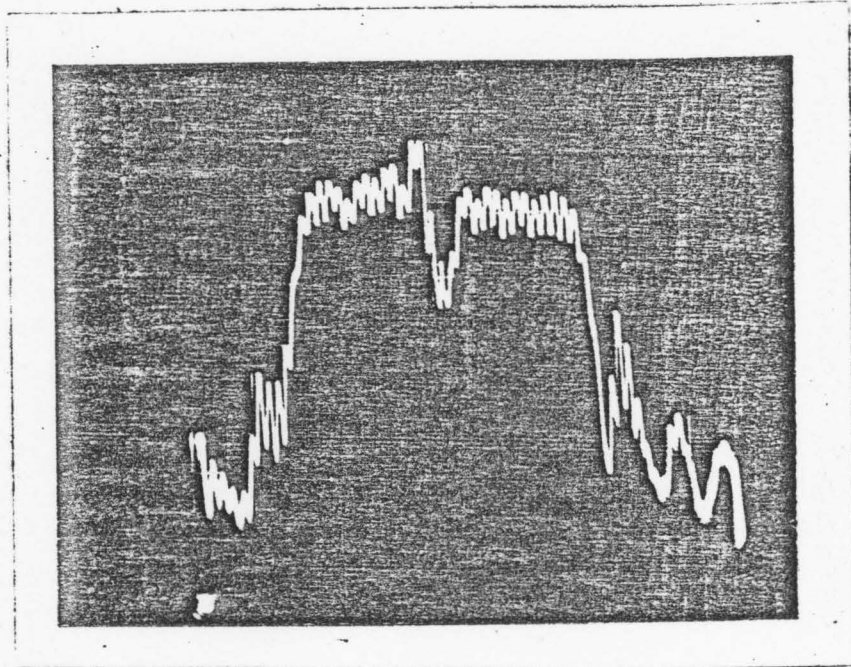
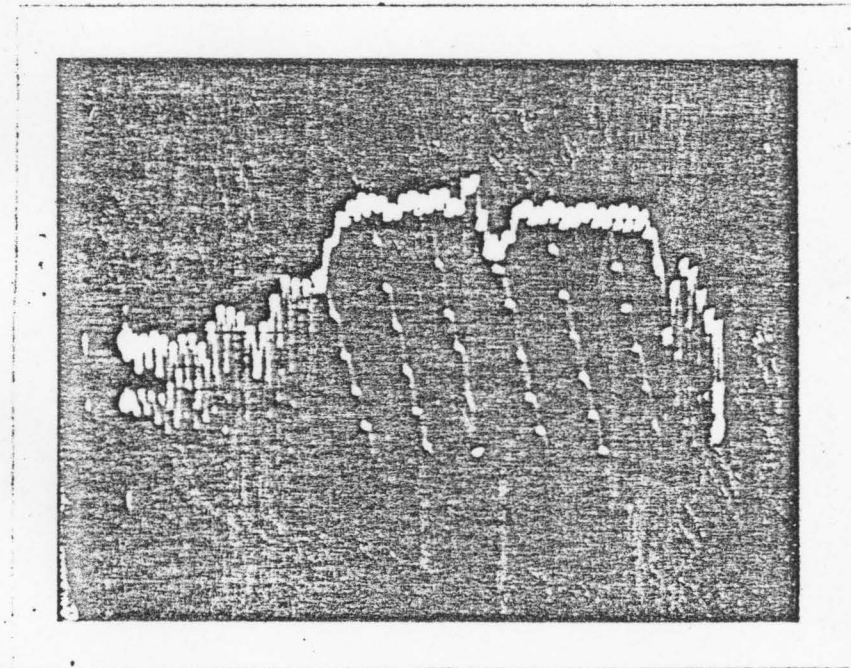


Figure 38: Observed response of filter #2.



(a)

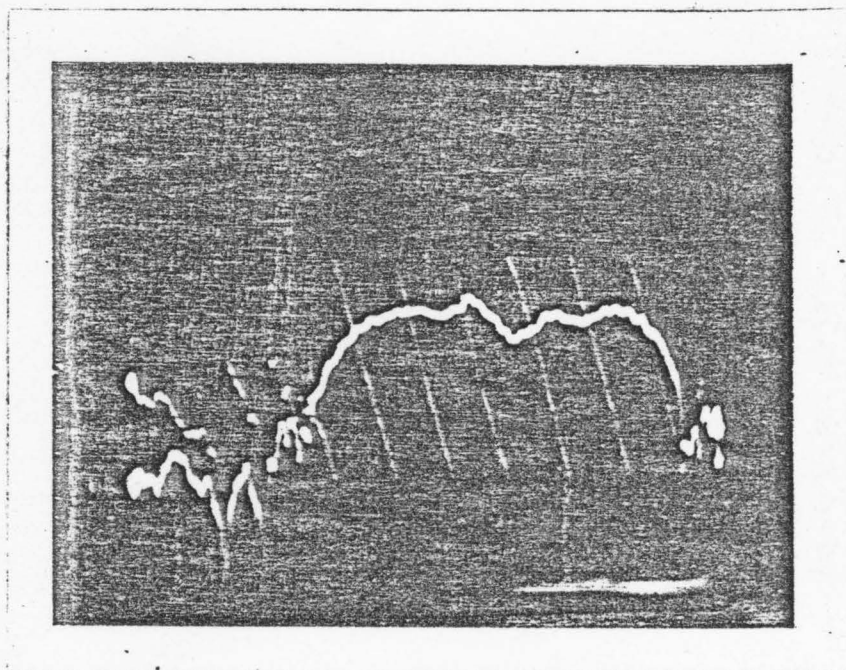


(b)

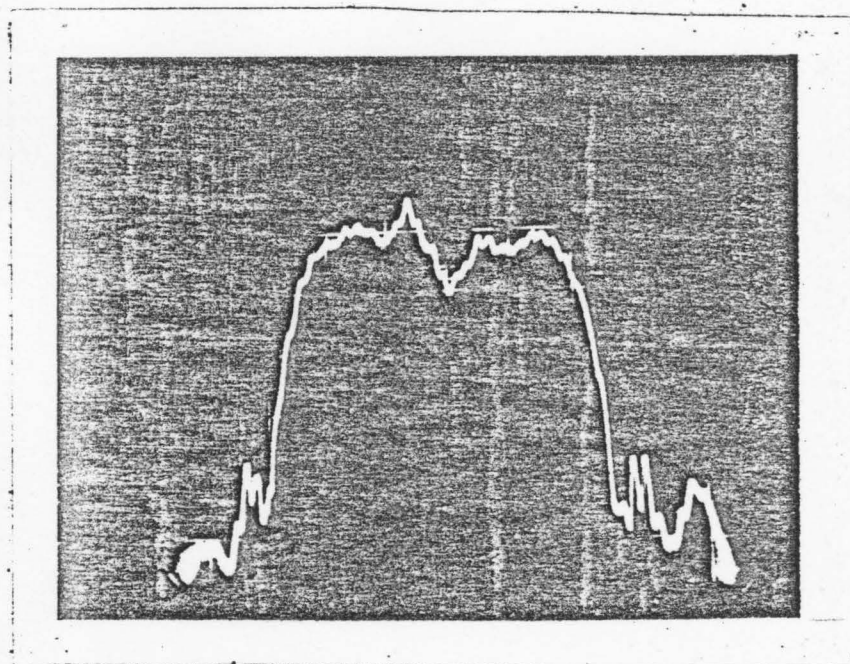
Figure 39: Photographs of response of filter #1.

(a) Magnitude response as measured on Alfred Network Analyzer

(b) Response as observed on Hewlett-Packard Phase-Magnitude Analyser



(a)

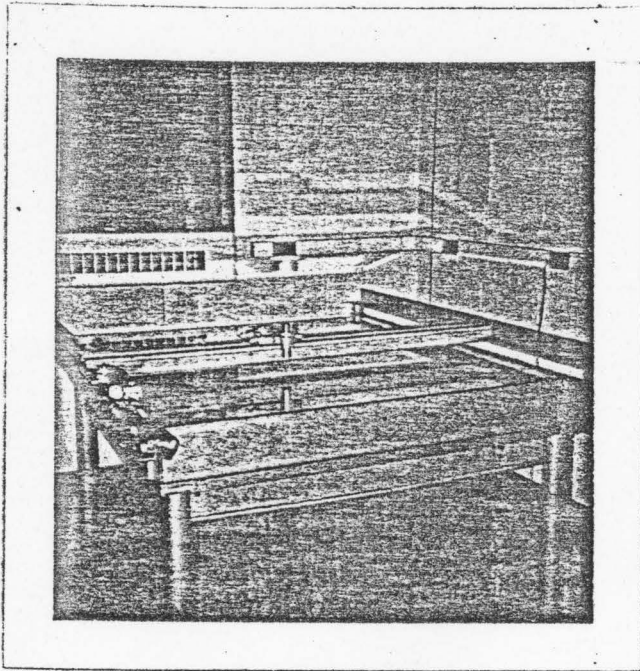


(b)

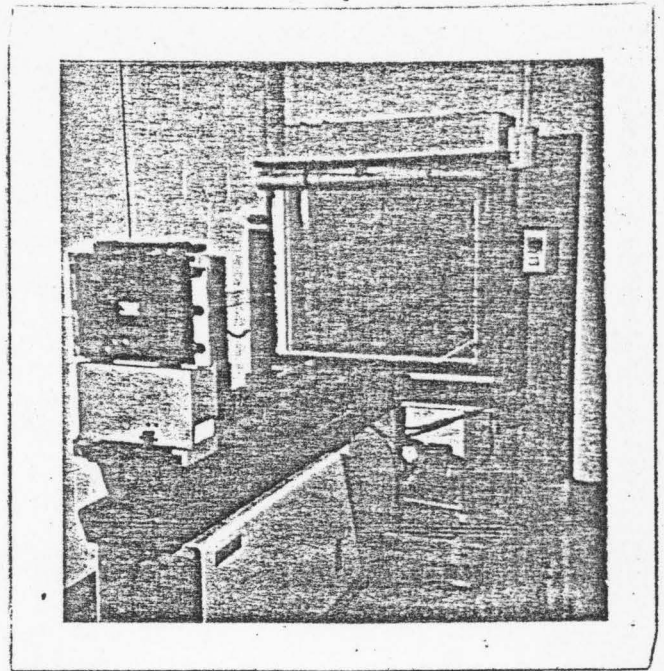
Figure 40: Photographs of Response of filter #2.

(a) Magnitude response as measured on Alfred Network Analyzer

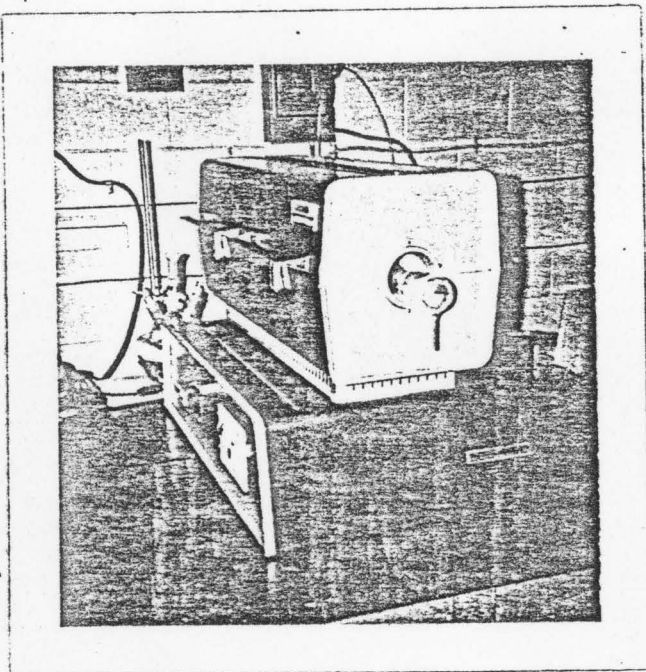
(b) Response as observed on Hewlett-Packard Phase-Magnitude Analyser



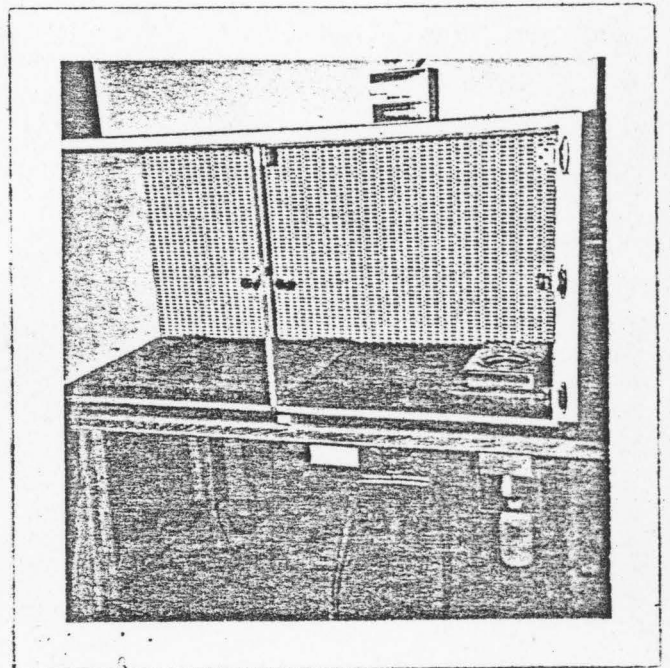
(a)



(b)



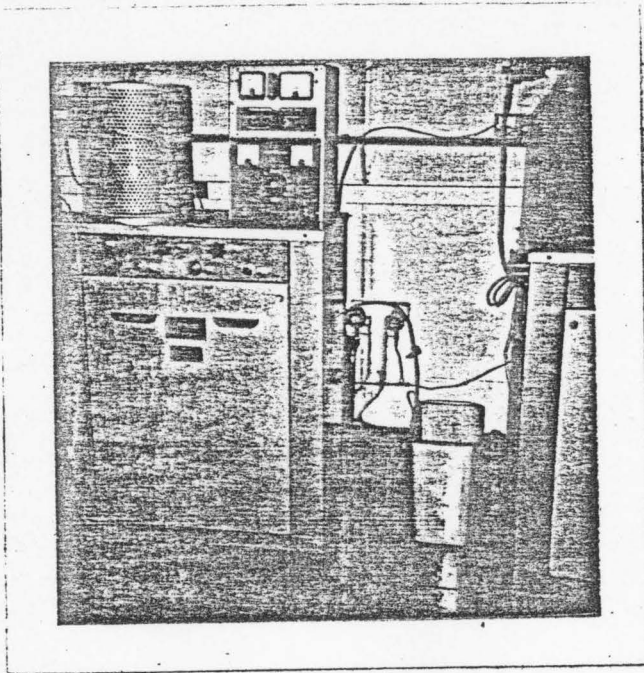
(c)



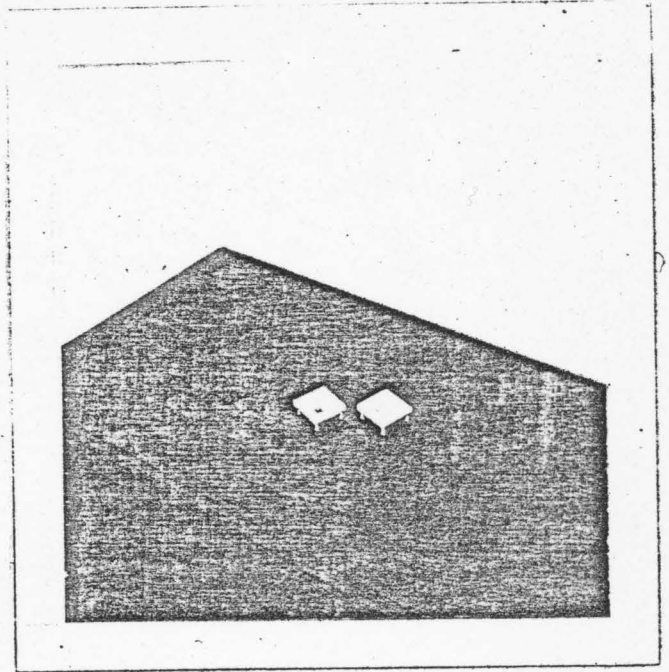
(d)

Figure 41: Photographs of equipment used in processing the surface-wave filters.

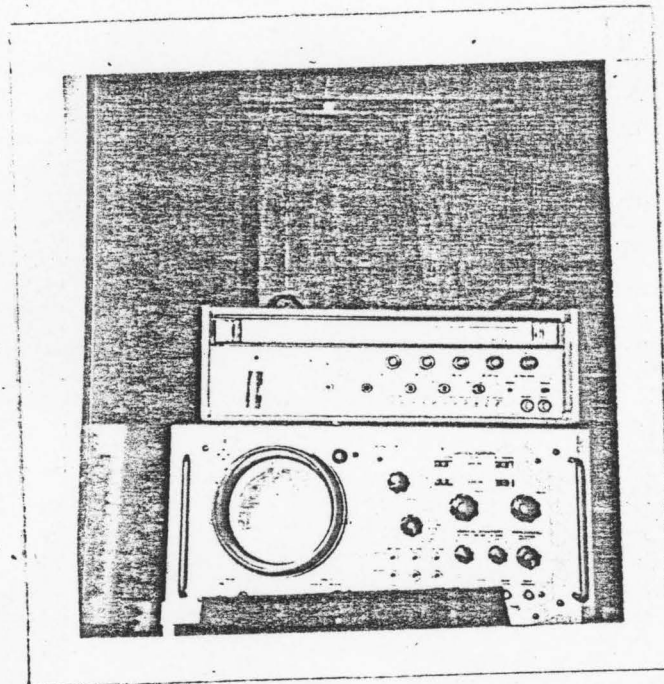
- (a) The Rubylith cutting table
- (b) The Photo-Reduction Camera
- (c) The annealing furnace
- (d) The Photo-resist spinner



(a)



(b)



(c)

Figure 42: Photographs of equipment used in processing the surface-wave filters.

- (a) The Vacuum evaporation system
- (b) The Sweep-Network Analyzer and Oscilloscope used in magnitude measurements
- (c) The completed filters shown in their test packages

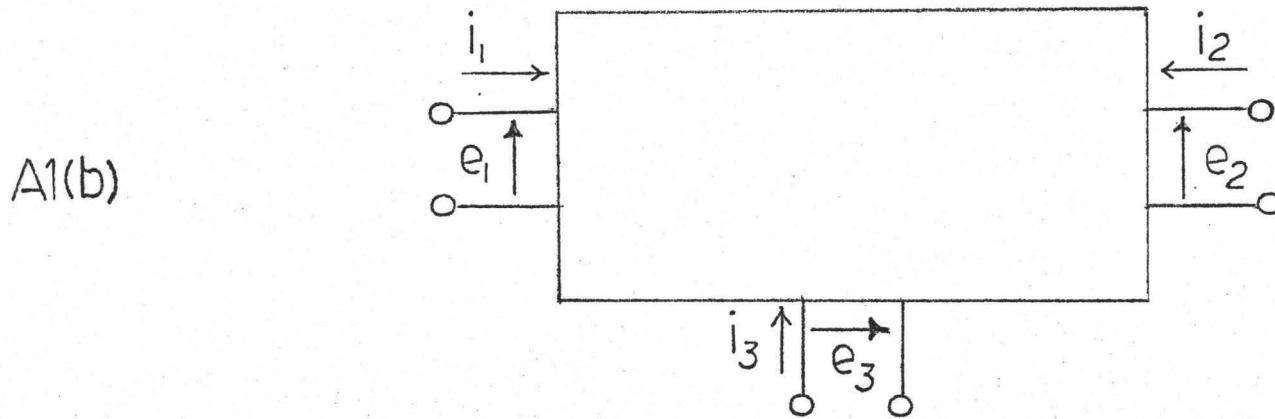
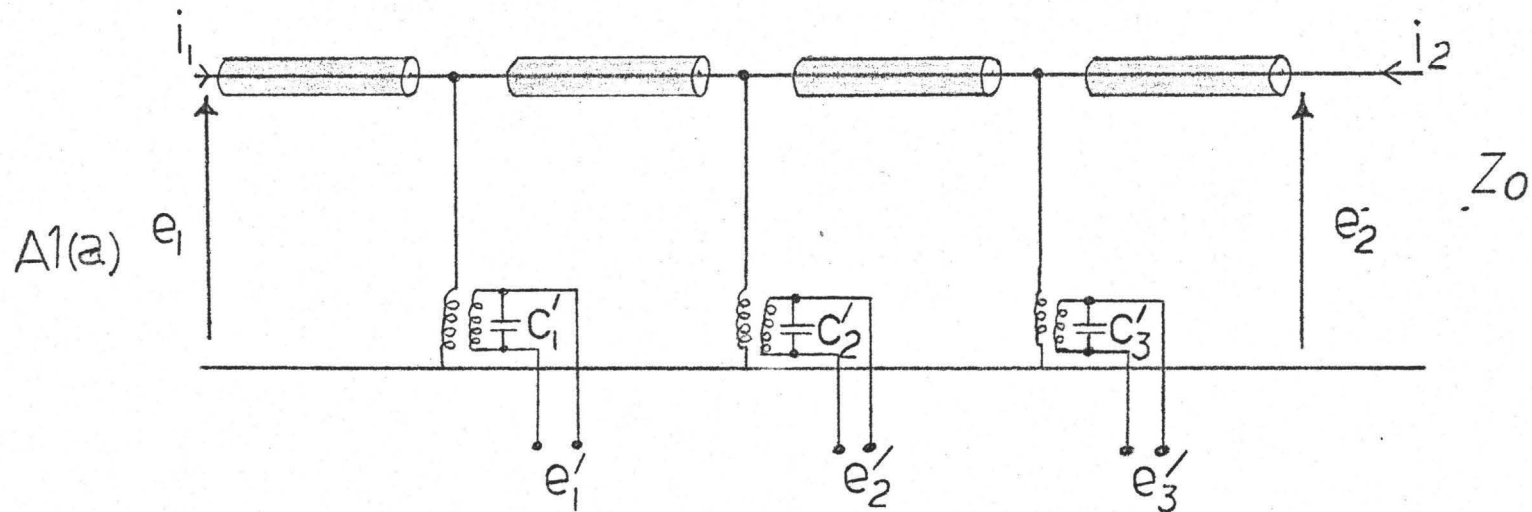


Figure A1: Surface-wave transducer characteristics based on the transmission line analogy.

(a) Uniform transmission line of characteristic frequency  $Z_0$  with periodically spaced excitation potentials

(b) 3-port electrical equivalent circuit of the complete transducer

References

- 1.
2. J.D. Maines, E.G.S. Paige, "Surface Acoustic-Wave Components, Devices and Applications", Proc. IEE, Volume 120, No. 10R, October 1973.
3. D.H. Hurlbart, "The Philosophy and Design of Acoustic Surface-Wave Filters", R.C.A. Engineer, 19, 6, April/May, 1974.
4. Clinton S. Hartmann, De Lamar, T. Bell Jr., Ronald C. Rosenfeld, "Impulse Model Design of Acoustic Surface Wave Filters", IEEE Transactions on Microwave Theory and Techniques, Volume MTT-21, No. 4, April 1973.
5. Paul H. Carr, "The Generation and Propagation of Acoustic Surface Waves at Microwave Frequencies", IEEE Transactions on Microwave Theory and Techniques, Volume MTT-17, No. 11, November 1969.
6. S.G. Joshi and R.M. White, "Excitation and Detection of Surface Elastic Waves in Piezoelectric Crystals", The Journal of the Acoustical Society of America, Volume 46, Number 1 (Part 1), 1969.
7. G.A. Coquin, H.F. Tiersten, "Analysis of the Excitation and Detection of Piezoelectric Surface Waves in Quartz by Means of Surface Electrodes", The Journal of the Acoustical Society of America, Volume 41, Number 4 (Part 2), 1967.

8. J.J. Campbell, W.R. Jones, "A Method for estimating optimal crystal cuts and propagation directions for excitation of piezoelectric surface waves", IEEE Transactions on Sonics and Ultrasonics, Volume SU-15, October 1968.
9. Kenneth M. Laskin, David W.T. Mih, Robert M. Tan, "A New Interdigital Electrode Transducer Geometry", IEEE Transactions on Microwave Theory and Techniques, Volume MTT-22, No. 8, August 1974.
10. A.J. De Vries, J.F. Dias, J.N. Rypkema, T.J. Wojcik "Characteristics of Surface-Wave Intergratable Filters (SWIFS), IEEE Transactions on Broadcast and Television Receivers BTR-13, Number 2, February 1971.
11. W.R. Smith, Henry M. Gerard, Jeffery H. Collins, Thomas M. Reeder, Herbert J. Shaw, "Analysis of Interdigital Surface Wave Transducers by Use of an Equivalent Circuit Model", IEEE Transactions on Microwave Theory and Techniques, Volume MTT-17, No. 11, November 1969.
12. Hwei P. Hsu, Fourier Analysis, Simon and Schuster Tech. Outlines, 1967.
13. G.L. Matthaei, David Y. Wong, Brian P. O'Shaughnessey, "Simplifications for the Analysis of Interdigital Surface Wave Devices", IEEE Transactions on Sonics and Ultrasonics, Volume SU-22, Number 2, March 1975.

14. Roger H. Tancrell, "Analytic design of Surface-Wave Bandpass Filters", IEEE Transactions on Sonics and Ultrasonics, Volume SU-21, No. 1, January 1974.
15. R. F. Mitchell, N.H.C. Reilley, "Equivalence of  $\delta$ -Function and Equivalent-Circuit Modesl for Interdigital Acoustic Surface Wave Transducers", Electronic Letters, Volume 8, No. 13, June 1972.
16. N.R. Ogg, D. Healey, "Acoustic Surface Waves and Non-Minimum Phase Shift Networks", RRE Memorandum 2770, 1972.